Université Mohamed Khider de Biskra
Faculté des Sciences et de la Technologie
Département de Génie Électrique

Thèse de Doctorat

Sciences et Technologies

Électrotechnique
Énergies Renouvelables

Présentée et soutenue par :
GHILANI Abdelmoumen

Le : 07, 05, 2026

Modélisation et optimisation d'une centrale solaire PV

Jury:

Mr. SAADI Ramzi	Prof.	Université de Biskra	Président
Mme. TERKI Amel	Prof.	Université de Biskra	Rapporteur
Mr. TEGANI Ilyes	MCA	C.U.Barika	Co-Rapporteur
Mr. NAIMI Djemai	Prof.	Université de Biskra	Examinateur
Mr. DRID Said	Prof.	Ecole Supérieur Nationale ER2SD. Batna	Examinateur

Année Universitaire : 2025–2026

Mohamed Khider University of Biskra
Faculty of Science and Technology
Department of Electrical Engineering

Doctoral Thesis

Sciences and Technologies

Electrotechnics
Renewable Energies

Presented and defended by:
GHILANI Abdelmoumen

On: 07, 05, 2026

Modelling and Optimisation of a PV Solar Power Plant

Jury:

Mr. SAADI Ramzi	Prof	University of Biskra	President
Mme. TERKI Amel	Prof	University of Biskra	Supervisor
Mr. TEGANI Ilyes	MCA	U.C. of Barika	Co-supervisor
Mr. NAIMI Djemai	Prof	University of Biskra	Examiner
Mr. DRID Said	Prof	Higher National School ER2SD of Batna	Examiner

Academic Year: 2025-2026

ملخص الأطروحة

يشهد قطاع الطاقة الكهروضوئية تطورًا متسارعًا جعله أحد أهم ركائز التحول الطاقوي العالمي، إلا أن تحسين كفاءة الأنظمة المربوطة بالشبكة وضمان استقرارها تحت ظروف التشغيل المتغيرة لا يزالان يمثلان تحديًا تقنيًا كبيرًا. وفي هذا السياق، تقدم هذه الأطروحة إطارًا متكاملًا يجمع بين النمذجة الدقيقة، والتحسين الذكي، والتحقق التجريبي، بهدف تطوير أنظمة كهروضوئية أكثر كفاءة وموثوقية. وقد شملت الدراسة مقارنة متقدمة بين البنية أحادية وثنائية الطابق، وتصميم منصة تجريبية حقيقية تعتمد على عاكس ثلاثي الطور، إضافة إلى تقييم خوارزميات ميتاهوريستية حديثة لتتبّع نقطة القدرة العظمى وتحليل استراتيجيات تحكم متقدمة لتحسين جودة القدرة والاستجابة الديناميكية. وأظهرت النتائج أداءً متميزًا للحلول المقترحة من حيث سرعة التتبع، وزيادة كفاءة استخراج القدرة، وتعزيز استقرار النظام، مما يجعل هذه الأطروحة مساهمة علمية وعملية واعدة في تطوير الجيل القادم من محطات الطاقة الشمسية المربوطة بالشبكة الكهربائية.

الكلمات المفتاحية: أنظمة PV متصلة بالشبكة، تحسين، تتبع نقطة القدرة العظمى، خوارزميات ميتاهيوريستية، استراتيجيات التحكم في العواكس

Résumé de la Thèse

Le secteur de l'énergie photovoltaïque connaît une expansion accélérée qui en a fait l'un des piliers les plus importants de la transition énergétique mondiale. Cependant, l'amélioration de l'efficacité des systèmes raccordés au réseau et la garantie de leur stabilité dans des conditions de fonctionnement variables constituent encore un défi technique majeur. Dans ce contexte, cette thèse présente un cadre intégré qui combine la modélisation précise, l'optimisation intelligente et la validation expérimentale, dans le but de développer des systèmes photovoltaïques plus efficaces et plus fiables. L'étude a inclus une comparaison avancée entre les architectures monophasée et à deux étages, la conception d'une plateforme expérimentale réelle basée sur un onduleur triphasé, ainsi que l'évaluation d'algorithmes métaheuristiques modernes pour le suivi du point de puissance maximale et l'analyse de stratégies de commande avancées visant à améliorer la qualité de l'énergie et la réponse dynamique. Les résultats ont montré des performances remarquables des solutions proposées en termes de rapidité de poursuite, d'augmentation de l'efficacité d'extraction de la puissance et de renforcement de la stabilité du système, ce qui fait de cette thèse une contribution scientifique et pratique prometteuse pour le développement de la prochaine génération de centrales solaires raccordées au réseau électrique

Mots-clés : systèmes PV connectés au réseau, optimisation, poursuite du point de puissance maximale, algorithmes métaheuristiques, stratégies de commande des onduleurs

Thesis Abstract

The photovoltaic energy sector is witnessing accelerated expansion that has made it one of the most important pillars of the global energy transition. However, improving the efficiency of grid-connected systems and ensuring their stability under varying operating conditions still represents a major technical challenge. In this context, this thesis presents an integrated framework that combines precise modeling, intelligent optimization, and experimental validation, with the aim of developing more efficient and reliable photovoltaic systems. The study included an advanced comparison between single-stage and two-stage topologies, the design of a real experimental platform based on a three-phase inverter, in addition to the evaluation of modern metaheuristic algorithms for maximum power point tracking and the analysis of advanced control strategies to improve power quality and dynamic response. The results showed remarkable performance of the proposed solutions in terms of tracking speed, increased power extraction efficiency, and enhanced system stability, making this thesis a promising scientific and practical contribution to the development of the next generation of grid-connected solar power plants.

Keywords: grid-connected PV systems, optimisation, maximum power point tracking, metaheuristic algorithms, inverter control strategies.

Acknowledgements and Dedication

First and foremost, I thank Allah Almighty for granting me strength, patience, and perseverance throughout the completion of this thesis. Without His guidance and blessings, none of this work would have been possible.

I extend my deepest gratitude to my beloved parents and family, whose unwavering support, encouragement, and sacrfiices have been the foundation of my academic journey. My sincere appreciation also goes to my friends, whose companionship and motivation continuously inspired me to move forward.

*A special and heartfelt acknowledgment is dedicated to my supervisor, **Prof. Amel TERKI**, for her continuous guidance, scientfiic support, and invaluable mentorship. Her patience, expertise, and constructive advice played a crucial role in shaping the quality and direction of this research.*

*I would like to express my sincere gratitude and deep appreciation to the esteemed members of the examination committee, particularly the Chair of the Committee, Professor **Ramzi Saadi**, and the examiners: Professor **Djemai Naimi** and our honoured guest Professor **Said Drid**, for their valuable guidance and scientfiic support, which have greatly enriched this work.*

*I would also like to express my profound appreciation to all the professors of the **Department of Electrical Engineering** at the University of Biskra.*

*My thanks are further extended to the members of the research laboratories **LGEB** and **LMSE**, whose collaboration, resources, and technical support greatly contributed to the success of this thesis.*

To everyone who supported me in any way—directly or indirectly—please accept my sincere gratitude. This achievement is as much yours as it is mine.

مع فائق الشكر والامتنان لكل من ساهم في إنجاز هذا العمل

Contents

List of Figures

List of Algorithms

List of Tables

Nomenclature

PV	Photovoltaic
MPPT	Maximum Power Point Tracking
GCI	Grid-Connected Inverter
DC	Direct Current
AC	Alternating Current
THD	Total Harmonic Distortion
PLL	Phase-Locked Loop
DSP	Digital Signal Processor
FLC	Fuzzy Logic Control
ANN	Artificial Neural Network
PSO	Particle Swarm Optimization
GWO	Grey Wolf Optimization
WOA	Whale Optimization Algorithm
CS	Cuckoo Search
P&O	Perturb and Observe
IncCond	Incremental Conductance
SRF	Synchronous Reference Frame
ICC	Indirect Current Control
DCC	Direct Current Control
DPC	Direct Power Control
SVPWM	Space Vector Pulse Width Modulation
$\mathbf{V_{DC}}$	DC-Link Voltage
$\mathbf{I_{inv}}$	Inverter Input Current
$\mathbf{V_{pv}}$	Photovoltaic Array Output Voltage
ω	Grid Angular Frequency
$\theta(t)$	Instantaneous Phase Angle
IEC 61727	International Standard for PV Grid Interface
IEEE 1547	Standard for Interconnection of Distributed Energy Resources
EN 61000-3-2	European Standard for Harmonic Emissions

General Introduction

General Introduction

Solar energy is considered one of the most important renewable energy sources globally, due to its wide and sustainable availability and progressively decreasing competitive costs over the years. This advantage makes it a fundamental element in reshaping the global energy mix and reducing dependence on fossil fuels, as well as contributing to the reduction of carbon emissions.

Photovoltaic (PV) power plants have witnessed remarkable technological progress in terms of physical components, mathematical modelling, control techniques, and methods of integration with electrical grids. With the significant expansion in the adoption of these plants at local and global grid levels, it has become essential to understand the dynamic performance of PV systems and optimise their operational processes to ensure a continuous and reliable electricity supply, and to maintain the stability of modern grids under various and changing operating conditions.

Operational challenges for these systems have become more complex with the increase in plant size and their grid integration, as such large and diverse environments require precise models and advanced control systems to ensure a balance between power quality, system stability, and efficiency in solar energy extraction. In addition, developments in maximum power point tracking (MPPT) algorithms and inverter control strategies have become key tools for maximising energy production and minimising operational losses, reflecting the importance of continuous research to develop an integrated framework that combines modelling, control, and experimental validation.

Motivation and Problem Statement

Despite the significant progress in photovoltaic technology, the practical implementation of high-efficiency and reliable solar power plants still faces numerous operational and technical challenges. The performance of grid-connected PV systems is directly affected by variations in solar irradiance, temperature changes, partial shading conditions, and grid dynamics. These factors can significantly reduce the extracted power, cause operational instability, and negatively impact power quality.

Furthermore, current research is often fragmented, with studies focusing on a single aspect of the system such as modelling, MPPT algorithm design, inverter control, or performance optimisation, without providing a comprehensive framework that integrates these elements. As a result, engineers and designers lack a practical, experimentally supported methodology to help them select the most appropriate system architecture, implement advanced MPPT algorithms, and optimise inverter control strategies within a unified perspective. This gap is particularly evident in countries like Algeria, where abundant solar potential does not always match the level of applied optimisation in practical systems.

Accordingly, this thesis aims to achieve two main objectives:

- To provide a precise, optimisation-oriented modelling framework capable of representing both the steady-state and dynamic behaviours of grid-connected PV systems under realistic operating conditions.
- To propose, evaluate, and experimentally validate advanced control strategies and optimised MPPT algorithms to enhance energy extraction efficiency, reduce losses, and ensure high-quality integration with the electrical grid.

Main Contributions of the Thesis

The thesis presents several scientific and technical contributions, summarised as follows:

- **Optimised Architectural Evaluation by Comparison of Single- and Two-Stage PV System Configurations**
  A comparative analytical study was conducted for single- and two-stage photovoltaic system configurations under varying levels of solar irradiance. The evaluation included efficiency, dynamic response, and compliance with grid-connection requirements. This analysis provides clear engineering guidelines for selecting the optimal architecture for designing and implementing grid-connected solar systems, in accordance with the application requirements and desired performance levels.
- **Design and Implementation of an Optimised Solar Inverter for Grid Injection**
  A three-phase, single-stage photovoltaic inverter with advanced industrial features was designed and implemented, utilising **Field-Stop IGBTs**, a **RLC Snubber Circuit** for protection against voltage transients, along with **Bipolar Gate Driver Circuits** and **Undervoltage Lockout Protection** to ensure reliable and safe operation. This inverter serves as a robust experimental platform for validating performance in grid-connected scenarios.
- **Comprehensive Experimental Validation of Metaheuristic Maximum Power Point Tracking (MPPT) Algorithms in a Single-Stage Three-Phase Grid-Connected PV System**
  Four advanced MPPT algorithms (GWO, WOA, CS, PSO) were evaluated using an actual three-phase, single-stage grid-connected PV system. The assessment focused on their capability to maximise the extracted power under challenging operating conditions, including uniform and partial shading, providing an accurate evaluation of performance and energy extraction efficiency.

– **Practical Evaluation of Advanced Inverter Control Strategies**
  Four advanced inverter control strategies (DPC, SRF, DCC, ICC) were tested on the same experimental platform to assess their ability to ensure power quality, dynamic response stability, and compliance with international grid-connection standards. The results confirm the practical applicability and reliability of these strategies in industrial systems.

Thesis Structure

The thesis is structured progressively to enable readers to build a comprehensive understanding of the topic:

– **Chapter 1:** Provides an overview of solar power system architectures, international standards, and MPPT techniques, establishing the research context and scientific foundation of the study.

– **Chapter 2:** Focuses on modelling and optimisation of control strategies, laying a strong theoretical base for developing high-efficiency grid-connected PV systems.

– **Chapter 3:** Presents simulation and performance evaluation, including efficiency analysis, dynamic response, and comparison of system architectures and control strategies.

– **Chapter 4:** Describes the design, implementation, and experimental validation of the system, analysing practical results to ensure alignment with simulation expectations, with emphasis on extracted power quality and system stability under real operating conditions.

Overall, In light of current challenges and the increasing requirements for integrating solar energy into electrical grids, this work represents a pivotal step toward achieving robust, efficient, and internationally compliant PV systems. The contributions presented go beyond theoretical analysis; they start with establishing a reference for international standards, advance to developing precise mathematical models, investigate optimal topologies in depth, and evaluate modern metaheuristic MPPT algorithms. Practically, the originality of this thesis is reflected in the custom design and physical implementation of the PV inverter that meets the highest safety and quality standards, alongside rigorous experimental validation of both tracking algorithms and advanced control strategies under real operating conditions. Finally, integrating these efforts into a unified methodology and comprehensive experimental reference aims to bridge the gap between academic research and industrial applications, providing an indispensable practical guide for engineers and researchers working in the design and operation of grid-connected PV systems.

Chapter I

Review of Photovoltaic System Architectures, Standards,and MPPT Techniques

I.1 Introduction

Photovoltaic (PV) power systems have emerged as a critical component of renewable energy solutions due to their sustainability and decreasing cost. However, the efficiency of PV systems depends on various factors, including environmental conditions, system architecture, energy management techniques, and technical standards. This chapter provides an overview of PV power systems, their classifications, conversion topologies, technical standards, and the importance of Maximum Power Point Tracking (MPPT) techniques.

I.2 Renewable energy in the world

According to the International Renewable Energy Agency (IRENA), by the end of 2023, the global installed capacity for renewable energy surpassed 3,869 gigawatts, with notable contributions from various energy sectors. Specifically, 1,407 gigawatts were allocated to renewable hydropower, 1,017 gigawatts to onshore wind energy, 1,412 gigawatts to photovoltaic solar power (PV), 6.87 gigawatts to solar thermal energy, and 0.027 gigawatts to other renewable energy sectors [1] .

These statistics highlight the continued progress in the global transition to renewable energy, with renewable sources accounting for 43% of the total installed energy capacity worldwide by the end of 2023. During this year, 473 gigawatts were added to global renewable energy capacity, marking the largest increase to date, with a growth rate of 13.9%. Notably, renewable energy accounted for 86% of the total global energy capacity additions, with solar energy alone contributing nearly three-quarters of this increase, adding 346 gigawatts, while wind energy contributed an additional 116 gigawatts [2].

I.2.1 Renewable Energy Development in Algeria

In Algeria,as illustrated in Figure I.1, the capacity for renewable energy production has witnessed significant growth, although it still represents a small portion of the country's overall energy mix. By the end of 2023, Algeria's total renewable energy capacity reached 590 megawatts, with contributions from various sources, including hydropower, wind energy, and solar power. In the field of hydropower, the capacity of power plants has remained stable at 129 megawatts since 2020 [2]. Meanwhile, in the wind energy sector, no substantial progress has been made, with wind capacity remaining at 10 megawatts since 2014, reflecting challenges in its development. On the other hand, photovoltaic solar energy has experienced significant growth, as shown in Figure I.1, with its capacity increasing from 3 megawatts in 2014 to 426 megawatts in 2023. Algeria continues to focus its efforts on expanding its solar energy potential and taking advantage of favorable climatic conditions for photovoltaic solar power generation [3].

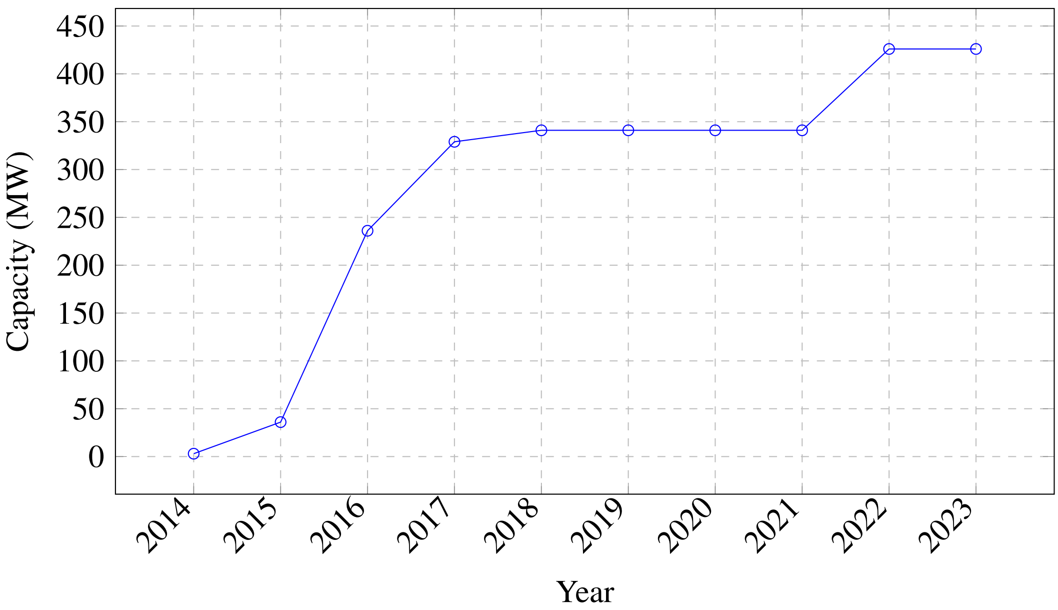

Figure I.1: Growth of photovoltaic solar energy Capacity in Algeria

In the broader African context, the renewable energy sector continues to evolve, with the total renewable energy capacity in the continent reaching 62,107 megawatts by the end of 2023. Despite this progress, Algeria, like many countries in the region, still faces significant challenges in fully leveraging its renewable energy potential. This requires continuous investments, the development of new technologies, and strategic planning to achieve both national and international energy goals [4].

I.3 Overview of Photovoltaic Power Plant Systems

I.3.1 Historical overview

The discovery of the photovoltaic effect dates back to the early 19th century. In 1839, the French physicist Alexandre Edmond Becquerel first observed a phenomenon that enabled the conversion of light into electrical energy. This principle later became the foundation for the operation of solar cells [5]. Over subsequent decades, numerous scientists contributed to advancing the understanding and practical application of this effect. Among the most notable figures were Charles Fritts, Edward Weston, Nikola Tesla, and Albert Einstein, the latter of whom was awarded the Nobel Prize in 1905 for his groundbreaking work on the photoelectric effect [6].

Despite these early discoveries, the large-scale development of photovoltaic technology was constrained by high production costs. A significant breakthrough occurred only in the late 1950s, coinciding with advancements in the semiconductor industry. By the 1960s, solar cells were primarily deployed in space applications, supplying electrical power to orbiting satellites, where they demonstrated exceptional reliability and efficiency [5].

The 1970s marked a significant milestone for photovoltaic technology, as advancements in manufacturing processes resulted in improved performance and significant cost reductions. During this period, the oil crisis further accelerated interest in solar energy, prompting efforts to commercialise solar cells and integrate them with practical applications [7, 8].

Initially, solar cells were primarily employed to supply power to remote locations beyond the reach of conventional electrical grids. They were widely adopted for powering standalone systems such as lighthouses, telecommunication infrastructure, and low-power electronic equipment. By the 1980s, solar cells had gained popularity as an energy source for consumer electronics, including calculators, wristwatches, portable radios, and lamps [6]. Simultaneously, the development of photovoltaic systems for residential and commercial use saw significant advancements. Both off-grid and grid-connected systems emerged, facilitating the expansion of solar energy in various sectors. In rural areas lacking access to electricity infrastructure, solar energy played a crucial role in powering essential applications such as water pumping, cooling systems, telecommunications, and household appliances [5].

The increasing adoption of photovoltaic technology during this period laid the groundwork for the widespread deployment of solar energy solutions in the following decades [7, 6].

I.3.2 Classification of the PV system

Photovoltaic (PV) technology is one of the most important parts of sustainable energy production. It uses interconnected photovoltaic cells to directly turn solar radiation into electricity [9]. The overall efficiency and operational performance of PV systems are contingent upon multiple factors, including the configuration of photovoltaic modules and prevailing environmental conditions. Generally, PV systems are classified into three primary categories, each distinguished by its specific operational framework and practical applications [10].

I.3.2.1 Stand-Alone Photovoltaic Systems

Stand-alone photovoltaic (PV) systems are specifically engineered to function independently of the electrical grid, making them particularly advantageous for deployment in remote locations or off-grid environments. As illustrated in Figure I.2,these systems are primarily designed to supply designated direct-current (DC) or alternating-current (AC) loads and can be broadly categorised into two distinct types: direct-coupled systems and battery-integrated systems. [11] Direct-coupled configurations don't store energy, so they only provide electricity during the day. This makes them perfect for uses like water pumping and ventilation systems [12]. However, because solar energy production isn't always steady, battery storage is often added to stand-alone PV systems to make sure of a steady flow of power, thereby mitigating the mismatch between energy generation and consumption [9].

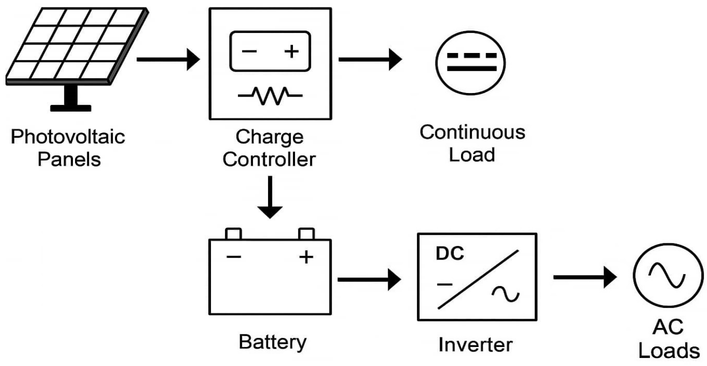

Figure I.2: Stand-Alone Photovoltaic Systems

I.3.2.2 Grid-Connected Photovoltaic Systems

As shown schematically in Figure I.3,grid-connected photovoltaic (PV) systems are designed to function in parallel with the electrical utility grid, enabling the seamless integration of solar-generated electricity into the grid infrastructure. A fundamental component of these systems is the inverter, which facilitates the conversion of direct current (DC) electricity, produced by PV modules, into alternating current (AC) electricity that aligns with the grid's voltage and power quality standards [9]. These systems play a crucial role in decreasing reliance on conventional power sources while also enhancing overall energy efficiency. In certain configurations, excess solar energy can be fed back into the grid, contributing to grid stability and reducing the need for additional power generation from traditional sources. Furthermore, by generating electricity in proximity to the point of consumption, grid-connected PV systems help minimise transmission losses and support the decentralisation of energy production, thereby improving the resilience and efficiency of the power grid [11].

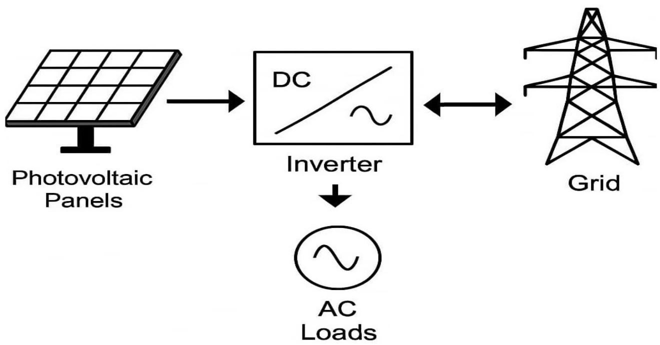

Figure I.3: Grid-Connected Photovoltaic Systems

I.3.2.3 Hybrid systems

Hybrid photovoltaic (PV) systems, as depicted in Figure I.4, represent an advanced configuration that integrates solar power generation with complementary energy sources such as diesel, gas, or wind generators [11]. These systems are particularly beneficial in regions characterised by intermittent solar radiation or where the availability of energy storage infrastructure is constrained [13]. By leveraging multiple energy sources, hybrid PV systems significantly enhance the reliability and stability of power supply, ensuring a more consistent and uninterrupted electricity generation process. This hybridisation makes them a highly viable solution for a broad spectrum of applications, ranging from remote off-grid areas to urban environments where energy security and efficiency are paramount [14].

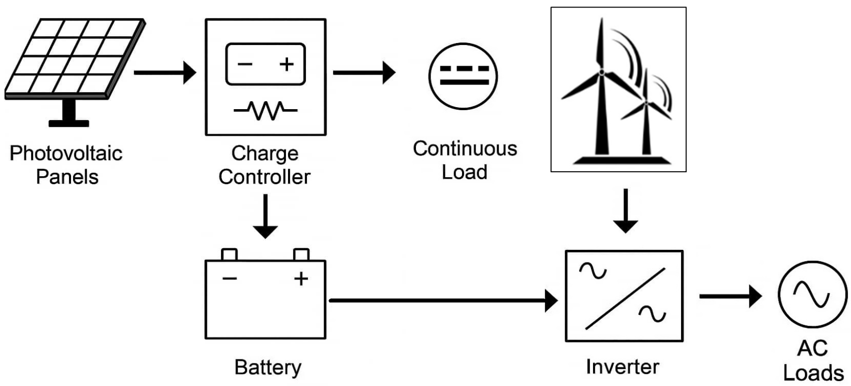

Figure I.4: Hybrid Photovoltaic Systems

I.3.3 Photovoltaic System Topologies

I.3.3.1 Central Inverters

Central inverters are widely used in large-scale photovoltaic (PV) systems, typically in three-phase, grid-connected applications with power ratings ranging from 10 kW to 1000 kW. In this configuration, as shown in Figure I.5 multiple PV arrays are connected in parallel to a single inverter that converts the direct current (DC) produced by the solar modules into alternating current (AC) for distribution to the grid or local consumption. This system is known for its high efficiency, particularly when using transformerless PV converters that minimise losses during the power conversion stage[15].

However, the central inverter system requires long DC cables, which contribute to power losses, and its performance can be affected by shading or mismatches between PV modules. Additionally, the reliance on a single inverter makes the system vulnerable to complete shutdown in case of inverter failure[16].Despite these challenges, central inverters remain the preferred solution for large-scale PV installations with uniform irradiance conditions, where simplicity, cost-effectiveness, and efficiency are prioritised [17].

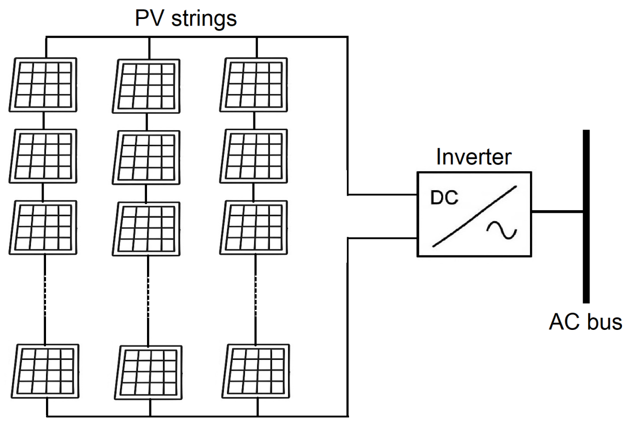

Figure I.5: Central inverter system configuration

I.3.3.2 String Inverters

String inverters are commonly used in photovoltaic (PV) systems with power ratings ranging from 1 kW to 3 kW. In this configuration, as shown in Figure I.6, each PV string is connected to its own inverter, which allows for individual Maximum Power Point Tracking (MPPT) for each string. This configuration enhances system reliability, as failure in one inverter does not affect the entire system. Additionally, the string topology reduces shading losses since each string operates independently, ensuring higher efficiency, especially when dealing with partial shading [18].

The main advantage of this topology is its ability to improve efficiency and reduce mismatch losses compared to centralised inverters. The system is also more flexible, allowing easy expansion by adding new strings to increase power output. However, the increased number of inverters raises the system's cost, which is a significant disadvantage. Additionally, while individual MPPT helps in minimising losses, power mismatches between strings are not entirely eliminated [19].

This topology provides better overall performance compared to central inverters, especially in systems where shading or orientation issues exist. It also reduces the need for anti-return diodes and enhances the system's redundancy. Despite these benefits, the cost and complexity of multiple inverters remain key challenges [20].

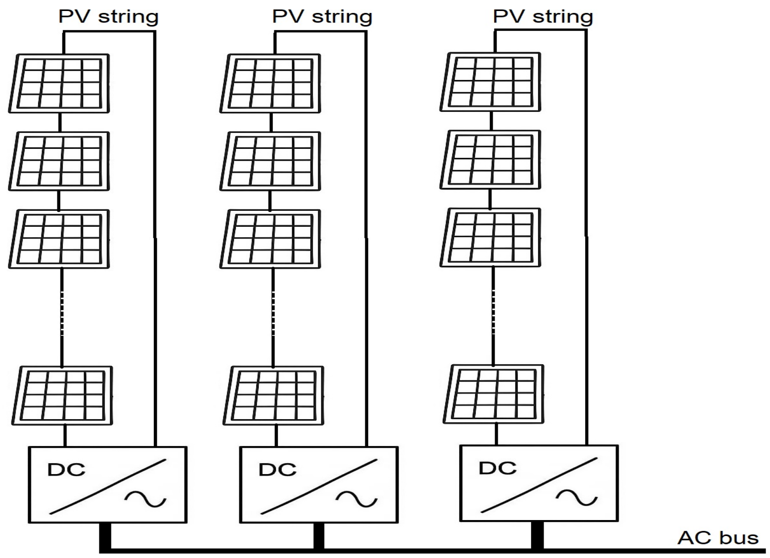

Figure I.6: String inverter configuration .

I.3.3.3 Multi-String Inverters

The multi-string inverter configuration is a hybrid solution that combines the advantages of string and centralised inverters. It provides a balance between cost reduction, DC loss minimisation, and shading sensitivity, as shown in Figure I.7.In this topology, each PV string is equipped with its own Maximum Power Point Tracking (MPPT) and DC-DC converter, allowing for individual control of each string [21].This results in improved energy output, especially in shaded conditions, while maintaining the simplicity and cost benefits of a central inverter. This configuration, which emerged in the PV market in 2002, is commonly used in systems with power ratings between 3 kW and 10 kW. It allows for the integration of inverters with varying power ratings and PV modules with different current-voltage (I-V) characteristics. The MPPT for each string enhances overall efficiency, making this configuration increasingly popular as a standard solution in PV systems [10]. However, despite its advantages, the multi-string inverter topology faces challenges. The system's reliability is lower than that of string inverters, and additional losses from the DC-DC converters can affect overall performance. Power mismatch remains an issue, and the use of multiple power electronics converters adds to the system's cost and complexity. The power limit for this configuration is typically 5 kW [19].

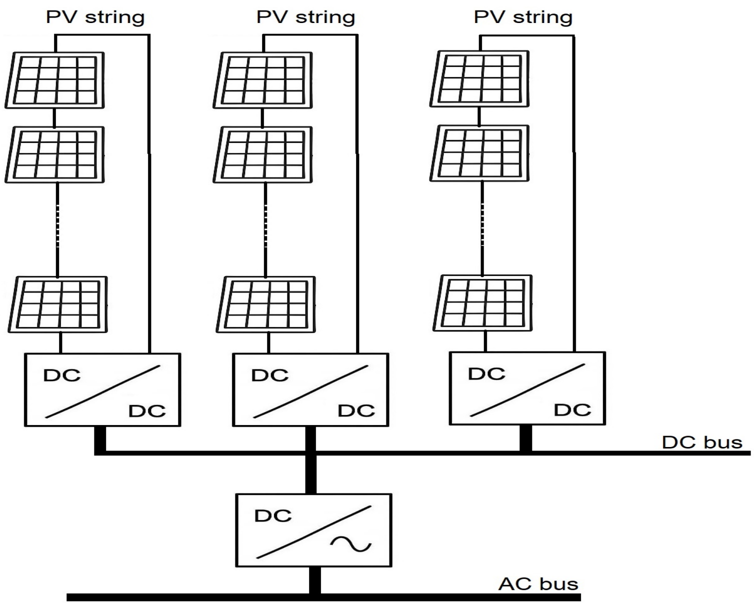

Figure I.7: Multi-string inverter configuration

I.3.3.4 Modular topology

In the topology illustrated in Figure I.8, a single photovoltaic (PV) module is directly connected to the grid through an integrated inverter that incorporates Maximum Power Point Tracking (MPPT) functionality. This configuration offers several notable advantages. It minimises mismatch losses by eliminating series or parallel connections with other modules, thereby enabling individualised power optimisation. The inclusion of separate MPPT for each module enhances the overall energy harvesting efficiency, especially under non-uniform irradiance conditions. Additionally, the plug-and-play nature of this setup facilitates ease of installation and system scalability[8].

Despite these benefits, the topology is associated with certain limitations. One key drawback is the relatively low efficiency due to the requirement to boost the inherently low DC voltage of the module to meet the grid-level voltage demands. Furthermore, the power conversion capacity is limited, making this approach suitable only for low-wattage applications. Since each unit handles only one PV module, this configuration is less appropriate for large-scale systems due to cost and complexity considerations[22].

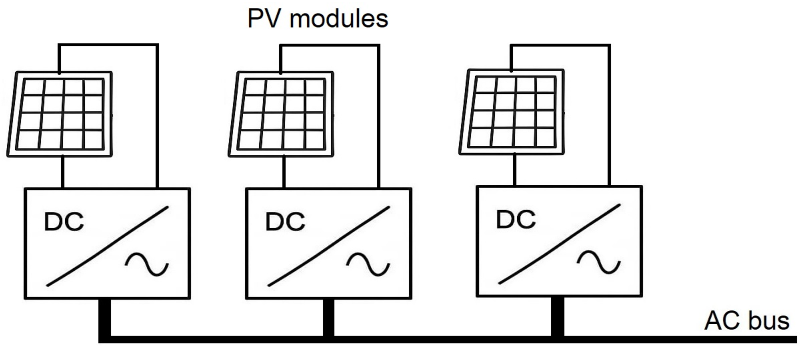

Figure I.8: Modular topology configuration

I.3.4 Photovoltaic power conversion configurations

The architecture of photovoltaic (PV) power conversion systems play a pivotal role in defining the efficiency, reliability, and overall performance of grid-connected PV systems. These architectures are generally categorized into single-stage and two-stage configurations, each offering distinct advantages and limitations. The selection of an appropriate topology is influenced by various factors, including power conversion efficiency, control complexity, cost, and compatibility with grid integration requirements [23]

I.3.4.1 Two-Stage Photovoltaic Power Conversion Architecture

The two-stage photovoltaic (PV) power conversion architecture,as illustrated in the figure I.9, consists of a DC-DC converter in the first stage, which plays a crucial role in Maximum Power Point Tracking (MPPT) for the PV module. By dynamically adjusting the voltage level, the converter ensures optimal energy extraction while stepping up the voltage to meet the requirements for subsequent processing and grid integration [24] [25].

In the second stage, an inverter is employed to enable grid compatibility. The inverter converts the DC power into AC while ensuring that both voltage and frequency conform to grid standards, thereby facilitating the efficient and stable injection of generated power into the electrical grid [26].

Despite its operational efficiency, this topology presents inherent limitations that may impede large-scale deployment. One of the primary drawbacks is the large physical footprint resulting from the high number of interconnected power electronic components. Additionally, the substantial initial cost, driven by the complex structural design requiring multiple power conversion stages, poses a significant challenge. Furthermore, the advanced control mechanisms associated with this architecture increase system complexity, which leads to higher operational and maintenance costs [24].

Moreover, the multiple conversion stages contribute to cumulative energy losses, which reduce overall power transfer efficiency and raise concerns about system reliability and stability. A notable technical issue associated with this topology is the degradation of power quality, particularly the increase in Total Harmonic Distortion (THD), which negatively impacts sensitive electrical loads. This, in turn, may affect grid stability and limit the overall performance of the system [25].

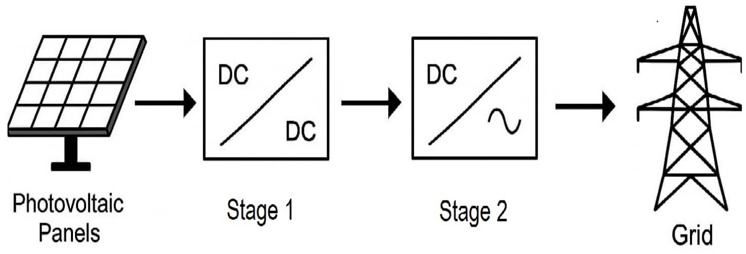

Figure I.9: Two-stage photovoltaic power conversion architecture.

I.3.4.2 Single-Stage Photovoltaic Power Conversion Architecture

This architecture employs a single-stage conversion approach as shown in Figure I.10, directly interfacing the photovoltaic (PV) array with the grid via an inverter. The inverter simultaneously performs Maximum Power Point Tracking (MPPT) and DC-AC conversion, ensuring optimal energy extraction while maintaining strict compliance with grid voltage and frequency requirements. By eliminating the intermediate DC-DC conversion stage, this topology simplifies the power conversion process, reducing system complexity and enhancing overall efficiency [24][27].

One of the primary advantages of the single-stage configuration is its compact design, which results in a reduced physical footprint and lower implementation costs compared to multi-stage architectures.[25] The direct power transfer mechanism minimizes energy losses associated with multiple conversion stages, thereby improving overall system efficiency. Additionally, the simplified control strategy reduces computational demands, contributing to increased system reliability and ease of maintenance [26].

However, despite its advantages, the single-stage topology introduces several challenges. The absence of an intermediate DC-DC converter limits voltage control flexibility, making it more difficult to optimize energy harvesting under varying solar irradiance conditions. Furthermore, the simultaneous execution of MPPT and grid synchronization imposes stringent control requirements on the inverter, thus increasing the complexity of its design and operation [23].

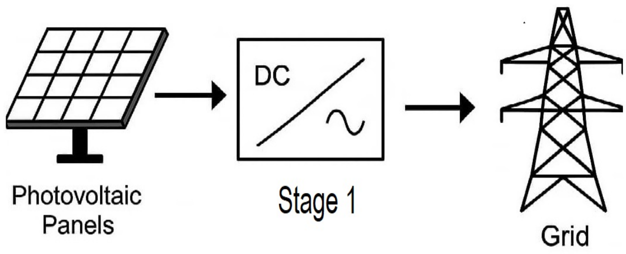

Figure I.10: Single-Stage Photovoltaic Power Conversion Architecture.

I.4 Global Standards for Optimal Integration and Performance of Grid-Connected PV Systems

Ensuring the quality of distributed energy in grid-connected photovoltaic (PV) systems is a fundamental requirement defined by international standards. These standards aim to regulate key technical parameters, such as Total Harmonic Distortion (THD), voltage and frequency limits, power factor (PF), leakage current, and DC injection levels, to ensure seamless and safe integration with the distribution grid.This is in accordance with standards like IEC 61727, IEEE 1547, and EN 61000-3-2. Compliance with these standards is critical for grid-connected photovoltaic inverters (GCI), which act as the interface between PV arrays and the electrical grid, converting DC to AC while maintaining operational stability and efficiency. Furthermore, these standards address essential aspects such as islanding detection, grounding, and automatic reconnection mechanisms after grid disturbances[28][29]. Galvanic isolation is a crucial technical factor in the design of photovoltaic inverters, as it significantly enhances safety and reduces operational risks. This isolation can be achieved through the use of high-frequency transformers on the DC side or low-frequency transformers on the grid side, in line with the national regulations of each country. However, the presence of galvanic isolation in grid-connected photovoltaic systems noticeably impacts the efficiency of DC-AC conversion, making it a key design consideration. The following tables present the technical requirements for these standards, including disconnection and reconnection criteria for grid-connected inverters under varying operational conditions[8].

Standard	Total Harmonic Distortion (THD)	DC Injection Level
IEC 61727	$\leq 5\%$	$\leq 0.5\%$ of rated current
IEEE 1547	$\leq 5\%$	$\leq 0.5\%$ of rated current

Table I.1: Limits for Power Quality (Total Harmonic Distortion & DC Injection)

Standard	Voltage Range (V)	Frequency Range (Hz)	Response Time Limit (seconds)
IEC 61727	± 10% of nominal voltage	49 - 51	≤ 2
IEEE 1547	± 10% of nominal voltage	59.3 - 60.5	≤ 2

Table I.2: Voltage and Frequency Tolerances for Normal Operation

Standard	Minimum Voltage (V)	Maximum Voltage (V)	Frequency Range for 50Hz	Frequency Range for 60Hz
IEC 61727	90% of nominal voltage	110% of nominal voltage	47 - 53	57 - 63
IEEE 1547	88% of nominal voltage	110% of nominal voltage	/	59.3 - 60.5

Table I.3: Disconnection and Reconnection Criteria for Grid-Connected PV Systems

In the context of IEEE 1547, synchronization requirements with the grid are vital to ensure system coordination with the electrical grid. The system requires the frequency and voltage to synchronize between the grid-connected system and the grid itself, along with automatic disconnection in the event of any unacceptable deviation from these parameters. The system automatically verifies compliance with the grid by synchronizing with its frequency and voltage, thus preventing interference that could destabilize the grid [30].

I.5 Review of Maximum Power Point Tracking (MPPT)

Maximum Power Point Tracking (MPPT) techniques are fundamental in enhancing the efficiency of photovoltaic (PV) solar energy systems. These techniques identify the optimal operating point that maximises power output under varying environmental conditions such as temperature and solar irradiance[31]. The primary benefit of MPPT is ensuring the highest possible energy extraction from solar panels at any given moment by dynamically adjusting the operating point in response to changing environmental conditions. Both conventional and advanced MPPT techniques play a critical role in improving the overall performance of solar energy systems. However, each technique faces unique challenges that necessitate innovative solutions to ensure optimal performance[32].

I.5.1 Conventional Techniques

The Perturb and Observe (P&O) method is one of the simplest and most widely used MPPT techniques. This method periodically adjusts the voltage or current while monitoring the corresponding power variation. If the power increases, the adjustment continues in the same direction; otherwise, it reverses. Despite its simplicity and ease of implementation, P&O suffers from oscillations around the maximum power point, particularly in cases of rapid irradiance variations. These oscillations can lead to energy losses, limiting overall system efficiency [33].

The Incremental Conductance (IncCond) method, on the other hand, performs simultaneous analysis of both voltage and current to determine the optimal power point more accurately than P&O. This technique evaluates the slope of the power curve, allowing for a more precise MPP tracking. However, its computational complexity increases energy consumption, making it challenging for resource-constrained systems where efficiency is a priority [32].

I.5.2 Advanced Techniques

Advanced MPPT techniques employ more sophisticated methods, such as Fuzzy Logic Control (FLC), which relies on a fuzzy inference system to fine-tune the optimal operating point of solar panels. This approach enables a rapid adaptive response to environmental fluctuations such as sudden changes in solar irradiance or temperature. However, the effectiveness of FLC depends heavily on the quality of rule design and membership function definition, requiring advanced expertise in tuning and calibration to achieve optimal performance[32][34].

Artificial Neural Networks (ANNs) represent another advanced MPPT approach. These networks use deep learning models to process historical and real-time data, allowing them to adapt to dynamically changing environmental conditions. While ANNs demonstrate high efficiency in adapting to variable conditions, their computational demands and requirement for extensive training datasets may limit their applicability in systems with constrained resources, posing challenges in practical implementations[35].

Metaheuristic algorithms such as Particle Swarm Optimisation (PSO) and Grey Wolf Optimisation (GWO) have also been explored for MPPT applications. These algorithms mimic natural behaviours, with PSO modelling bird flocking patterns and GWO emulating the hunting dynamics of grey wolves. These approaches offer advantages such as reduced oscillations and improved system stability. However, their high computational requirements may restrict their application in low-power scenarios[31].

I.5.3 Challenges of Real-Time MPPT Implementation

MPPT techniques face multiple challenges when implemented in real-time PV systems. One of the most significant issues is partial shading, which results in multiple local MPPs. This complicates the tracking process and increases the difficulty of identifying the global MPP, potentially leading to reduced efficiency. If shading occurs on parts of the solar array, conventional algorithms may mistakenly track a local MPP instead of the global MPP, reducing overall power output[35].

Another major challenge is the rapid fluctuation of environmental conditions, such as sudden changes in solar irradiance due to cloud movement or abrupt temperature variations. These fluctuations require immediate and precise algorithmic responses to maintain optimal system performance. However, many conventional algorithms struggle to achieve real-time adaptability, impacting system efficiency under rapidly changing environmental conditions[31].

Additionally, integrating MPPT algorithms with other system components, such as grid-connected inverters and energy storage systems, poses further challenges. MPPT algorithms must ensure seamless coordination with these components while maintaining grid stability and power quality. In scenarios involving sudden environmental changes such as shading or irradiance fluctuations, the system must dynamically adjust the MPP to align with other system components, presenting a challenge in maintaining synchronisation between algorithms and hardware.

I.5.4 Potential Solutions and Future Research Directions

A promising solution to address the challenges of MPPT implementation in real-time photovoltaic systems involves the use of high-performance digital signal processors (DSPs) such as the Texas Instruments F28379D. These processors are well-suited for handling complex computational tasks with high speed and precision, ensuring minimal delays in system response. The F28379D offers significant power efficiency, as it reduces energy consumption during processing, which is crucial for maintaining optimal system performance under fluctuating environmental conditions. Moreover, this DSP can be seamlessly integrated with other system components, such as inverters and energy storage systems, facilitating effective coordination and rapid adaptation to changing conditions in photovoltaic systems [36].

Future research efforts should focus on the integration of Field Programmable Gate Arrays (FPGAs) for MPPT applications. FPGAs provide the advantage of parallel processing, which can significantly enhance the speed and accuracy of tracking the maximum power point. In addition, the incorporation of edge AI techniques could further improve real-time decision-making in MPPT. By leveraging machine learning models tailored for embedded systems, edge AI could enable adaptive and intelligent control of MPPT algorithms. Combining AI-driven methods with conventional techniques could lead to hybrid MPPT approaches, balancing computational efficiency with tracking accuracy, offering improved performance in a variety of operational conditions [37][38].

I.6 Conclusion

This chapter reviewed the historical development of renewable energy, highlighting the role of photovoltaic (PV) solar energy in meeting global and national sustainable energy demands, particularly in Algeria. It presented the classifications and structural configurations of PV systems, along with an analysis of solar energy conversion methods.

International standards for the optimal integration and performance of grid-connected PV systems were also examined, underlining the importance of compliance to ensure system stability and efficiency. Furthermore, various Maximum Power Point Tracking (MPPT) techniques were discussed, comparing traditional and modern approaches while addressing challenges posed by dynamic environmental conditions.

The review concludes that the development of advanced MPPT methods, such as heuristic algorithms (PSO and GWO), combined with high-performance DSP processors, offers promising potential for enhancing the efficiency of grid-connected PV systems.

Chapter II

Modelling and Control of Grid-Connected Photovoltaic Power Plants

II.1 Introduction

Achieving high performance and operational reliability in photovoltaic (PV) power systems hinges on two fundamental pillars: accurate system modelling and the optimisation of control strategies. These components form the technical backbone of this chapter, which is structured in two main parts. The first part develops a complete mathematical model of the grid-connected PV system, starting from the PV cell and progressing through the power conversion chain to the grid interface. The second part presents the control strategies that rely on this model: Maximum Power Point Tracking (MPPT) algorithms, inverter control techniques, and phase synchronisation via Phase-Locked Loops (PLL). This separation provides a clear, sequential foundation for the real-time implementation of high-efficiency, grid-connected PV systems.

II.2 Modelling of the Grid-Connected PV System

The overall system consists of a PV array, a DC-DC converter (optional), a DC-link capacitor, a three-phase inverter, an output filter and the utility grid. In this section we develop the mathematical equations that describe the dynamic behaviour of each component, starting from the PV cell and progressing towards the grid interface. These equations will be used later for control design.

II.2.1 Modelling of the Photovoltaic Generator

II.2.1.1 Simplified Equivalent Electrical Model of a Photovoltaic Cell

Accurate modelling of photovoltaic (PV) cells is essential for the effective design, simulation, and control of solar energy systems. Among the various modelling approaches, the single-diode equivalent circuit remains the most widely adopted, as it captures the fundamental electrical behaviour of PV cells while preserving mathematical simplicity. It serves as the foundation for most analytical and simulation-based studies in photovoltaic engineering [39].

As depicted in Figure II.1, the simplified equivalent circuit consists of four key components. The photocurrent source I_{ph} represents the current generated by incident solar irradiance and is directly proportional to the irradiance level. A diode accounts for the non-linear current–voltage (I-V) behaviour of the p–n junction within the cell. The series resistance R_s models the ohmic losses due to the semiconductor material and electrical contacts, while the shunt resistance R_p represents leakage paths caused by defects and non-idealities in the junction [40].

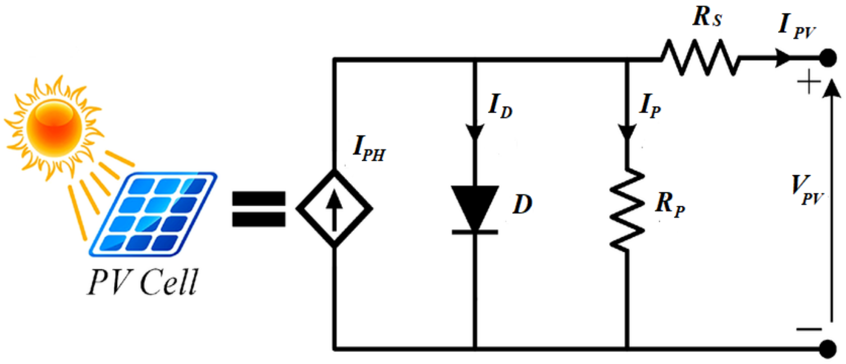

Figure II.1: Simplified equivalent circuit of a photovoltaic cell.

The output current I_{pv} of the PV cell is described by the following non-linear equation:

$$I_{pv} = I_{ph} - I_0 \left(\exp\left(\frac{q(V_{pv} + I_{pv}R_s)}{nkT} \right) - 1 \right) - \frac{V_{pv} + I_{pv}R_s}{R_p} \qquad \text{(II.1)}$$

where:

- I_0 is the diode's reverse saturation current,
- q is the elementary charge (1.602×10^{-19} C),
- k is Boltzmann's constant (1.381×10^{-23} J/K),
- T is the cell temperature in Kelvin,
- n is the diode ideality factor,

Despite its simplifications, this model offers sufficient accuracy for most engineering applications. It reproduces the non-linear characteristics of PV cells and accounts for the influence of environmental conditions, such as irradiance and temperature, on their electrical performance. Consequently, it is commonly employed alongside parameter extraction techniques to model commercial PV modules and assess their behaviour under real-world conditions [41].

II.2.1.2 Effect of Solar Irradiance and Temperature on Photovoltaic Cell Characteristics

Figure II.2 illustrates the current–voltage (I–V) and power–voltage (P–V) characteristics of a photovoltaic (PV) cell under standard test conditions. These curves identify three critical operating points: the *short-circuit current* (I_{sc}), the *open-circuit voltage* (V_{oc}), and the *maximum power point* (MPP), denoted by the coordinates (V_{mpp}, I_{mpp}). The MPP represents the operating condition at which the cell delivers its maximum power and optimal efficiency [42].

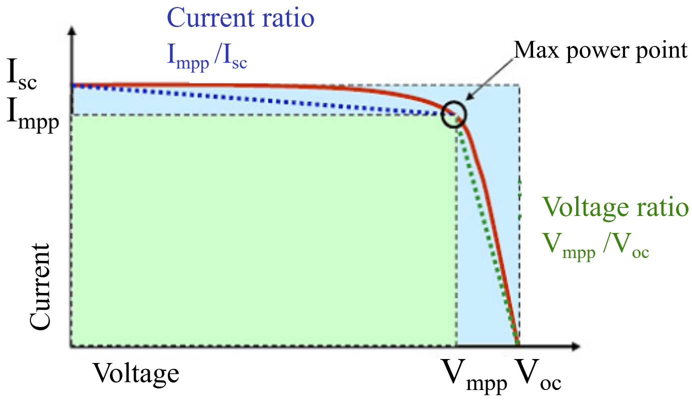

Figure II.2: Characteristics of a PV cell.

The performance of a PV cell is significantly influenced by solar irradiance. As the irradiance level (G) increases, the short-circuit current (I_{sc}) increases almost linearly, whereas the open-circuit voltage (V_{oc}) increases logarithmically and to a lesser extent. This behaviour can be approximated by the relation:

$$I_{\text{sc}} \approx I_{\text{sc,ref}} \cdot \frac{G}{G_{\text{ref}}} \tag{II.2}$$

where $I_{\text{sc,ref}}$ is the short-circuit current at reference irradiance G_{ref}.

This response results from the fact that photocurrent generation is directly proportional to incident irradiance. Consequently, higher irradiance levels lead to increased power output, mainly due to the higher I_{ph}. This trend is illustrated in Figure II.3, which shows how the I–V and P–V characteristics shift with changing irradiance.

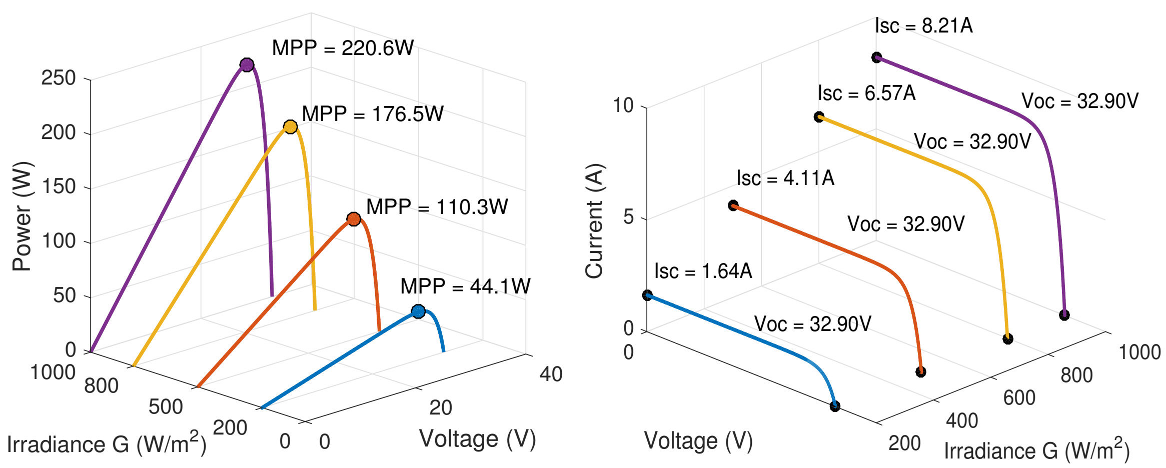

(a) Power–Voltage (P–V) characteristics (b) Current–Voltage (I–V) characteristics

Figure II.3: Influence of irradiance on the electrical characteristics of a PV cell.

In contrast, temperature has a different impact. As temperature increases, the open-circuit voltage (V_{oc}) decreases significantly, while the short-circuit current (I_{sc}) experiences only a slight increase. The temperature dependence of V_{oc} can be approximated by:

$$V_{oc} \approx V_{oc,ref} + \beta \cdot (T - T_{ref}) \tag{II.3}$$

where β is the temperature coefficient (typically negative), T is the actual cell temperature, and T_{ref} is the reference temperature. As power output is the product of voltage and current, the reduction in V_{oc} leads to a net decrease in available power [29, 43].

These environmental effects highlight the importance of integrating *maximum power point tracking* (MPPT) techniques, which dynamically adjust the operating point to ensure optimal energy extraction under varying conditions.

In hot climates such as arid and desert regions, elevated temperatures can severely degrade PV efficiency. These environments combine high irradiance with high ambient temperatures, making it essential to adapt the system design to mitigate temperature-induced losses and maintain reliable performance [33].

II.2.1.3 Effect of Partial Shading on Photovoltaic System Performance

Partial shading is widely recognised as one of the most detrimental factors affecting the efficiency, reliability, and energy yield of photovoltaic (PV) systems. This issue is particularly prominent in urban and semi-urban environments, where transient shading from nearby structures, vegetation, or moving clouds is common. Unlike uniform irradiance reduction, partial shading results in a non-uniform distribution of solar energy across the PV array, causing electrical mismatches between interconnected cells or modules [44].

This mismatch leads to multiple local maxima in the power–voltage (P–V) characteristics of the array, as illustrated in Figure II.4, complicating the identification of the global maximum power point (GMPP). Conventional maximum power point tracking (MPPT) algorithms, which are typically designed for unimodal P–V curves, may become trapped in a local peak. Consequently, the overall harvested energy is reduced, impairing system performance [33]. Moreover, shaded cells may experience reverse bias conditions due to current being forced through them by adjacent unshaded cells. This can result in localised overheating—commonly referred to as “hot spots”—which not only reduce efficiency but may also cause permanent damage to the affected modules if appropriate protection mechanisms are not in place. To mitigate such risks, two primary types of protection diodes are integrated into PV modules: **blocking diodes**, which prevent reverse current flow and safeguard against system-wide failures, and **bypass diodes**, which are connected in parallel with groups of series-connected cells. Bypass diodes allow current to flow around shaded or defective cells, thereby reducing power losses and preventing thermal damage. Typically, a standard PV panel with 36 cells is equipped with three bypass diodes—one for every 12 cells—providing an adequate level of protection [45].

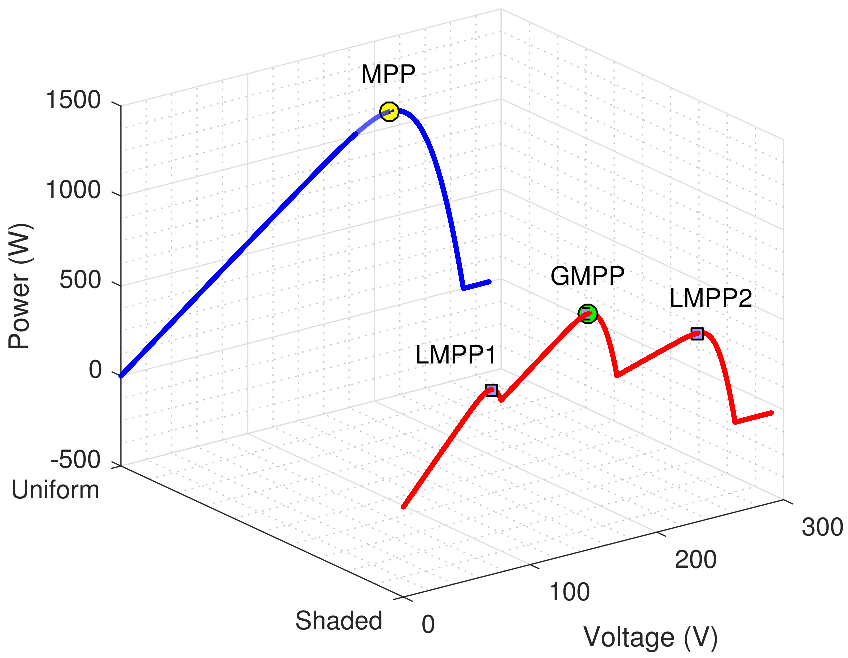

Figure II.4: Effect of partial shading on the P–V characteristics of a PV module.

The challenges posed by partial shading have stimulated extensive research and technological development. Mitigation strategies can be broadly categorised into four main approaches [8]:

1. **Enhanced MPPT Algorithms**: Advanced methods have been proposed to overcome the limitations of conventional MPPT under partial shading. These include techniques such as power curve slope analysis, load-line tracking, segmented search algorithms (e.g., dividing rectangles), incremental conductance, instantaneous power optimisation, Fibonacci search, artificial neural networks (ANNs), and particle swarm optimisation (PSO).

2. **Alternative Array Configurations**: Modifying the electrical connections within the PV array—using layouts such as total cross-tied, bridge-linked, or dynamically reconfigurable topologies—can help distribute mismatch losses more evenly and improve the array's tolerance to shading.

3. **Architectural Innovations in PV Systems**: Decentralised architectures, including micro-inverters or module-integrated power electronics (MIPE), allow for independent power point tracking at the module level. These are particularly effective in conditions of spatially varying irradiance.

4. **Advanced Power Converter Topologies**: Emerging converter designs—such as multilevel inverters, voltage injection units, module-integrated DC–DC converters, and multiple-input converters—offer improved adaptability and energy extraction under shaded conditions.

II.2.2 Modelling of the DC-DC Boost Converter

In grid-connected photovoltaic (PV) systems based on a dual-stage architecture, the DC-DC adaptation stage plays a pivotal role in conditioning the energy flow before injection into the grid [44]. This stage is interposed between the PV array and the inverter, where it serves to elevate and stabilise the inherently variable DC voltage V_{pv}, which is the output of the photovoltaic generator. The aim is to supply a higher and regulated DC voltage V_s to the input of the inverter, appropriate for synchronised grid interaction [46].

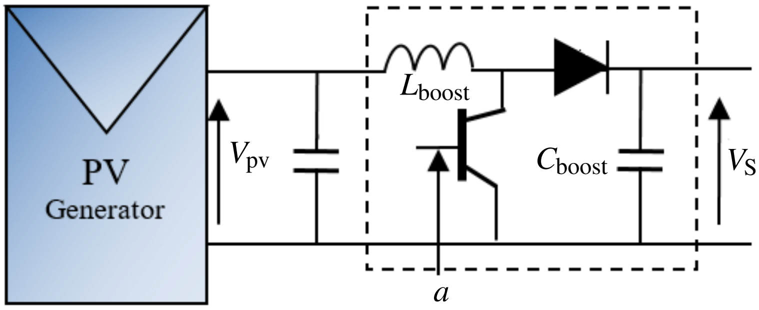

Figure II.5: Equivalent circuit of the boost converter

A boost converter is commonly employed in this stage. It consists of a power inductor, a high-frequency switching device, a freewheeling diode, and one or more output filter capacitors. The converter operates by periodically switching the power transistor at high frequency, thereby increasing the output voltage V_s relative to the PV voltage V_{pv}. Simultaneously, it enables the implementation of a Maximum Power Point Tracking (MPPT) algorithm that dynamically adjusts the duty cycle to maximise energy extraction under changing irradiance and temperature conditions [39].

Correct sizing of the passive components is essential to ensure low ripple and high efficiency. The peak current through the inductor is estimated as:

$$I_{L_{\max}} = 2 \cdot \frac{V_s}{V_{pv}} \cdot I_s \tag{II.4}$$

The inductance required for stable operation is given by [44]:

$$L_{\text{boost}} = a \cdot \frac{V_{pv}}{f_d \cdot \Delta I_L} \tag{II.5}$$

While the output capacitance is calculated as:

$$C_{\text{boost}} = a \cdot \frac{I_s}{\Delta V_s \cdot f_d} \tag{II.6}$$

During each switching cycle, the boost converter operates in two distinct modes [47] [48]:

- **Switch ON:** the inductor stores energy from the PV input:

$$\frac{di_L(t)}{dt} = \frac{V_{pv}}{L} \tag{II.7}$$

- **Switch OFF:** the inductor delivers energy to the load:

$$\frac{di_L(t)}{dt} = \frac{V_{pv} - V_s}{L} \tag{II.8}$$

By applying the state-space averaging method over one switching period, the averaged inductor current equation is obtained as:

$$\frac{di_L}{dt} = a\left(\frac{V_{pv}}{L}\right) + (1-a)\left(\frac{V_{pv} - V_s}{L}\right) \tag{II.9}$$

After simplification:

$$\frac{di_L}{dt} = \frac{V_{pv} - (1-a)V_s}{L} \tag{II.10}$$

Similarly, the averaged capacitor voltage equation is expressed as:

$$\frac{dV_s}{dt} = a\left(-\frac{i_s}{C}\right) + (1-a)\left(\frac{i_L - i_s}{C}\right) \tag{II.11}$$

which yields:

$$\frac{dV_s}{dt} = \frac{(1-a)i_L - i_s}{C} \tag{II.12}$$

This modelling approach relies on several idealised assumptions to simplify the analysis, including the use of lossless components, operation in continuous conduction mode (CCM), and a sufficiently high switching frequency to justify the use of averaged equations. Despite their ideal nature, these assumptions hold reasonably well in high-frequency switching converters with well-designed filter elements, thereby enabling the effective implementation of control algorithms such as MPPT or DC voltage regulation.

Finally, the duty cycle a, which represents the proportion of time the switch remains in the ON state during each switching period, is defined by:

$$a = 1 - \frac{V_{pv}}{V_s} \tag{II.13}$$

This relationship defines the fundamental voltage conversion ratio of the boost topology. It serves as the core control variable used to regulate the output voltage V_s in accordance with the operating point of the photovoltaic generator and the downstream inverter requirements. By continuously adjusting the duty cycle a, the system is capable of maintaining a stable and optimised DC-link voltage, even under fluctuating irradiance and temperature conditions.

II.2.3 Modelling of the DC-Link Capacitor

The DC-link acts as the primary interface between the variable output of the photovoltaic generator (or the DC-DC boost stage) and the inverter input. It is generally modelled as an electrolytic capacitor whose role is to stabilise the intermediate voltage and absorb fluctuations resulting from variations in solar irradiance or dynamic load changes. The voltage dynamics across the capacitor are governed by the first-order differential equation [49][50]:

$$C \cdot \frac{dV_{DC}}{dt} = I_{PVs} - I_{inv} \tag{II.14}$$

Where:

- C is the DC-link capacitance,
- V_{DC} is the intermediate DC voltage,
- I_{PVs} is the current supplied from the PV side (via the DC-DC converter or directly),
- I_{inv} is the current drawn by the inverter.

The inverter current I_{inv} depends on the switching state of each leg, described by logical control signals S_1, S_2, and S_3:

$$I_{inv} = S_1 \cdot I_a + S_2 \cdot I_b + S_3 \cdot I_c \tag{II.15}$$

II.2.4 Modelling of the Three-Phase Inverter

The three-phase inverter is responsible for converting the constant DC-link voltage V_{DC} into three-phase AC voltages synchronised with the grid. It consists of three legs, each composed of two power switches (IGBTs or MOSFETs) operating in complementary mode. The switching logic is defined such that if $S_i = 1$, the upper switch conducts while the lower one is open, and vice versa when $S_i = 0$.

Based on these signals, the line-to-line voltages are:

$$V_{ab} = V_{DC}(S_1 - S_2), \quad V_{bc} = V_{DC}(S_2 - S_3), \quad V_{ca} = V_{DC}(S_3 - S_1) \tag{II.16}$$

From these, and assuming a balanced system ($V_a + V_b + V_c = 0$), the phase voltages are derived as:

$$\begin{cases} V_a = \frac{V_{DC}}{3}(2S_1 - S_2 - S_3) \\ V_b = \frac{V_{DC}}{3}(2S_2 - S_1 - S_3) \\ V_c = \frac{V_{DC}}{3}(2S_3 - S_1 - S_2) \end{cases} \tag{II.17}$$

Or in matrix form:

$$\begin{bmatrix} V_a \\ V_b \\ V_c \end{bmatrix} = \frac{V_{DC}}{3} \cdot \begin{bmatrix} 2 & -1 & -1 \\ -1 & 2 & -1 \\ -1 & -1 & 2 \end{bmatrix} \cdot \begin{bmatrix} S_1 \\ S_2 \\ S_3 \end{bmatrix} \tag{II.18}$$

This matrix formulation is not only central to inverter output modelling but also forms the basis for modern control strategies. It provides a direct mapping between the switching logic and the instantaneous output voltages, thereby enabling the real-time generation of reference signals required for current control or voltage tracking—especially in advanced modulation techniques such as Space Vector PWM (SVPWM) or Direct Torque Control (DTC).

II.2.5 Modelling of the Output Filter and Grid Interface

The inverter is interfaced with the utility grid via three-phase inductive filters (L_r). These filters serve to attenuate high-frequency switching harmonics and ensure that the injected current waveforms are nearly sinusoidal. The dynamics of each phase, according to Kirchhoff's voltage law, are given by [50]:

$$\begin{cases} \frac{dI_a}{dt} = \frac{V_a - R_r I_a - E_a}{L_r} \\ \frac{dI_b}{dt} = \frac{V_b - R_r I_b - E_b}{L_r} \\ \frac{dI_c}{dt} = \frac{V_c - R_r I_c - E_c}{L_r} \end{cases} \tag{II.19}$$

Where:

- I_a, I_b, I_c: currents injected into the grid,
- V_a, V_b, V_c: phase voltages generated by the inverter,
- E_a, E_b, E_c: grid voltages,
- R_r: filter resistance,
- L_r: filter inductance.

II.2.6 Complete State-Space Model of the Power Conversion Chain

The energy conversion chain in a grid-connected photovoltaic (PV) system, as illustrated in Figure II.6, comprises three main interconnected components: the DC-link capacitor, the three-phase inverter, and the grid interface via inductive filters. The sequence of models presented above forms an integrated representation of the dynamic behaviour of a grid-connected PV conversion system. Precise regulation of V_{DC} and control of injection currents is crucial to ensure stable, safe, and standards-compliant operation, including requirements for power factor, harmonic distortion (THD), and voltage–frequency synchronisation.

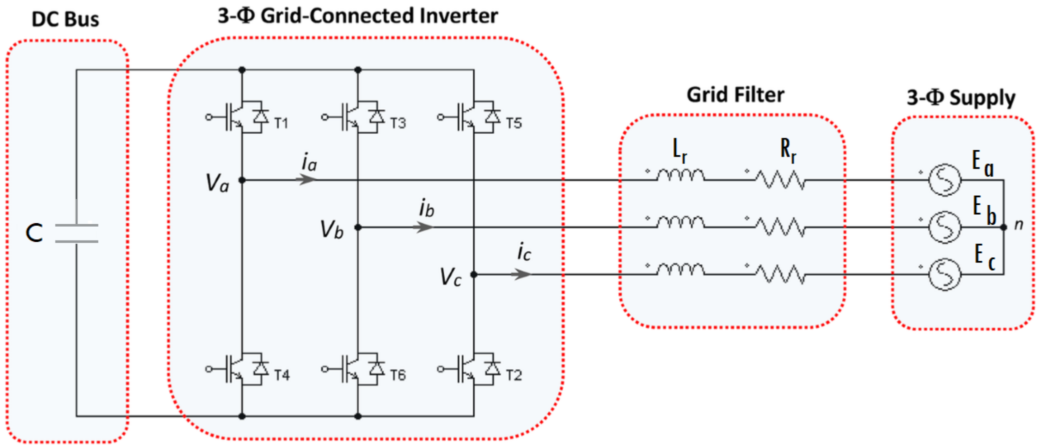

Figure II.6: Schematic diagram of the grid-connected PV energy conversion chain: DC-Link → Inverter → Filter → Grid

II.3 Control Strategies for Grid-Connected PV Systems

The previous section established a complete mathematical model of the grid-connected PV system, including the PV generator, DC-DC converter (optional), DC-link, inverter, filter and grid. Based on this model, we now develop the control strategies that ensure optimal power extraction and grid injection. These controls are divided into three levels: Maximum Power Point Tracking (MPPT) to extract the maximum power from the PV array, inverter control to regulate the injected current/power, and synchronisation control (PLL) to align the inverter output with the grid.

II.3.1 Maximum Power Point Tracking (MPPT) Control

Maximum Power Point Tracking (MPPT) techniques are essential in photovoltaic (PV) energy systems, ensuring that the PV array consistently operates at the point of maximum power output under varying environmental conditions such as solar irradiance and temperature. This optimal operating point is known as the Maximum Power Point (MPP).

The current–voltage (I–V) characteristics of a PV cell are highly sensitive to changes in these environmental parameters, resulting in a shifting MPP on the power–voltage (P–V) curve. Consequently, a fixed operating point is insufficient, and real-time tracking algorithms are necessary to dynamically adjust the system's operating point to match the MPP [51].

MPPT techniques typically regulate the duty cycle of a DC–DC converter or adjust the PV reference voltage $V_{\text{pv-ref}}$, depending on the system configuration. In single-stage systems, the MPPT controller directly modifies the converter's operation to extract maximum power.

Over the years, various MPPT strategies have been proposed, generally classified into two main categories: conventional and intelligent algorithms[39].

II.3.1.1 Indirect MPPT Algorithms Based on Linear Relations

A simpler category of conventional MPPT methods, known as indirect algorithms, relies on pre-established proportional relationships between the optimal parameters (optimal voltage V_{OP} and optimal current I_{OP}) and the characteristic parameters of the PV module (open-circuit voltage V_{OC} and short-circuit current I_{CC}). Depending on the controlled variable, these methods are classified as voltage regulation or current regulation.

II.3.1.1.1 Fraction of V_{OC} Method This method compares the PV generator voltage V_{PV} with a reference voltage that corresponds to the estimated optimal voltage V_{OP}. The voltage error is then used to adjust the duty cycle of the DC–DC converter so that V_{PV} follows V_{OP}. The reference voltage is obtained from the linear relation:

$$V_{OP} = k_V \cdot V_{OC} \tag{II.20}$$

where k_V is a voltage factor that depends on the specific PV generator and the operating temperature (typically between 0.70 and 0.80). This method is easy to implement but suffers from low accuracy under temperature variations and cannot adapt to partial shading conditions.

II.3.1.1.2 Fraction of I_{CC} Method This method is based on the first-order linear relation between the optimal current I_{OP} and the short-circuit current I_{CC}:

$$I_{OP} = k_I \cdot I_{CC} \tag{II.21}$$

The factor k_I typically ranges from 0.78 to 0.92, depending on the PV module and temperature. The maximum power point is reached by forcing the converter's current to follow a reference equal to I_{OP}. Like the previous method, it requires only one sensor (either voltage or current) but exhibits poor performance under changing irradiance, temperature, and especially partial shading.

II.3.1.2 Conventional MPPT Algorithms

Among conventional approaches, the Perturb and Observe (P&O) and Incremental Conductance (INC) algorithms are widely implemented due to their simplicity and reasonable performance [52].

The P&O algorithm operates by periodically perturbing the system—by adjusting either the converter's duty cycle or V_{ref}—and observing the resulting change in output power. If the power increases (i.e., $\Delta P > 0$), the perturbation continues in the same direction; otherwise, it reverses. As illustrated in Algorithm 1, this approach is easy to implement but often induces steady-state oscillations around the MPP and may misinterpret irradiance changes as MPP shifts [53].

Algorithm 1 Pseudo-code of Perturb and Observe (P&O) Algorithm

Initialize V_{ref}, P_{prev}
while true **do**
  Measure current voltage V and current I
  Compute power $P = V \cdot I$
  if $P > P_{\text{prev}}$ **then**
    Continue perturbation in the same direction
  else
    Reverse the direction of perturbation
  end if
  Update V_{ref}
  Set $P_{\text{prev}} \leftarrow P$
end while

Alternatively, the Incremental Conductance (INC) algorithm relies on the fact that the derivative of power with respect to voltage equals zero at the MPP [54]:

$$\frac{dP}{dV} = \frac{d(IV)}{dV} = I + V\frac{dI}{dV} = 0, \tag{II.22}$$

which leads to the decision criterion:

$$\frac{dI}{dV} = -\frac{I}{V}. \tag{II.23}$$

By comparing $\Delta I/\Delta V$ to $-I/V$, the algorithm determines the direction in which to adjust the operating point. As illustrated in Algorithm 2, the INC algorithm evaluates the instantaneous conductance and its variation to track the MPP with improved accuracy under varying irradiance conditions [55]:

$$
\begin{cases}
\frac{\Delta I}{\Delta V} > -\frac{I}{V} & \Rightarrow \text{Decrease } V_{\text{ref}}, \\
\frac{\Delta I}{\Delta V} < -\frac{I}{V} & \Rightarrow \text{Increase } V_{\text{ref}}, \\
\frac{\Delta I}{\Delta V} = -\frac{I}{V} & \Rightarrow \text{At MPP.}
\end{cases}
$$

Algorithm 2 Pseudo-code of Incremental Conductance (INC) Algorithm

Initialize V_{ref}
while true **do**
Measure current V and I
Compute $\Delta V = V - V_{\text{prev}}$
Compute $\Delta I = I - I_{\text{prev}}$
if $\Delta V \neq 0$ **then**
if $\frac{\Delta I}{\Delta V} = -\frac{I}{V}$ **then**
Keep V_{ref}
else if $\frac{\Delta I}{\Delta V} > -\frac{I}{V}$ **then**
Decrease V_{ref}
else
Increase V_{ref}
end if
end if
Update $V_{\text{prev}} \leftarrow V$, $I_{\text{prev}} \leftarrow I$
end while

In summary, both P&O and INC algorithms are effective in tracking the MPP, yet each presents limitations. The P&O method is computationally light and easy to implement, but it suffers from oscillations and ambiguity under rapidly changing conditions. On the other hand, the INC algorithm improves tracking accuracy and response to irradiance fluctuations, albeit at the cost of higher complexity.

II.3.1.3 Optimisation Problem Formulation for MPPT

The Maximum Power Point Tracking (MPPT) task can be formulated as a constrained optimisation problem, where the objective is to determine the optimal PV operating voltage that maximises the extracted power from the photovoltaic generator.

Let $V_{\text{pv-ref}}$ denote the control variable corresponding to the PV reference voltage. The objective function is defined by the generated PV power:

$$P_{\text{pv}}(V_{\text{pv-ref}}) = V_{\text{pv-ref}} \times I_{\text{pv}}(V_{\text{pv-ref}}) \tag{II.24}$$

The optimisation objective is therefore to maximise the PV output power while satisfying the operating constraints imposed by the PV array and the grid-connected inverter.

The lower voltage bound is determined according to the minimum DC-link voltage required to guarantee proper operation and synchronisation of the three-phase grid-connected inverter, and can be approximated as:

$$V_{\text{pv,min}} = \sqrt{3}\, U_{\text{grid}} \tag{II.25}$$

where U_{grid} is the RMS line voltage of the utility grid. The upper bound corresponds to the open-circuit voltage of the PV array V_{OC}. Therefore, the admissible operating range is given by:

$$\sqrt{3}\, U_{\text{grid}} \leq V_{\text{pv-ref}} \leq V_{\text{OC}} \tag{II.26}$$

Consequently, the MPPT optimisation problem can be expressed as:

$$\begin{aligned} \underset{V_{\text{pv-ref}}}{\text{maximise}} \quad & P_{\text{pv}}(V_{\text{pv-ref}}) \\ \text{subject to} \quad & \sqrt{3}\, U_{\text{grid}} \leq V_{\text{pv-ref}} \leq V_{\text{OC}} \end{aligned} \tag{II.27}$$

Under partial shading conditions, the resulting power-voltage characteristic becomes multimodal with several local maxima, making conventional MPPT techniques less effective and motivating the use of metaheuristic optimisation algorithms for accurate global maximum power point tracking.

II.3.1.4 Advanced Metaheuristic MPPT Algorithms

While conventional MPPT algorithms like Perturb and Observe (P&O) and Incremental Conductance (INC) offer simple implementation and acceptable performance, they often suffer from limitations such as steady-state oscillations, slow convergence under rapidly changing irradiance, and inability to escape from local maxima in partial shading conditions.

To overcome these drawbacks, researchers have turned to intelligent and nature-inspired metaheuristic optimisation techniques. These methods, including Particle Swarm Optimisation (PSO), Grey Wolf Optimisation (GWO), Cuckoo Search (CS), and Whale Optimisation Algorithm (WOA), offer adaptive, robust, and high-precision tracking of the Global Maximum Power Point (GMPP) in dynamic and complex environments.

This subsection presents the operational principles and mathematical formulations of the most prominent intelligent MPPT algorithms used in PV applications.

II.3.1.4.1 Particle Swarm Optimisation (PSO) for MPPT Particle Swarm Optimisation (PSO) is a population-based metaheuristic algorithm inspired by the collective behaviour of swarms, such as birds flocking or fish schooling. This social behaviour, referred to as swarm intelligence, allows particles to explore a solution space cooperatively to find the optimal result [56]. In photovoltaic (PV) systems, PSO is widely used for Maximum Power Point Tracking (MPPT), especially under complex irradiance conditions that may cause multiple local maxima on the power–voltage (P–V) curve [57][58].

Each individual in the swarm, called a particle, represents a candidate reference voltage $V_{\text{pv-ref}}$ applied to the PV converter. Initially, these particles are randomly distributed over the search space. During each iteration, each particle evaluates the output power at its current voltage and updates its velocity and position based on its best previous voltage P_{best} and the best global voltage found by the entire swarm G_{best} [59].

The velocity update equation is given by:

$$V_i^{(k+1)} = w \cdot V_i^{(k)} + c_1 \cdot r_1 \cdot \left(P_{\text{best}_i} - V_{\text{pv-ref}_i}^{(k)}\right) + c_2 \cdot r_2 \cdot \left(G_{\text{best}} - V_{\text{pv-ref}_i}^{(k)}\right) \tag{II.28}$$

The position update, which corresponds to the updated reference voltage, is expressed as:

$$V_{\text{pv-ref}_i}^{(k+1)} = V_{\text{pv-ref}_i}^{(k)} + V_i^{(k+1)} \tag{II.29}$$

Where:

- $V_i^{(k)}$: velocity of particle i at iteration k,
- w: inertia weight controlling the trade-off between exploration and exploitation,
- c_1, c_2: acceleration coefficients for cognitive and social components,
- r_1, r_2: random values uniformly distributed in the interval [0, 1],
- P_{best_i}: best personal voltage position of particle i,
- G_{best}: best voltage position found by the entire swarm.

The fitness function is the output power of the PV system. After each update, the new position is retained if the corresponding power improves:

$$P\left(V_{\text{pv-ref}_i}^{(k+1)}\right) > P\left(V_{\text{pv-ref}_i}^{(k)}\right) \tag{II.30}$$

The PSO-based MPPT procedure involves the following steps:

1. Initialise the swarm: number of particles, inertia weight w, acceleration coefficients c_1 and c_2, and random initial velocities and positions.
2. For each particle, measure the PV voltage and current to calculate the output power.
3. Update each particle's velocity and reference voltage using the governing equations.

4. Update the personal best and global best positions based on the evaluated power.

5. Repeat the process until a maximum number of iterations is reached or the improvement becomes negligible.

This method enables efficient convergence to the Global Maximum Power Point (GMPP) while maintaining low computational complexity and high adaptability. Figure II.7 illustrates the general flowchart of the PSO-based MPPT approach [33][60].

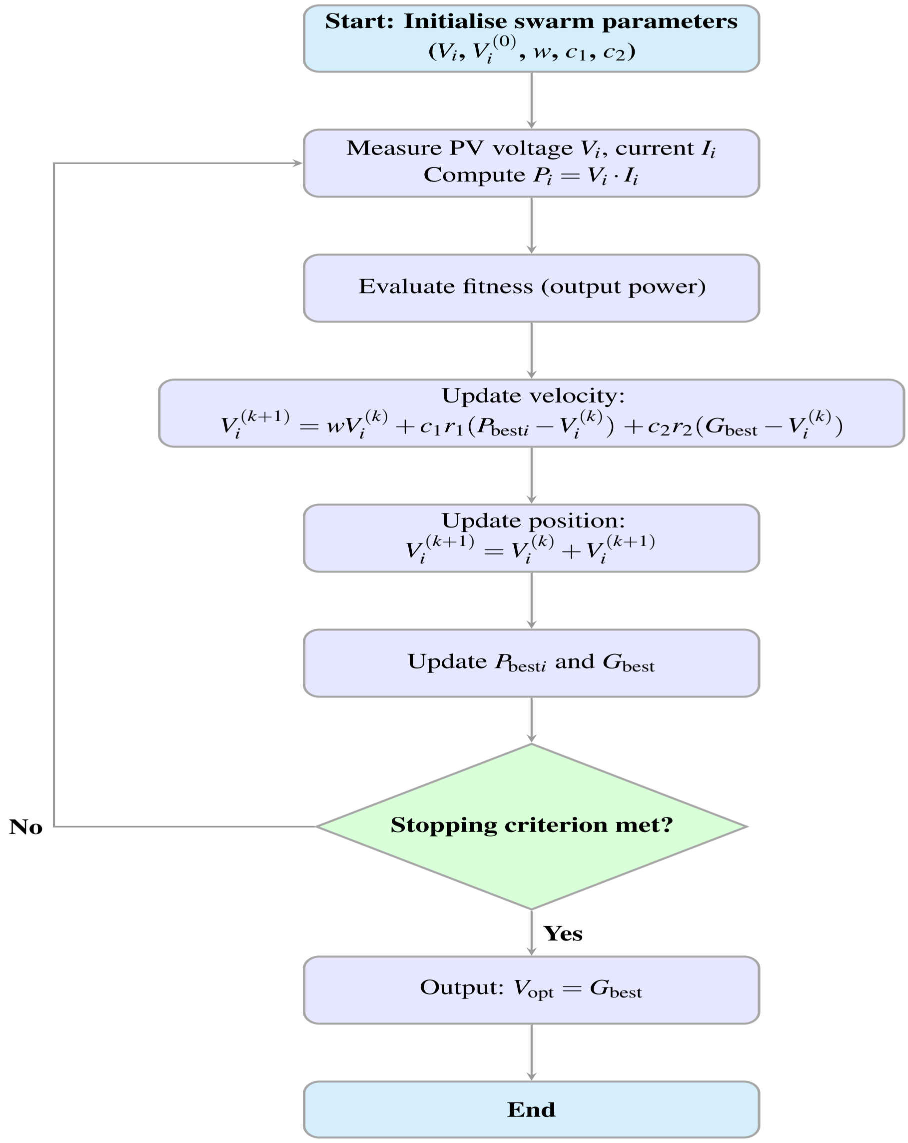

Figure II.7: Flowchart of the Particle Swarm Optimisation (PSO) algorithm for MPPT

II.3.1.4.2 Grey Wolf Optimisation (GWO) for MPPT The Grey Wolf Optimisation (GWO) algorithm is a nature-inspired metaheuristic designed to mimic the social hierarchy and hunting behaviour of grey wolves. It has demonstrated excellent performance in solving non-linear optimisation problems and has been successfully applied to Maximum Power Point Tracking (MPPT) in photovoltaic (PV) systems [35].

In nature, grey wolves live in structured social groups, where the leadership hierarchy is divided into four categories:

- **Alpha** (α): the leader of the pack, representing the best solution.
- **Beta** (β): the second-best solution, assisting the alpha.
- **Delta** (δ): the third-best solution, supporting both alpha and beta.
- **Omega** (ω): the rest of the pack, following the leadership hierarchy.

The hunting mechanism of grey wolves typically involves three phases: *pursuing the prey*, *encircling it*, and *launching the final attack*. This coordinated behaviour is mathematically formulated to guide the optimisation process [61][62].

In the MPPT context, each grey wolf represents a candidate reference voltage $V_{\text{pv-ref}}$ applied to the PV system. Initially, a population of wolves is randomly distributed across the search space. The fitness of each wolf is evaluated based on the output power at its corresponding voltage. The top three wolves (α, β, and δ) are used to guide the movement of the remaining wolves.

The position update of a wolf is calculated with respect to each of the top three leaders using the following equations:

$$\vec{D}_\alpha = \left|\vec{C}_1 \cdot \vec{X}_\alpha - \vec{X}\right|, \quad \vec{X}_1 = \vec{X}_\alpha - \vec{A}_1 \cdot \vec{D}_\alpha \tag{II.31}$$

$$\vec{D}_\beta = \left|\vec{C}_2 \cdot \vec{X}_\beta - \vec{X}\right|, \quad \vec{X}_2 = \vec{X}_\beta - \vec{A}_2 \cdot \vec{D}_\beta \tag{II.32}$$

$$\vec{D}_\delta = \left|\vec{C}_3 \cdot \vec{X}_\delta - \vec{X}\right|, \quad \vec{X}_3 = \vec{X}_\delta - \vec{A}_3 \cdot \vec{D}_\delta \tag{II.33}$$

The updated position of the current wolf is then computed as the average of the three guided positions:

$$\vec{X}(k+1) = \frac{1}{3}\left(\vec{X}_1 + \vec{X}_2 + \vec{X}_3\right) \tag{II.34}$$

Where $\vec{X}$ corresponds to $V_{\text{pv-ref}}$ in this context. The coefficient vectors $\vec{A}_i$ and $\vec{C}_i$ are defined as:

$$\vec{A}_i = 2a \cdot \vec{r}_{1i} - a, \quad \vec{C}_i = 2 \cdot \vec{r}_{2i}, \quad \text{for } i = 1,2,3 \tag{II.35}$$

Here, a is a linearly decreasing control parameter from 2 to 0 over the course of iterations, and $\vec{r}_{1i}$, $\vec{r}_{2i}$ are random vectors with values in [0,1].

After the new reference voltage $V_{\text{pv-ref}}^{(k+1)}$ is calculated, it is applied to the PV system. The power output is then measured and compared to the previous value:

$$P\left(V_{\text{pv-ref}}^{(k+1)}\right) > P\left(V_{\text{pv-ref}}^{(k)}\right) \Rightarrow \text{Accept the new position} \tag{II.36}$$

The iterative process continues until a stopping criterion is met, either a maximum number of iterations or a sufficiently small improvement in power. The GWO algorithm is summarised by the following steps [63]:

1. Initialise the population of candidate $V_{\text{pv-ref}}$ values.
2. Evaluate the power output for each position and assign rankings to determine α, β, and δ.
3. Update all positions using the three leaders and the encircling equations.
4. Map new positions to reference voltages and measure the power output.
5. Accept new positions if they yield higher power, and repeat until convergence.

Figure II.8 illustrates how the positions of the wolves evolve and converge during the optimisation process. The complete procedural logic is also depicted in the flowchart of Figure II.9.

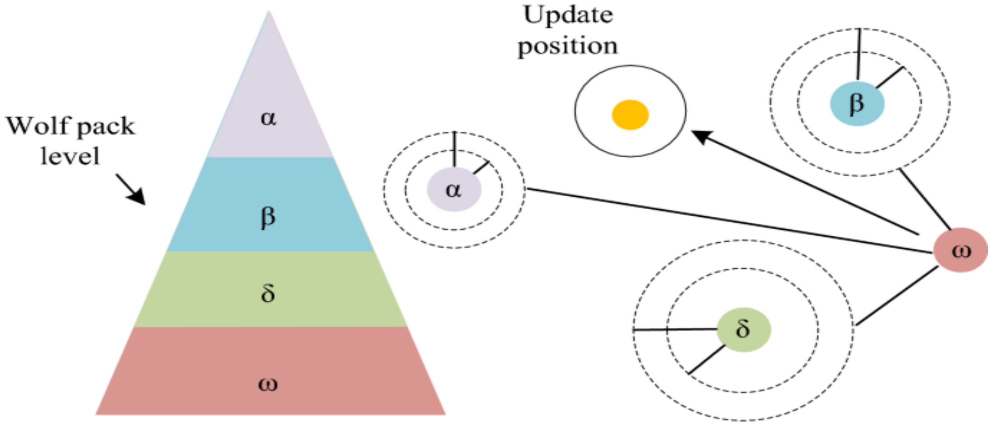

Figure II.8: Illustration of grey wolf position updates in the search space.

The GWO algorithm provides an efficient and flexible approach for real-time MPPT in PV systems. It combines simplicity, minimal parameter tuning, and fast convergence, making it suitable for implementation in embedded controllers of modern solar inverters.

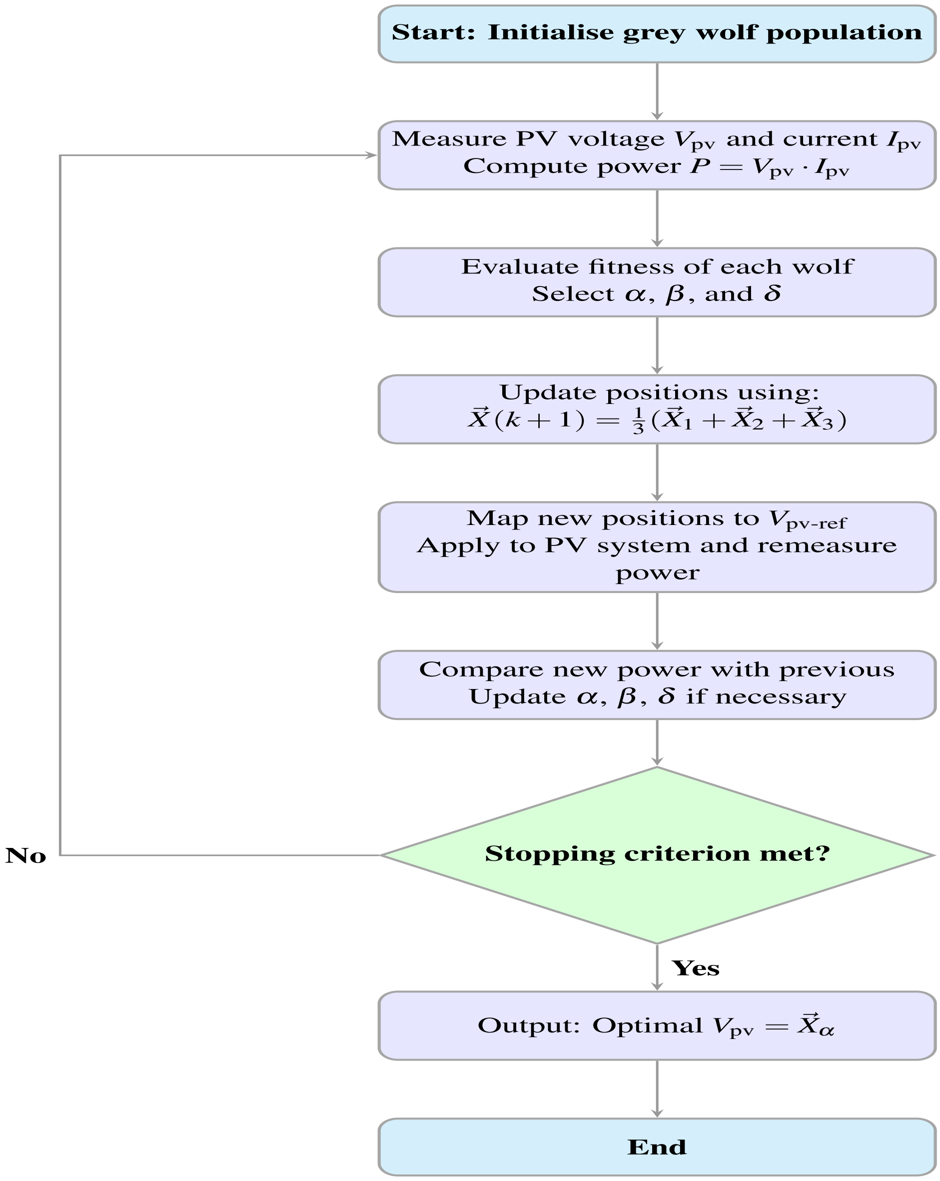

Figure II.9: Flowchart of the Grey Wolf Optimisation (GWO) algorithm for MPPT

II.3.1.4.3 Cuckoo Search (CS) for MPPT The **Cuckoo Search (CS)** algorithm is a nature-inspired metaheuristic based on the obligate brood parasitism of some cuckoo species, which lay their eggs in the nests of other host birds. This strategy, along with a powerful random walk technique known as Lévy flight, forms the foundation of the CS optimisation method. Its simplicity and strong global search ability make it particularly suitable for complex optimisation problems such as Maximum Power Point Tracking (MPPT) in photovoltaic (PV) systems [64].

In nature, certain cuckoos—such as *Tapera*—imitate the appearance and egg colouration of host birds to increase the chances of egg survival. If a host bird identifies a foreign egg, it may discard it or abandon the nest entirely. These behaviours are mimicked in CS through discovery and replacement mechanisms, which enhance the diversity of the solution population.

In the context of MPPT, each cuckoo represents a candidate reference voltage $V_{\text{pv-ref}}$. The objective is to dynamically adjust this voltage to ensure that the PV system operates at its Global Maximum Power Point (GMPP), even under rapidly changing environmental conditions.

The CS algorithm is governed by three idealised rules:

1. Each cuckoo lays one egg at a time and places it in a randomly selected nest.
2. The best nests with the highest-quality eggs (i.e., those yielding the highest power output) are carried over to the next generation.
3. The number of available nests is fixed, and a host bird may discover a foreign egg with a probability $P_a \in [0,1]$. If discovered, the host abandons the nest or replaces it with a new one.

To generate new solutions, the algorithm employs **Lévy flights**, a form of random walk with steps drawn from a heavy-tailed probability distribution. This feature enables long-range exploration of the search space, preventing premature convergence to local optima [65].

The update rule for generating a new solution $X_i^{(k+1)}$ for a given cuckoo is:

$$X_i^{(k+1)} = X_i^{(k)} + \alpha \cdot \text{Lévy}(\lambda) \tag{II.37}$$

Where:

- $X_i^{(k)}$: current solution (reference voltage),
- α: step size scaling factor (commonly set to 1),
- Lévy(λ): random step drawn from a Lévy distribution with exponent $1 < \lambda \leq 3$.

The **fitness function** is the output power of the PV system $P(V_{\text{pv-ref}})$. A new solution is accepted if it results in improved power output:

$$P\left(V_{\text{pv-ref}}^{(k+1)}\right) > P\left(V_{\text{pv-ref}}^{(k)}\right) \tag{II.38}$$

The CS algorithm proceeds as follows [66] [67]:

1. **Initialisation:** Generate an initial population of nests (candidate voltages).
2. **Solution Generation:** Use Lévy flights to generate new solutions (cuckoo eggs).
3. **Comparison and Replacement:** Evaluate each new solution and replace inferior ones in the population.

4. **Discovery and Abandonment:** A fraction P_a of the worst nests is replaced with new random solutions.

5. **Convergence Check:** Repeat until the maximum number of iterations is reached or convergence is achieved.

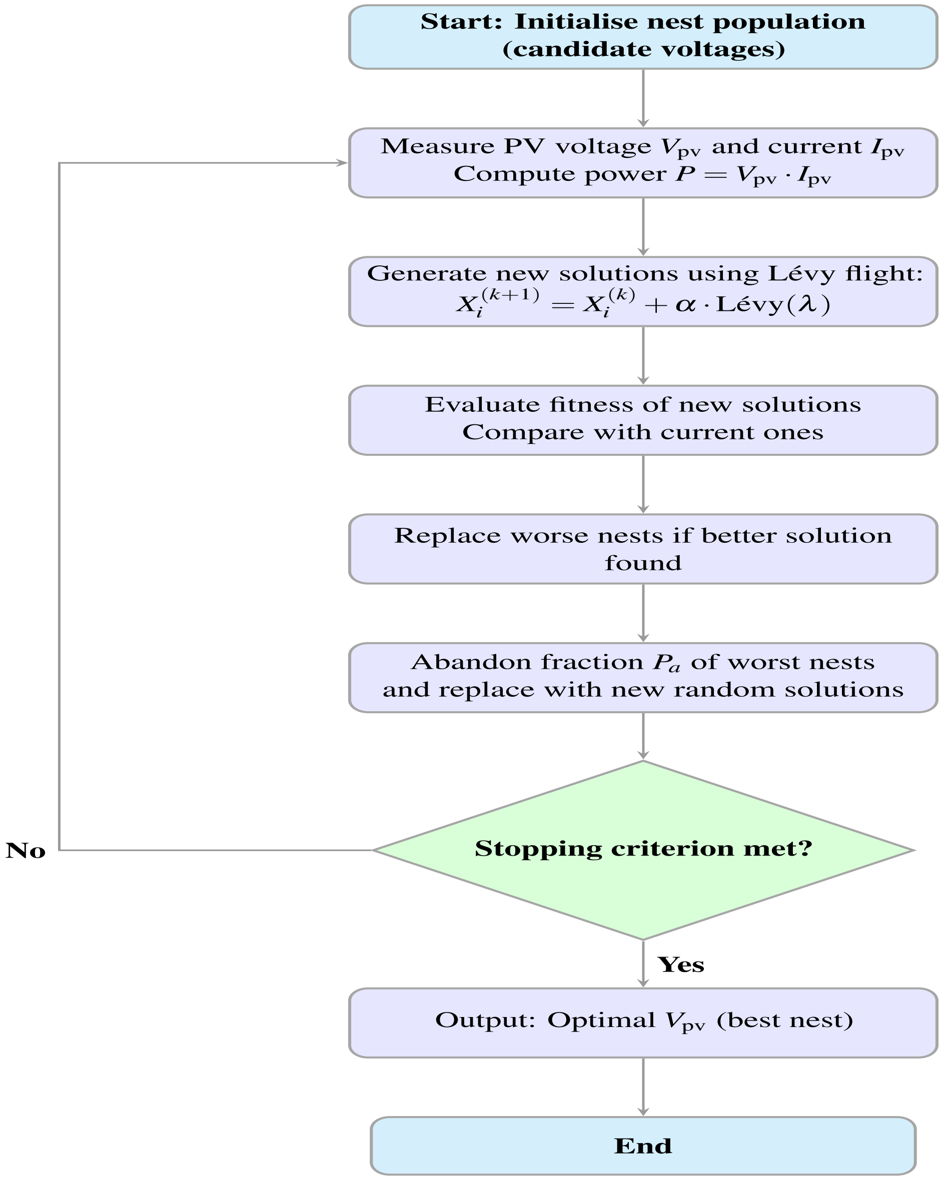

Figure II.10: Flowchart of the Cuckoo Search (CS) algorithm for MPPT

The CS method offers several advantages in MPPT applications, including robust global search capability, efficient handling of non-linearities, and minimal tuning requirements. Its stochastic nature and reliance on Lévy flights make it particularly effective under partial shading and fast-changing irradiance scenarios, positioning it as a strong candidate for real-time implementation in PV control systems.

These intelligent MPPT methods offer high tracking accuracy under dynamic and complex conditions. The choice between PSO, GWO, CS, or WOA depends on the specific application requirements, such as convergence speed, response stability, and computational constraints.

II.3.1.4.4 Whale Optimization Algorithm (WOA) for MPPT The Whale Optimization Algorithm (WOA) is a recent metaheuristic optimisation technique inspired by the bubble-net hunting strategy of humpback whales. In nature, humpback whales generate spiral-shaped bubbles to encircle and trap prey, a behaviour that has been mathematically modelled to guide the optimisation process in various engineering problems, including Maximum Power Point Tracking (MPPT) in photovoltaic (PV) systems [44].

In this context, each search agent (whale) represents a candidate solution, typically corresponding to a reference voltage or duty cycle of the PV system. The aim of WOA is to dynamically adjust this parameter to extract the maximum possible power under varying environmental conditions, including partial shading scenarios [68][69].

The WOA consists of three main strategies:

- **Encircling the Prey:** Whales estimate the current best solution and update their positions relative to this best agent.
- **Bubble-Net Attacking Method:** This strategy combines spiral-shaped position updates and shrinking encircling mechanisms to refine the search.
- **Exploration Phase:** Whales search globally by moving towards randomly selected search agents, encouraging diversity and avoiding local optima.

The position of each whale is updated based on the following model:

$$X^{(k+1)} = \begin{cases} X^*(k) - A \cdot D, & \text{if } p < 0.5 \\ D' \cdot e^{b \cdot l} \cdot \cos(2\pi l) + X^*(k), & \text{if } p \geq 0.5 \end{cases} \quad \text{(II.39)}$$

where:

$$D = |C \cdot X^*(k) - X(k)| \quad \text{(II.40)}$$

$$A = 2a \cdot r_1 - a \quad \text{(II.41)}$$

$$C = 2 \cdot r_2 \quad \text{(II.42)}$$

$$a = 2 - \frac{2k}{\text{MaxIteration}} \quad \text{(II.43)}$$

$$l = (a-1) \cdot r_3 + 1 \quad \text{(II.44)}$$

$$p = r_4 \quad \text{(II.45)}$$

Here:

- $X(k)$: Current position of the whale (e.g., reference voltage $V_{\text{pv-ref}}$),
- $X^*(k)$: Best solution found so far,
- D: Distance between the whale and the best solution,
- A, C: Coefficients controlling convergence behaviour,
- r_1, r_2, r_3, r_4: Random numbers in $[0,1]$,
- a: Decreasing control parameter to balance exploration and exploitation.

The algorithm proceeds as follows:

1. **Initialisation:** Randomly initialise the whale population across the search space.
2. **Fitness Evaluation:** Calculate the output power $P(V_{\text{pv-ref}})$ for each whale.
3. **Leader Update:** Identify the whale with the highest power output as X^*.
4. **Position Update:** Update each whale's position using the encircling or spiral strategy based on probability p.
5. **Termination:** Repeat until convergence or a maximum number of iterations is reached.

The updated reference voltage $V_{\text{pv-ref}}^{(k+1)}$ is used to control the DC–DC converter and maximise power output. The selection criterion for improvement is defined by:

$$P\left(V_{\text{pv-ref}}^{(k+1)}\right) > P\left(V_{\text{pv-ref}}^{(k)}\right) \tag{II.46}$$

Algorithm 3 presents the Whale Optimization Algorithm (WOA) applied to MPPT. This algorithm outlines how whale agents explore and exploit the search space to locate the Global Maximum Power Point (GMPP).

WOA offers several advantages for MPPT applications, including high global search efficiency, minimal parameter requirements, and robust performance under non-uniform irradiance conditions. Its bio-inspired structure enables adaptive tuning of control variables to optimise PV system output dynamically and reliably.

Algorithm 3 Whale Optimization Algorithm (WOA) applied to MPPT

Initialisation: Randomly initialise whale population $X_i(0)$ within the search space.
for $k = 1$ to MaxIteration **do**
  for each whale $X_i(k)$ **do**
    Measure V_{pv} and I_{pv}
    Compute power: $P_i = V_{\text{pv}} \cdot I_{\text{pv}}$
    Evaluate fitness
  end for
  Identify best whale $X^*(k)$ with highest P
  for each whale $X_i(k)$ **do**
    Generate random numbers r_1, r_2, r_3, $r_4 \in [0,1]$
    Compute coefficients:

$$\begin{aligned} a &= 2 - \frac{2k}{\text{MaxIteration}} \\ A &= 2a \cdot r_1 - a \\ C &= 2 \cdot r_2 \\ l &= (a-1) \cdot r_3 + 1 \\ p &= r_4 \end{aligned}$$

    Compute distance: $D = |C \cdot X^*(k) - X_i(k)|$
    if $p < 0.5$ **then**
      $X_i(k+1) = X^*(k) - A \cdot D$ ▷ Encircling the prey
    else
      $X_i(k+1) = D \cdot e^{b \cdot l} \cdot \cos(2\pi l) + X^*(k)$ ▷ Spiral bubble-net
    end if
  end for
  Apply $V_{\text{pv-ref}} = X_i(k+1)$ to the PV system
  Measure new power $P_i^{(k+1)}$
  if $P_i^{(k+1)} > P_i^{(k)}$ **then**
    Update best solution $X^*(k+1)$
  end if
end for
Output: Optimal reference voltage $V_{\text{pv}} = X^*$

II.3.2 Inverter Control Strategies

The inverter constitutes a fundamental element in grid-connected photovoltaic (PV) systems, performing the crucial function of converting direct current (DC) generated by solar modules into alternating current (AC) that is synchronised with the utility grid in terms of voltage, frequency, and phase angle. The effectiveness and reliability of this conversion process are inherently dependent on the control strategy adopted. Modern control strategies are designed to achieve multiple objectives, including optimal energy conversion, dynamic voltage and current regulation, enhanced power quality, and strict adherence to international grid codes and standards.

A high-level control architecture typically involves the continuous measurement of system variables—such as grid voltage, grid current, and inverter output signals—followed by real-time signal processing within a dedicated monitoring and control unit. This unit generates the appropriate gating or modulation signals to ensure that the inverter operates in a manner consistent with the grid's dynamic requirements [23]. The conceptual framework of this control loop is depicted in Figure II.11, which outlines the primary functional blocks involved in the real-time control of a grid-connected inverter.

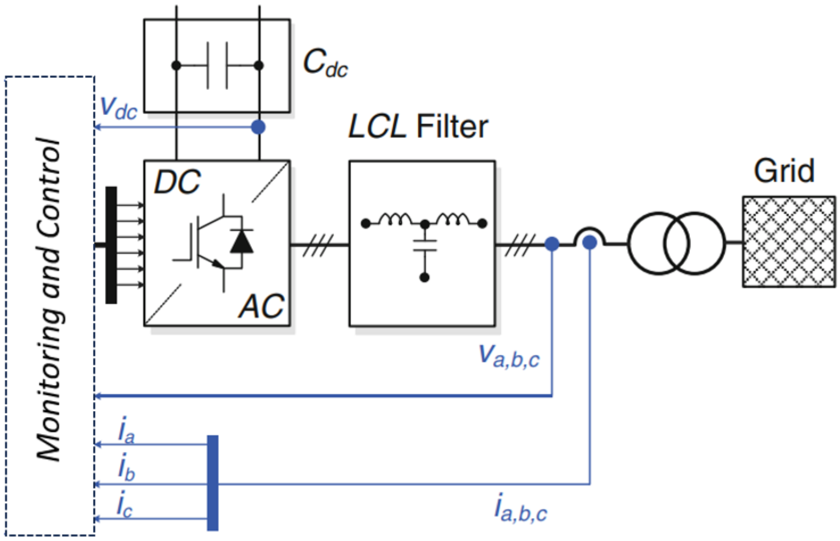

Figure II.11: General control structure for grid-connected PV inverters

Several control techniques have been extensively investigated and deployed, varying in terms of control objectives, algorithmic complexity, transient response, and implementation feasibility. Among the most established are Synchronous Reference Frame Control (SRF), Direct Current Control (DCC), Indirect Current Control (ICC), and Direct Power Control (DPC). The subsequent subsections provide a comprehensive analysis of these methodologies.

II.3.2.1 Synchronous Reference Frame Control (SRF)

The synchronous reference frame (SRF) control strategy, commonly referred to as the *dq* method, is extensively adopted in grid-connected PV systems due to its ability to decouple active and reactive power components. By transforming three-phase alternating quantities into a rotating coordinate system aligned with the grid voltage vector, the control simplifies regulation tasks into DC quantities, thereby facilitating precise control and dynamic performance [39].

As depicted in the general control framework (see Figure II.12), the control structure consists of an outer voltage regulation loop and an inner current control loop. The outer loop regulates the DC-link voltage by comparing it to a reference value $V_{dc,ref}$, typically provided by a Maximum Power Point Tracking (MPPT) algorithm to ensure optimal extraction of power from the PV generator. The error between the measured and reference DC voltages is processed by a proportional–integral (PI) controller, which generates the direct-axis current reference $i_d^*(t)$. To ensure unity power factor operation, the quadrature-axis current reference $i_q^*(t)$ is typically set to zero [70].

The current control loop operates in the rotating dq frame, where the three-phase inverter output currents are transformed using the Park transformation. The instantaneous phase angle $\theta(t)$ of the grid voltage is extracted using a Phase-Locked Loop (PLL) and used in the transformation process:

$$\begin{bmatrix} x_d \\ x_q \end{bmatrix} = \frac{2}{3} \begin{bmatrix} \cos(\theta) & \cos(\theta - 120^\circ) & \cos(\theta + 120^\circ) \\ -\sin(\theta) & -\sin(\theta - 120^\circ) & -\sin(\theta + 120^\circ) \end{bmatrix} \begin{bmatrix} x_a \\ x_b \\ x_c \end{bmatrix} \tag{II.47}$$

The measured $i_d(t)$ and $i_q(t)$ are compared to their references $i_d^*(t)$ and $i_q^*(t)$, and the resulting errors are processed by two independent PI controllers. To improve dynamic performance and decouple the control axes, cross-coupling terms involving the grid frequency ω and filter inductance L are added. For example, the direct-axis voltage reference is given by:

$$v_d^*(t) = K_{p,i}(i_d^*(t) - i_d(t)) + K_{i,i}\int (i_d^*(t) - i_d(t))dt + \omega L i_q(t) \tag{II.48}$$

The final voltage references $v_d^*(t)$ and $v_q^*(t)$ are inverse-transformed back to the three-phase frame using the inverse Park transformation and used to generate the switching signals through Pulse Width Modulation (PWM). This method ensures accurate current tracking, effective power injection, and robust operation under various grid conditions [71].

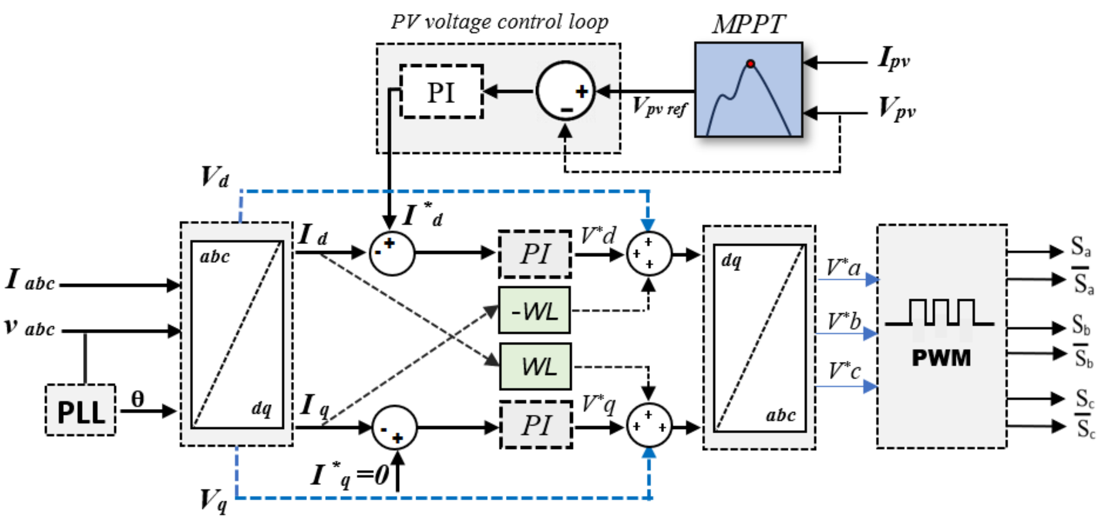

Figure II.12: Control diagram of the Synchronous Reference Frame (SRF) method.

II.3.2.2 Direct and Indirect Current Control Strategies

Current control techniques are widely used in grid-connected photovoltaic inverters to regulate the injected current and ensure proper power transfer to the utility grid. Among the most commonly used methods are the Indirect Current Control (ICC) and Direct Current Control (DCC) strategies.

Both approaches share a similar general structure. First, the MPPT algorithm generates the reference voltage V_{pvref} corresponding to the maximum available PV power. A PI controller then regulates the DC-link voltage V_{dc}, producing the peak current reference I_{sp}. In addition, a PLL is employed to synchronize with the grid and extract the phase angle $\theta(t)$.

The three-phase current references are generated as follows:

$$
\begin{aligned}
i_{sa}^*(t) &= I_{\text{sp}}(t)\sin(\theta(t)) \\
i_{sb}^*(t) &= I_{\text{sp}}(t)\sin(\theta(t) - 120^\circ) \\
i_{sc}^*(t) &= I_{\text{sp}}(t)\sin(\theta(t) - 240^\circ)
\end{aligned}
\tag{II.49}
$$

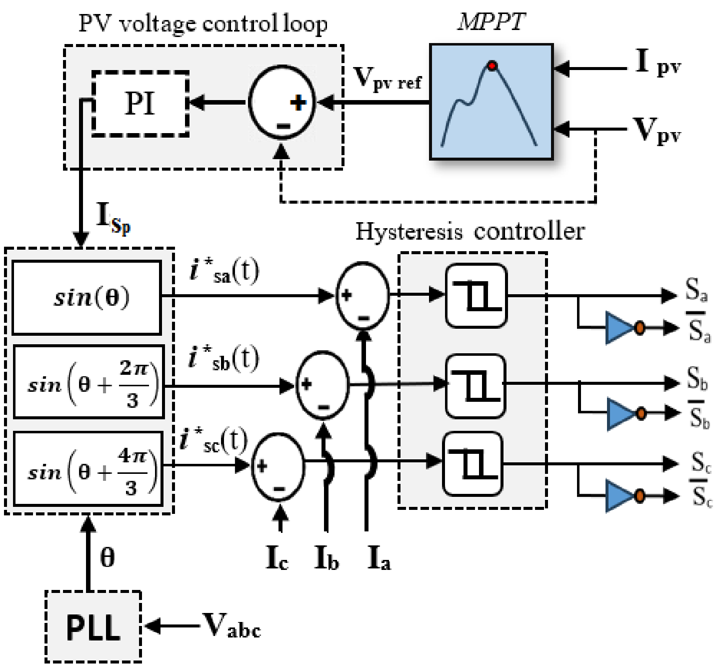

Figure II.13: General structure of current control strategies .

The main difference between ICC and DCC lies in the current tracking technique used by the inverter controller.

In the ICC method, hysteresis current control is generally adopted. The inverter switching states are directly determined according to the instantaneous current error:

$$
|\Delta i(t)| = |i_s^*(t) - i_s(t)| < \Delta i_{\max} \tag{II.50}
$$

This technique is simple and provides fast dynamic response, but it suffers from variable switching frequency and higher current ripple.

Conversely, the DCC method commonly employs sinusoidal PWM or similar modulation techniques with a fixed switching frequency:

$$v_{\mathrm{PWM}}(t) = f(i_s^*(t) - i_s(t)) \tag{II.51}$$

II.3.2.3 Direct Power Control (DPC)

In the Direct Power Control (DPC) method, the inverter switching states are determined directly without the use of an inner current control loop. The control strategy is based on the estimation of instantaneous active and reactive power components in the stationary (α, β) reference frame. These powers are calculated from the measured grid voltages and inverter output currents using the following expressions [72]:

$$p(t) = v_\alpha(t) \cdot i_\alpha(t) + v_\beta(t) \cdot i_\beta(t) \tag{II.52}$$

$$q(t) = v_\alpha(t) \cdot i_\beta(t) - v_\beta(t) \cdot i_\alpha(t) \tag{II.53}$$

The calculated instantaneous active and reactive powers are compared with their respective reference values $p^*(t)$ and $q^*(t)$, resulting in two error signals $e_p(t)$ and $e_q(t)$. These errors are evaluated against hysteresis bands to generate two digital control signals, S_p and S_q, that determine whether the power needs to be increased or decreased [73].

At the same time, the position of the grid voltage vector θ_n is detected, allowing the identification of the present sector within the (α, β) plane. This plane is divided into twelve equal sectors, each covering 30° of the full 360° space vector diagram (see Figure II.14).

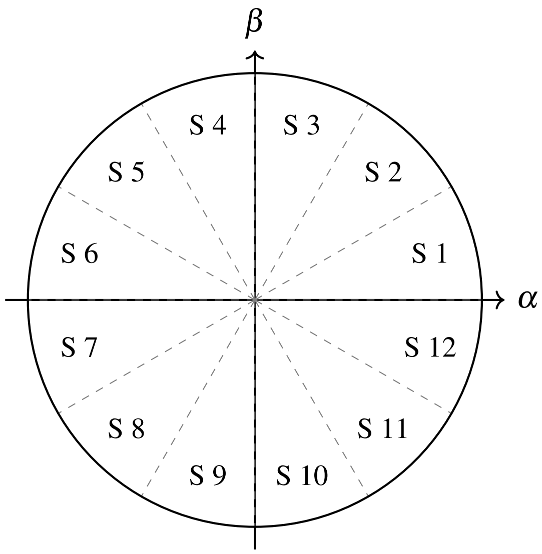

Figure II.14: Division of the (α, β) plane into 12 sectors for DPC switching.

The inverter switching state is then selected based on the combination of S_p, S_q, and the sector number. A predefined switching table is used for this purpose, as shown in Table II.1. This table determines the appropriate switching vector (e.g., 101, 000, 111, etc.) to be applied in each case, optimising the inverter operation in terms of active and reactive power regulation [74].

Table II.1: Switching sequence per sector based on S_p and S_q.

S_p	S_q	Θ_1	Θ_2	Θ_3	Θ_4	Θ_5	Θ_6	Θ_7	Θ_8	Θ_9	Θ_{10}	Θ_{11}	Θ_{12}
1	0	101	111	100	000	110	111	110	000	011	111	001	000
1	1	111	111	000	000	111	111	000	000	111	111	000	000
0	0	101	100	100	110	110	010	010	011	011	001	001	101
0	1	100	110	110	010	010	011	011	011	101	101	101	100

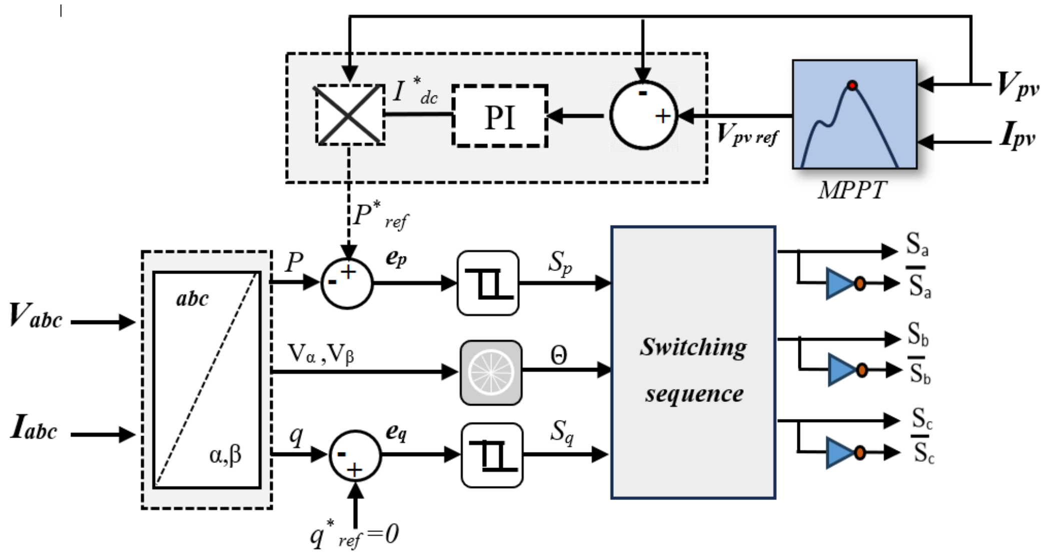

Figure II.15: Control diagram of the Direct Power Control (DPC) method.

II.3.3 Synchronisation Control: Phase-Locked Loop (PLL)

In grid-connected photovoltaic (PV) systems, accurate synchronisation with the utility grid is a critical prerequisite for ensuring stable and standards-compliant power injection. This task involves estimating the grid's fundamental voltage characteristics—namely frequency, amplitude, and phase angle—with high precision. To achieve this, a **three-phase Phase-Locked Loop (PLL)** is typically employed, offering robust phase and frequency tracking under both steady-state and transient conditions [75][17].

The synchronisation process begins with the measurement of three-phase grid voltages $V_a(t), V_b(t), V_c(t)$, which are transformed into the stationary orthogonal reference frame (α, β) using the Clarke transformation:

$$\begin{bmatrix} V_\alpha(t) \\ V_\beta(t) \end{bmatrix} = \frac{2}{3} \begin{bmatrix} 1 & -\frac{1}{2} & -\frac{1}{2} \\ 0 & \frac{\sqrt{3}}{2} & -\frac{\sqrt{3}}{2} \end{bmatrix} \begin{bmatrix} V_a(t) \\ V_b(t) \\ V_c(t) \end{bmatrix} \tag{II.54}$$

These orthogonal voltages are then transformed into the rotating dq reference frame through the Park transformation, which depends on an estimated phase angle $\theta'(t)$:

$$\begin{bmatrix} V_d(t) \\ V_q(t) \end{bmatrix} = \begin{bmatrix} \cos(\theta'(t)) & \sin(\theta'(t)) \\ -\sin(\theta'(t)) & \cos(\theta'(t)) \end{bmatrix} \begin{bmatrix} V_\alpha(t) \\ V_\beta(t) \end{bmatrix} \tag{II.55}$$

The objective of the PLL is to regulate the angle $\theta'(t)$ such that the direct-axis voltage component $V_d(t)$ converges to zero. This condition implies that the rotating reference frame is aligned with the voltage vector, and thus $\theta'(t) \to \theta(t)$, where $\theta(t)$ is the true phase angle of the grid [76].

The error signal $e(t) = V_d(t)$ is processed through a Proportional–Integral (PI) controller to produce the estimated angular frequency $\omega'(t)$:

$$\omega'(t) = K_p \cdot V_d(t) + K_i \int V_d(t)\, dt + \omega_c \tag{II.56}$$

Here, K_p and K_i are the PI gains, and ω_c is the nominal grid frequency (e.g., $2\pi \times 50\,\mathrm{rad/s}$). The phase angle $\theta'(t)$ is obtained by integrating $\omega'(t)$:

$$\theta'(t) = \int \omega'(t)\, dt \tag{II.57}$$

This closed-loop system dynamically adjusts $\theta'(t)$ to match the grid's actual phase $\theta(t)$, ensuring synchronisation even in the presence of noise, harmonics, or transient disturbances [77].

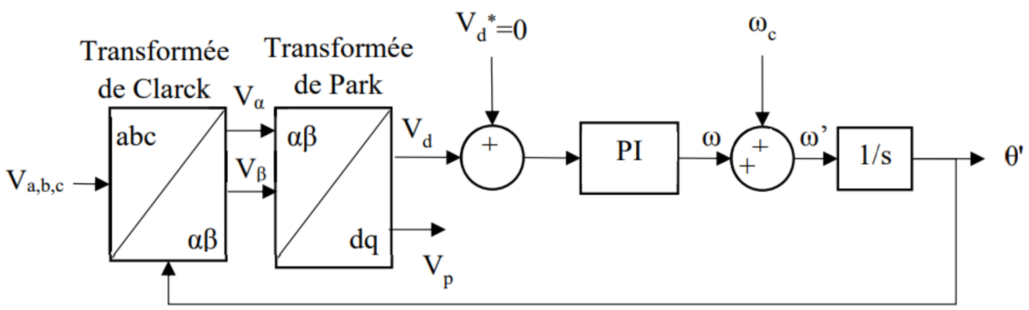

Figure II.16: Block diagram of the three-phase PLL using Clarke and Park transformations.

This configuration is widely adopted in advanced control techniques such as Synchronous Reference Frame (SRF) and Direct Current Control (DCC), where precise phase tracking is essential for generating accurate current or voltage references[39][78].

II.4 Conclusion

This chapter has established the methodological foundation of the thesis through the construction of a rigorous mathematical model for the grid-connected photovoltaic (PV) system, complemented by the integration of contemporary control strategies. Particular attention was given to the modelling and explanation of intelligent Maximum Power Point Tracking (MPPT) algorithms, given their pivotal role in ensuring optimal energy extraction under varying environmental conditions. Additionally, inverter control techniques were outlined with a focus on compliance with international standards governing grid interconnection, thereby enhancing system reliability and operational stability.

Within this comprehensive theoretical and technical framework, the chapter lays the groundwork for the subsequent phase of validation. The models and control schemes developed here are intended to serve as a solid basis for performance simulation and real-time experimentation, enabling a precise evaluation of system behaviour and the identification of potential areas for improvement.

As we transition to the following chapter, the focus shifts from theoretical formulation to practical verification — a crucial step in demonstrating the feasibility and effectiveness of the proposed solutions under realistic operating conditions. Ultimately, the true scientific value lies not only in what can be theorised, but in what can be empirically substantiated.

Chapter III

Simulation and Performance Evaluation of Grid-Connected PV Systems

III.1 Introduction

Achieving high performance and operational reliability in grid-connected photovoltaic (PV) systems is a fundamental objective that demands accurate modelling of system components and the development of effective control strategies. In this context, simulation provides a vital preparatory step before practical implementation, offering a safe and flexible environment for analysing system behaviour under various operating conditions. It serves as an indispensable tool for assessing performance in scenarios that are otherwise difficult to realise in practice, whether due to technical constraints or uncontrollable environmental factors that hinder field experimentation.

This stage enables the identification of potential technical issues, the refinement of system design, and the selection of optimal configurations in terms of power conversion topology, maximum power point tracking (MPPT) algorithms, and control strategies. As such, this chapter lays the theoretical and practical groundwork for the deployment of advanced solutions in subsequent stages, highlighting the crucial role of simulation in the development pathway of PV systems.

Within this framework, a comprehensive performance assessment is conducted, encompassing efficiency, dynamic response, and overall system effectiveness. The insights derived from this evaluation inform practical recommendations and guide the design of an integrated system that meets the required technical and environmental standards for optimal operation.

III.2 PV Power Plant Sizing and Parameter Definition

In the context of this study, a 150 kW solar photovoltaic (PV) power plant has been dimensioned to serve as a representative model for performance evaluation and control strategy implementation. The selected capacity reflects a typical scale for decentralised renewable energy systems, which are increasingly deployed for both standalone and grid-connected applications.

This PV plant configuration can be considered either as a fully autonomous power generation unit or as a functional subcomponent within a larger-scale PV installation of equivalent nominal capacity. Such flexibility enhances the generality of the findings and broadens the applicability of the developed methodologies across diverse practical contexts.

The plant comprises a total of 365 high-efficiency PV modules arranged in 73 series-connected strings, each consisting of five modules. This configuration was selected to maximise the DC-side voltage and current within the operational limits of the chosen inverter topology. Table IV.1 presents the key electrical characteristics of the SPR-415E-WHT-D module under standard test conditions (STC), which serves as the baseline component for the array design.

Table III.1: Electrical specifications of the SPR-415E-WHT-D PV module under STC.

Parameter	Value
Rated Maximum Power (P_{max})	415 W
Voltage at P_{max} (V_{mp})	72.9 V
Current at P_{max} (I_{mp})	5.69 A
Open-Circuit Voltage (V_{oc})	85.3 V
Short-Circuit Current (I_{sc})	6.09 A
Number of Cells per Module	128

The single-diode model, widely adopted for PV cell characterisation, is used to simulate the electrical behaviour of the array. Figure III.1 illustrates the implemented configuration, providing the foundation for subsequent simulation and control analysis.

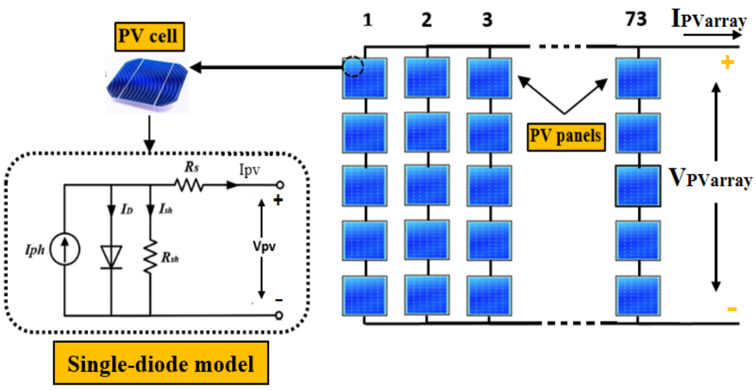

Figure III.1: Configuration of the PV power plant with the single-diode equivalent circuit of the PV cell.

III.3 Comparison of Single-and Two-Stage PV System Topologies

This comparison is essential for understanding how system topology influences energy extraction efficiency and compliance with power quality standards under varying solar irradiance conditions. Accordingly, this section presents a comparative analysis of single-stage and two-stage photovoltaic (PV) configurations operating under time-varying irradiance profiles.

As described in Chapter 1, the two-stage topology comprises a PV array connected to a boost converter, followed by a DC-link capacitor and a grid-connected inverter. In contrast, the single-stage configuration connects the PV array directly to the inverter, eliminating the intermediate DC conversion stage [27].

To optimise energy harvesting in both architectures, the Incremental Conductance (Inc-Cond) algorithm was adopted for maximum power point tracking (MPPT), due to its high accuracy, particularly during rapid irradiance changes. At the inverter level, a Synchronous

Reference Frame (SRF) control method was implemented to ensure synchronised and grid-compliant current injection while maintaining power quality.

The objective of this study is to evaluate system efficiency, power losses, and the performance of the MPPT algorithm across both configurations.

The results offer a comprehensive insight for engineers and researchers, supporting informed design decisions for grid-connected PV systems. This is achieved through a rigorous comparative analysis of the respective advantages and limitations of each topology under identical operating conditions. The key simulation parameters used in both cases are summarised in Table III.2, ensuring consistency in the evaluation criteria.

Table III.2: Simulation Parameters

Parameter	**Value**
Grid voltage (U_{grid})	220 V
Grid frequency (f)	50 Hz
Filter inductance and resistance ($L_{\text{filter}}, R_{\text{filter}}$)	0.09 H, 1.1 Ω
Boost inductor (L_{boost})	3 mH
Boost input capacitor (C_{boost})	320 μF
DC-link capacitor (C_{DC})	150,000 μF

Time-domain simulations were carried out using MATLAB/Simulink, as illustrated in Figures III.3 and III.4, employing identical PV array and grid settings in both systems to ensure a fair comparison. A variable solar irradiance profile was constructed to emulate realistic environmental conditions, as shown in Figure III.2.

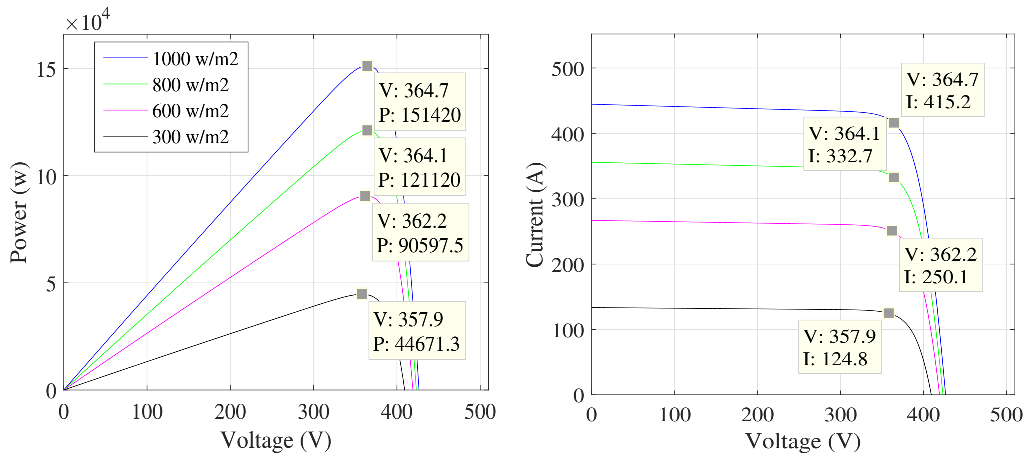

Figure III.2: I–V and P–V characteristics of the PV power plant under different irradiance levels.

Figures III.5 and III.6 illustrate the simulation results for voltage, current, and output power from the photovoltaic (PV) array, in addition to the power injected into the grid for both investigated topologies: single-stage and two-stage.

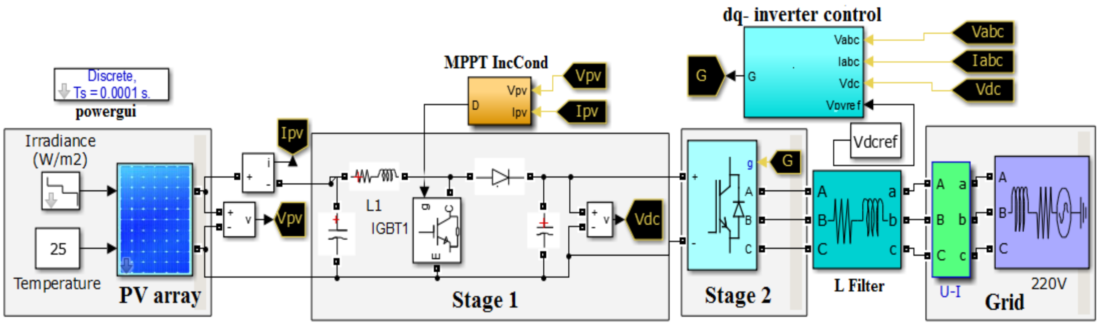

Figure III.3: Simulink implementation of the two-stage PV system topology.

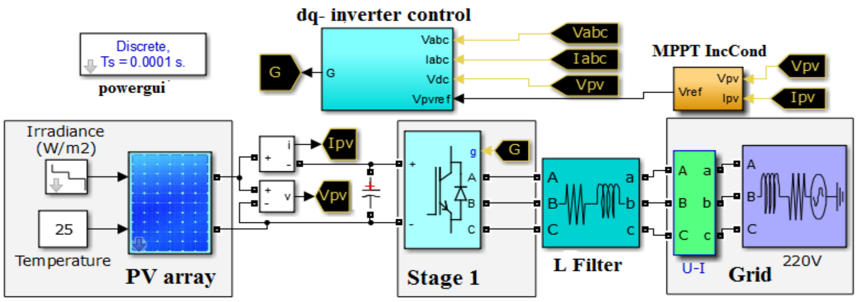

Figure III.4: Simulink implementation of the single-stage topology.

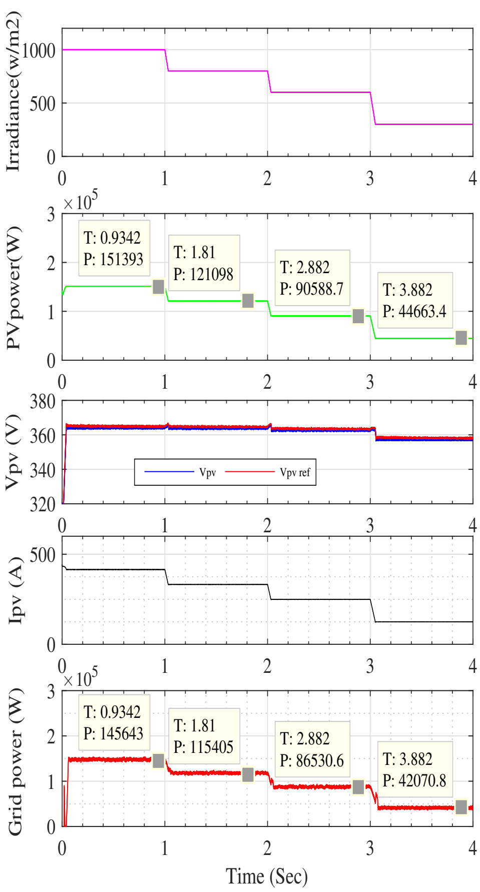

Figure III.5: Dynamic response of the single-stage topology.

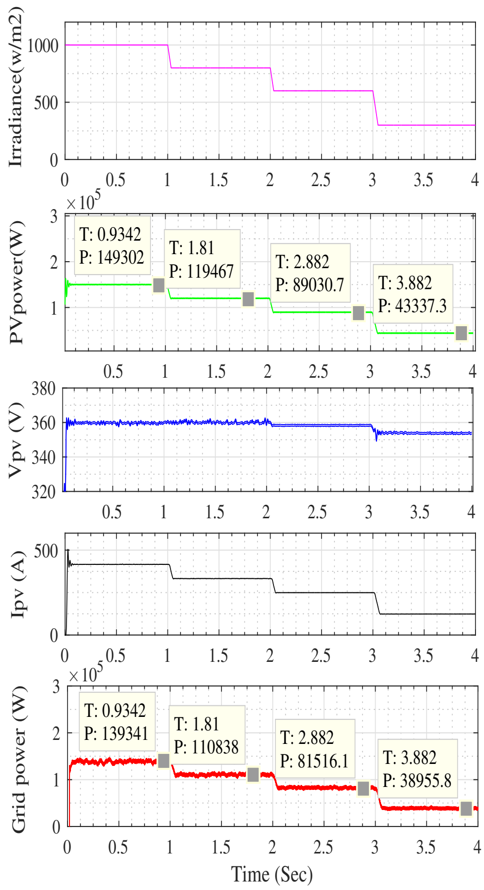

Figure III.6: Dynamic response of the two-stage topology.

These results clearly demonstrate the superior performance of the single-stage configuration, particularly in terms of maximum power point tracking (MPPT) using the Incremental Conductance (IncCond) algorithm. This topology exhibits faster response and more precise tracking, especially under dynamically varying irradiance conditions.

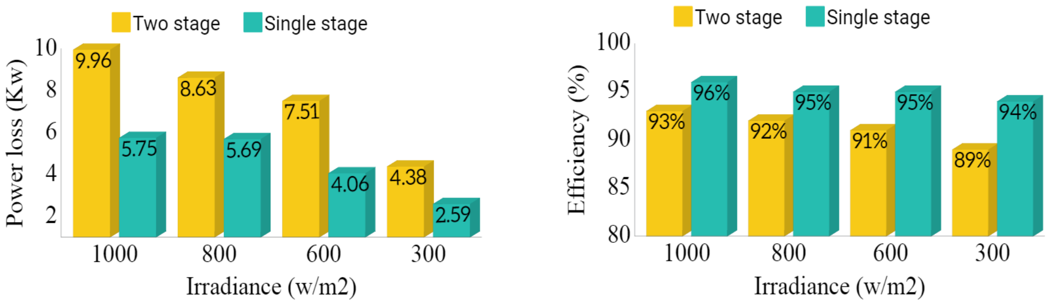

Figure III.7: Quantitative comparison of power losses and efficiencies between single-stage and two-stage PV topologies.

To quantitatively assess system performance, Figure III.7 presents a direct comparison of power losses for both topologies under varying irradiance levels (1000, 800, 600, and 300 W/m^2). According to the simulation data, total losses in the two-stage system amounted to 9.96 kW, 8.63 kW, 7.51 kW, and 4.38 kW, respectively. In contrast, the single-stage topology recorded significantly lower losses: 5.75 kW, 5.69 kW, 4.06 kW, and 2.59 kW. This reduction can be primarily attributed to the absence of the DC–DC boost converter in the single-stage structure, which minimises the number of active conversion components and their associated switching and conduction losses.

This distinction in losses directly translates into a notable difference in system efficiency. The single-stage topology achieved operational efficiencies of 96%, 95%, 95%, and 94% across the irradiance levels, whereas the two-stage system yielded lower efficiencies of 93%, 92%, 91%, and 89%, respectively. Notably, the efficiency gap between the two topologies narrows progressively with decreasing irradiance, reaching its lowest margin at 300 W/m^2.

This convergence in performance at low irradiance can be explained by the inherent limitations of energy generation from the PV array under such conditions. At reduced irradiance, the operating currents are significantly lower, thereby diminishing the impact of switching losses and rendering the structural differences between the two systems less influential on the overall performance. However, despite this convergence, the single-stage topology consistently retains a marginal advantage, which highlights its inherent design efficiency and robustness across a wide range of environmental conditions.

From a control perspective, the single-stage architecture benefits from integrating the MPPT algorithm directly within the inverter. This structural integration allows for faster and more accurate adaptation to real-time irradiance fluctuations, in contrast to the two-stage topology, which relies on coordination between separate converter and inverter control units.

Moreover, eliminating the intermediate DC–DC conversion stage reduces overall system complexity, lowers maintenance costs, and improves the quality of the power delivered to the grid.Practically speaking, these findings hold significant relevance for grid-connected PV systems deployed on a large scale, particularly in regions where solar irradiance varies frequently or unpredictably. The data indicate that the single-stage topology offers not only superior efficiency but also greater flexibility and responsiveness, positioning it as an optimal choice for next-generation PV systems that demand high reliability and stable output.

In conclusion, the single-stage configuration emerges as a technically and economically favourable solution, offering enhanced energy conversion efficiency, reduced power losses, simplified architecture, and overall system cost savings. These insights provide a strong foundation for the following chapters, which will focus on the development of optimised control strategies based on this topology to ensure grid code compliance and maximise energy harvesting, all within a framework of long-term reliability and technological sustainability.

III.4 MPPT Algorithm Assessment under Realistic Operating Scenarios

Building upon the findings of the previous section, which highlighted the superior performance of the single-stage topology in terms of efficiency, power loss reduction, and system simplicity, this section presents a detailed assessment of advanced control strategies responsible for enhancing the system's ability to reliably track the maximum power point (MPPT), particularly under dynamically changing operating conditions.

In this context, the performance of five MPPT algorithms is examined: the conventional Incremental Conductance (INC) method, along with four widely recognised metaheuristic techniques—Grey Wolf Optimiser (GWO), Particle Swarm Optimisation (PSO), Cuckoo Search (CUKO), and Whale Optimisation Algorithm (WOA). These algorithms have been selected based on their prevalence in the scientific literature and their proven capability to handle nonlinear, complex search spaces inherent to PV system operation.

The evaluation is conducted under three representative operating scenarios: uniform irradiance, dynamically varying irradiance and temperature, and partial shading affecting PV module performance. Each algorithm is analysed with respect to its tracking speed, stability, efficiency, and adaptability to fluctuating environmental conditions.

The ultimate aim of this study is to identify the most suitable and efficient algorithm for integration with the single-stage PV system topology, thereby ensuring optimal energy harvesting, enhanced grid power quality, and reduced system-level transients. These findings serve as a critical step towards the development of advanced, practically deployable control frameworks for next-generation grid-connected photovoltaic systems.

III.4.1 Performance under Uniform Irradiance

Uniform irradiance conditions serve as a fundamental reference for assessing the baseline behaviour of MPPT algorithms in the absence of external disturbances. This scenario facilitates a clear evaluation of each algorithm's capability to reach and maintain the Maximum Power Point (MPP), providing insights into convergence speed, response stability, and tracking accuracy under minimal operational stress.

In this context, the five selected algorithms were implemented on the same photovoltaic system under a constant irradiance of 1000 W/m^2, As previously illustrated in Figure III.2, the maximum power point (MPP) is located at a voltage of and a power output of $V = 364.7\,\text{V}$ and a power output of $P = 151420\,\text{W}$. The transient responses of each technique were recorded and compared against this reference point.

The following figures present the simulation results of the studied algorithms, enabling a quantitative assessment of their effectiveness in tracking the maximum power point.

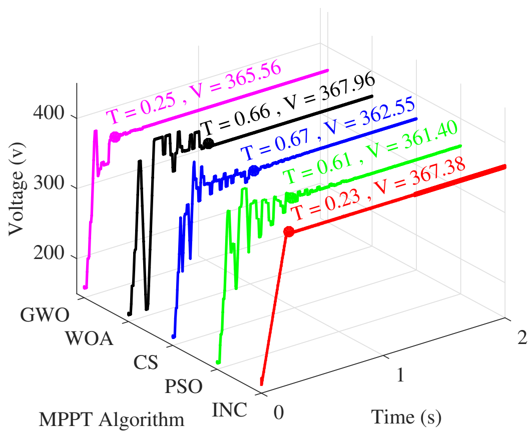

Figure III.8: Dynamic voltage response $V(t)$ under uniform irradiance.

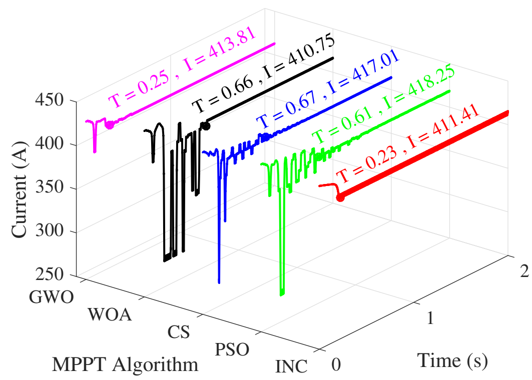

Figure III.9: Dynamic current response $I(t)$ under uniform irradiance.

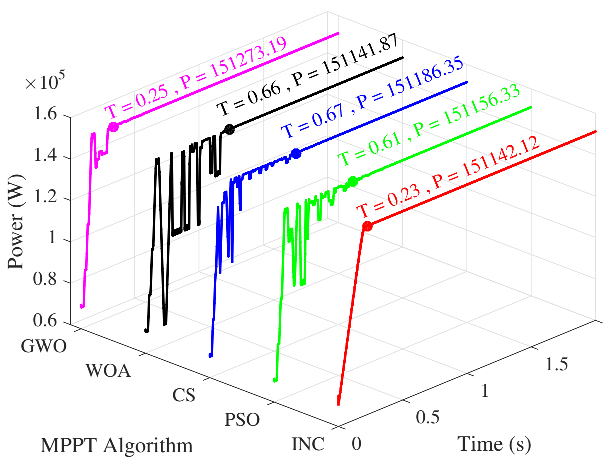

Figure III.10: Time-domain power tracking performance $P(t)$ of MPPT algorithms under uniform irradiance.

To provide a clearer comparative perspective based on the results presented in Figures III.8, III.9, and III.10, Table III.3 offers a quantitative summary of the steady-state performance of five MPPT algorithms under uniform irradiance. The table details their power outputs, voltage levels, convergence times, and deviations from the reference MPP.

Table III.3: MPPT Algorithm Performance under Uniform Irradiance ($G = 1000$ W/m^2)

Algorithm	**Tracking Time (s)**	**Power (W)**	ΔP (W)	**Voltage (V)**	ΔV (V)
GWO	0.25	151273.19	146.81	365.56	0.86
WOA	0.66	151141.87	278.13	367.96	3.26
CS	0.67	151186.35	233.65	362.55	2.15
PSO	0.61	151156.33	263.67	361.40	3.30
INC	0.23	151142.12	277.88	367.38	2.68

Based on these results in Table III.3, the Grey Wolf Optimiser (GWO) demonstrated the most accurate tracking behaviour, achieving the closest match to the reference MPP (151 420 W at 364.7 V), with a minimal power deviation of 146.81 W and a voltage error of just 0.86 V. Furthermore, GWO exhibited a rapid convergence time of 0.25 s, indicating strong suitability for real-time PV system control.

In contrast, the Incremental Conductance (INC) algorithm achieved the fastest response (0.23 s), albeit with reduced accuracy, showing a power deviation of 277.88 W and a voltage offset of 2.68 V. Among the remaining metaheuristic methods, the Cuckoo Search (CS) algorithm—despite its slower convergence time (0.67 s)—demonstrated relatively better voltage tracking than both PSO and WOA. Nevertheless, all three algorithms (WOA, PSO, and CS) recorded power deviations exceeding 230 W.

Overall, the tested algorithms performed reliably under stable irradiance. The GWO method stood out by combining high tracking accuracy, fast convergence, and minimal voltage deviation. These results underscore its potential for deployment in single-stage PV systems operating in consistent environmental conditions. However, further testing under variable irradiance, temperature changes, and partial shading remains essential to validate each algorithm's robustness and real-world applicability.

III.4.2 Performance under variable Irradiance and Temperature.

To evaluate the robustness and adaptability of maximum power point tracking (MPPT) algorithms under realistic environmental conditions, a dynamic test scenario was implemented in which both solar irradiance and ambient temperature were varied simultaneously, as illustrated in Figure III.11. This setup replicates the typical fluctuations encountered in real-world photovoltaic systems and presents a significant challenge to the algorithms, which are required to respond promptly and accurately to continuously shifting operating points while maintaining overall system stability.

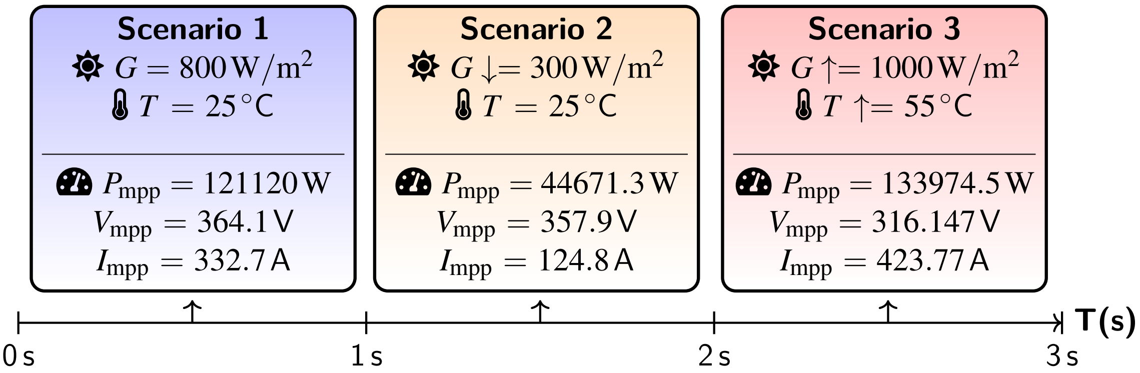

Figure III.11: Stepwise irradiance and temperature changes with corresponding MPP values.

The performance of each algorithm was assessed based on its ability to accurately track the maximum power point (MPP) under each dynamic condition. Figures III.12, III.13, and III.14 highlight the photovoltaic system characteristics and the corresponding MPPs under each irradiance and temperature combination. Particular emphasis was placed on three key criteria: tracking accuracy, response speed, and resilience to transient disturbances, as these factors have a direct impact on the overall energy harvesting efficiency.

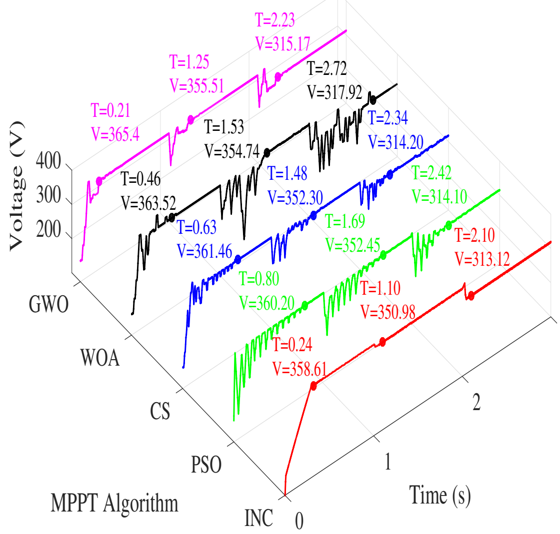

Figure III.12: Voltage response, $V(t)$.

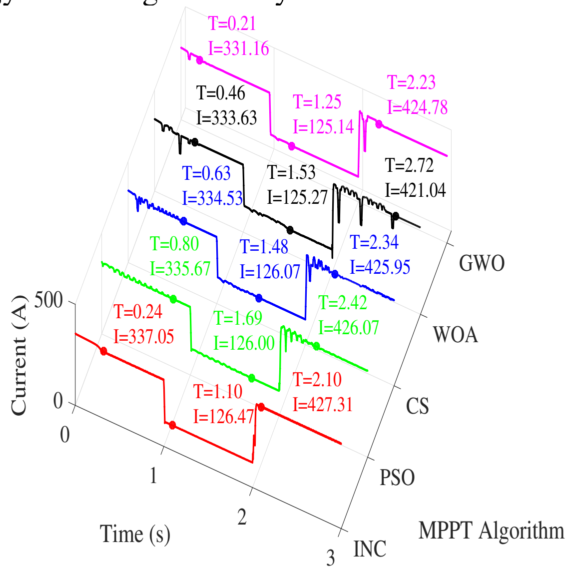

Figure III.13: Current response, $I(t)$.

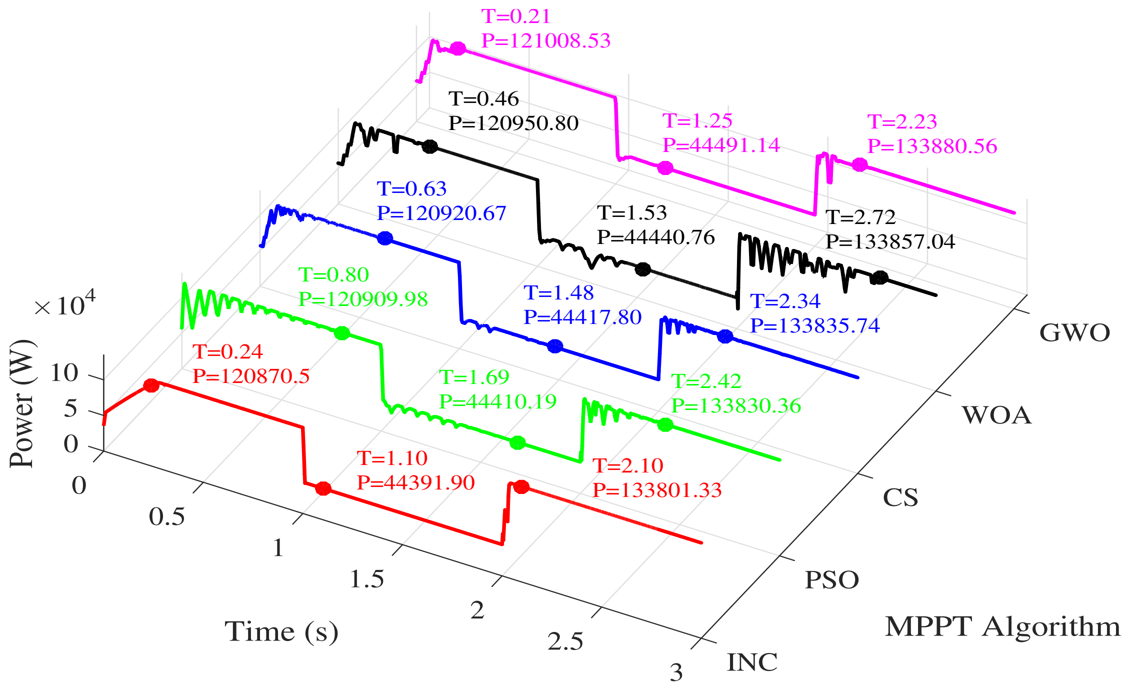

Figure III.14: Power response over time, $P(t)$.

To support visual analysis and emphasise the relative performance of each method, bar charts were generated based on the results presented in Figures III.12, III.13, and III.14 . These visual representations offer a clearer comparative perspective on the strengths and limitations of the tested MPPT techniques under varying environmental conditions.

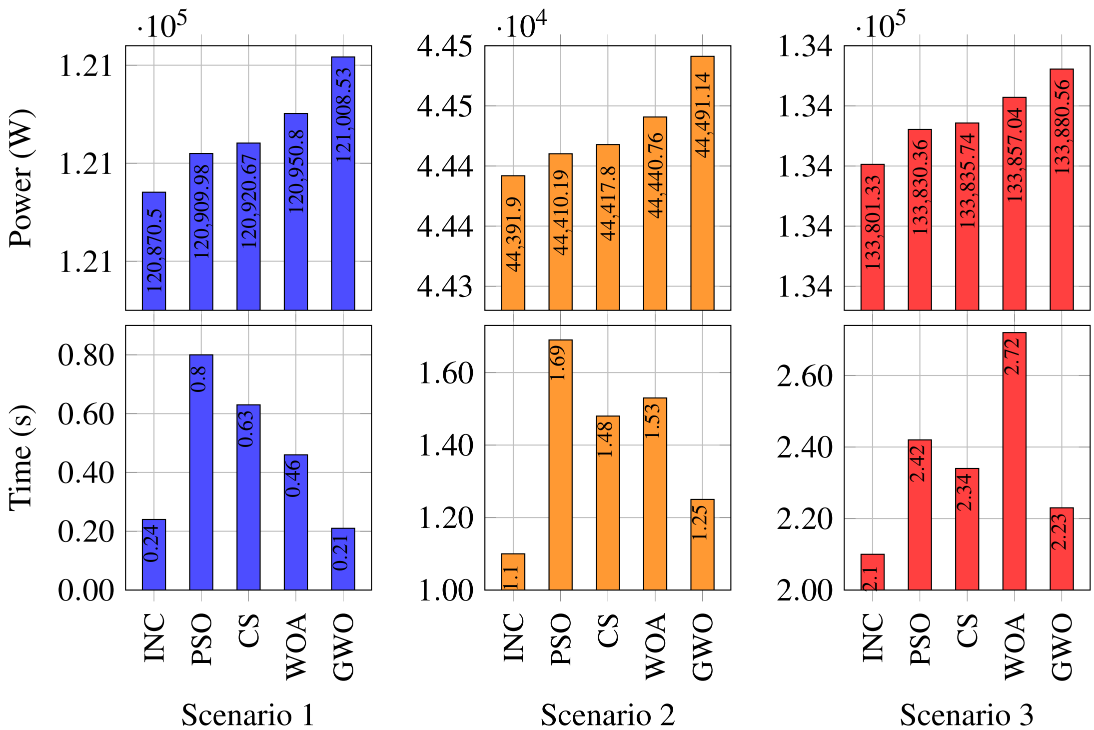

Figure III.15: Comparison of MPPT algorithms across three scenarios.

Based on the bar chart presented in Figure III.15,the results across the three test scenarios reveal distinct differences in the performance of the maximum power point tracking (MPPT) algorithms under dynamic operating conditions of the photovoltaic system.

III.4.2.0.1 Scenario 1: High irradiance and moderate temperature. As shown in Figure III.11,for the first scenario ($P_{\text{mpp}} = 121120$ W at $V = 364.1$ V), the differences among the algorithms were relatively limited, as all methods succeeded in reaching values close to the reference power. The Grey Wolf Optimisation (GWO) algorithm achieved the highest accuracy (121008.53 W, with only 111.5 W deviation), while the Incremental Conductance (INC) method demonstrated extremely fast response (0.24 s) but suffered from partial loss of accuracy. Both Particle Swarm Optimisation (PSO) and Cuckoo Search (CS) provided balanced outcomes between speed and accuracy, with their performance being closely aligned. The Whale Optimisation Algorithm (WOA) also tracked the power point effectively, though with a slightly longer convergence time.

III.4.2.0.2 Scenario 2: Reduced irradiance. As illustrated in Figure III.11,in the second scenario, where irradiance dropped significantly ($P_{\text{mpp}} = 44671.3$ W at $V = 357.9$ V), the contrast between algorithms became more pronounced. Once again, GWO maintained close proximity to the reference point (44491.14 W with a deviation of 180.2 W). Although INC converged quickly (1.10 s), its tracking error was the highest (around 280 W), highlighting its limitation under low-irradiance conditions. By contrast, both CS and WOA achieved better accuracy than INC, albeit at the expense of slightly longer response times (up to 1.53 s). PSO delivered moderate performance with acceptable accuracy and response speed, making it a practical compromise when a balance between speed and precision is required.

III.4.2.0.3 Scenario 3: Increased irradiance with elevated temperature. As depicted in Figure III.11,the third scenario, characterised by both increased irradiance and elevated temperature ($P_{\text{mpp}} = 133974.6$ W at $V = 316.15$ V), posed the most challenging conditions for the algorithms. All methods succeeded in approaching the reference power, but GWO retained a clear advantage, recording 133880.6 W with a minor deviation (93.9 W). Both CS and PSO demonstrated strong accuracy with comparable response times. WOA exhibited the slowest convergence (2.72 s), while INC maintained a relatively quick response (2.10 s) but with reduced accuracy compared with the metaheuristic-based techniques.

III.4.2.0.4 General comparison. Overall, the comparison highlights a trade-off between tracking speed and accuracy. INC consistently remained the fastest across all scenarios, yet it was the least precise, particularly under fluctuating irradiance. Conversely, the metaheuristic algorithms—especially GWO—demonstrated a strong capacity to achieve a balanced compromise between speed and accuracy, rendering them more suitable for practical applications in single-stage photovoltaic systems. Both PSO and CS emerged as viable alternatives, offering stable and well-balanced performance, while WOA proved effective in terms of accuracy but at the cost of longer response times.

III.4.3 Performance under Partial Shading

Partial shading conditions introduce localized reductions in solar irradiance on certain PV modules, resulting in multiple local maxima in the power–voltage (P–V) characteristic. This scenario represents a significant operational challenge for MPPT algorithms, as they must distinguish the global maximum power point (GMPP) from multiple local maxima to maintain optimal energy extraction.

Figure III.16 illustrates the I–V and P–V characteristics of the PV modules under partial shading, highlighting the formation of multiple peaks and the reduced overall power output. Evaluating algorithm performance under these conditions provides critical insights into tracking accuracy, convergence speed, and the robustness of each MPPT strategy in realistic, non-uniform irradiance environments.

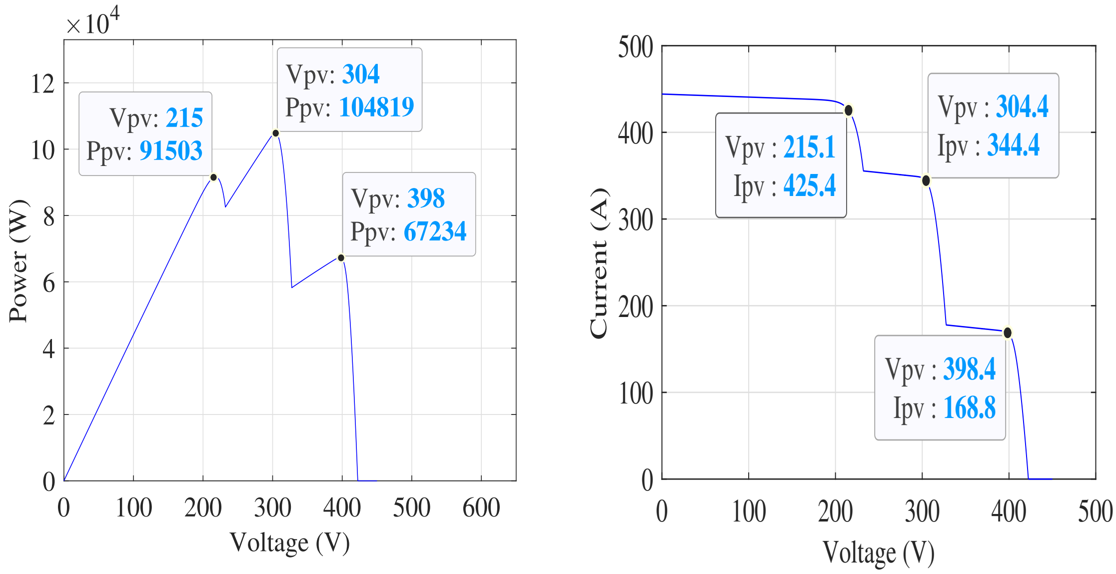

(a) P–V characteristic under partial shading. (b) I–V characteristic under partial shading.

Figure III.16: P–V and I–V characteristics of the PV system under partial shading conditions.

The following figures III.17, III.18, and III.19 present the simulation results of the studied MPPT algorithms, providing a quantitative basis for assessing their effectiveness in accurately tracking the global maximum power point under these complex conditions.

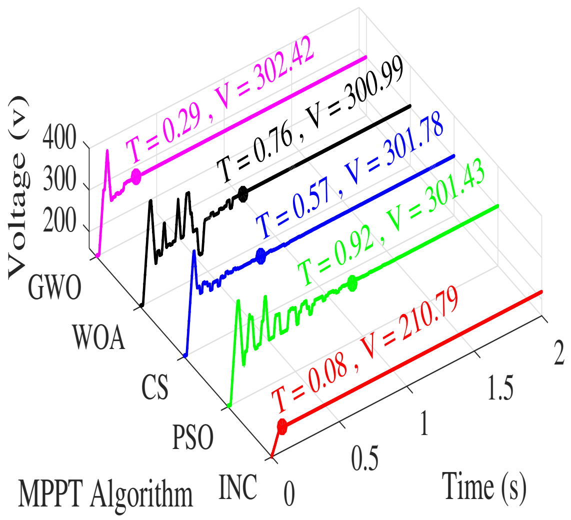

Figure III.17: Voltage response, $V(t)$.

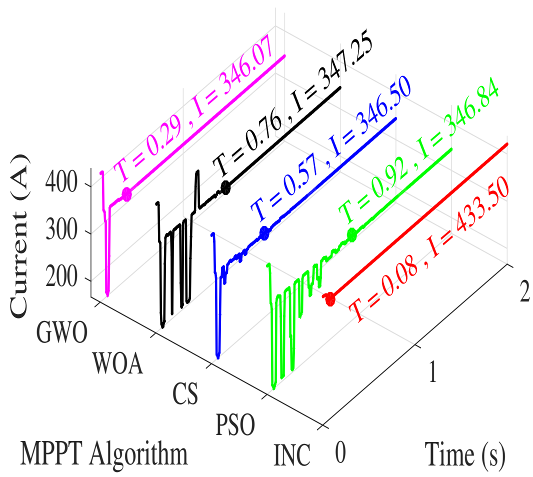

Figure III.18: Current response, $I(t)$.

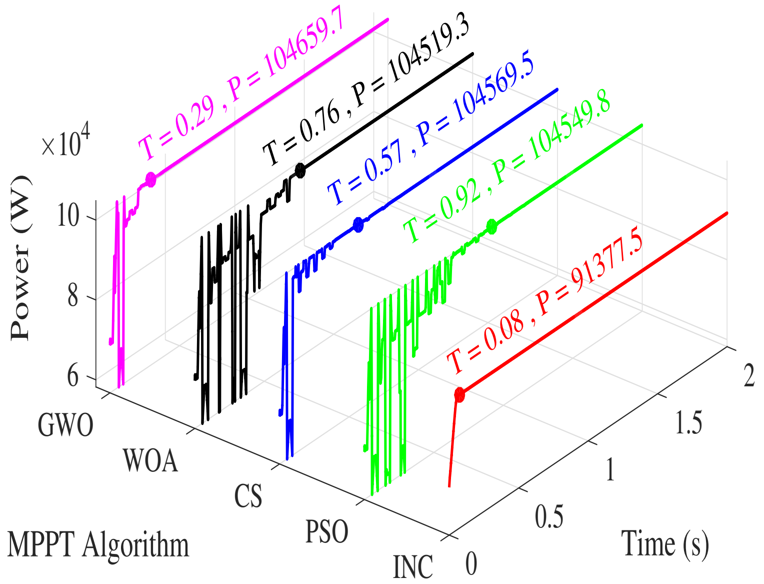

Figure III.19: Power response over time, $P(t)$.

Table III.4 summarises the simulation results obtained from different MPPT algorithms under partial shading conditions. The parameters include the tracking time, extracted power, operating voltage, and their respective deviations from the global maximum power point (GMPP).

Table III.4: Comparison of MPPT algorithm performance under partial shading conditions.

Algorithm	**Tracking Time (s)**	**Power (W)**	ΔP (W)	**Voltage (V)**	ΔV (V)
GWO	0.29	104,659.7	-159.3	302.42	-1.58
WOA	0.76	104,519.3	-299.7	300.99	-3.01
CS	0.57	104,569.5	-249.5	301.78	-2.22
PSO	0.92	104,549.8	-269.2	301.43	-2.57
INC	0.08	91,375.5	-13,443.5	210.79	-93.21

The results presented in Figures III.19 and Table III.4 indicate that the Grey Wolf Optimiser (GWO) achieved the fastest and most accurate convergence, closely matching the GMPP with a power deviation of only 159 W and a voltage deviation of 1.6 V. The Whale Optimisation Algorithm (WOA), Cuckoo Search (CS), and Particle Swarm Optimisation (PSO) also exhibited satisfactory tracking behaviour, maintaining their power deviation below 0.3% from the global optimum.In contrast, the conventional Incremental Conductance (INC) algorithm remained stuck at a local maximum, yielding 91.38 kW at 210.8 V — about 12.8% below the global optimum. This occurs because the deterministic nature of the INC method prevents it from escaping local peaks under non-uniform irradiance.Overall, all metaheuristic-based algorithms demonstrated effective global search capability under partial shading. Among them, GWO exhibited the best balance between convergence speed and tracking precision, confirming its superior adaptability to complex, multi-peak power characteristics.

III.5 Performance Evaluation of Grid-Connected Inverter Control Strategies

As highlighted in Chapter 1, grid-connected photovoltaic (PV) systems are required to comply with stringent power-quality standards, particularly in terms of total harmonic distortion (THD), frequency stability, and phase balance. To ensure a fair and consistent evaluation of inverter performance, all investigated control strategies were implemented and simulated using the same grid-connected PV plant model, whose structure is illustrated in Figure III.4.

This unified modelling framework enables a direct and rigorous comparison of the different control approaches under identical operating conditions. In this study, four widely adopted inverter control strategies are examined: Direct Power Control (DPC), Synchronous Reference Frame (SRF), Indirect Current Control (ICC), and Direct Current Control (DCC).

The simulated voltage and current waveforms, along with their corresponding THD values, for the four control approaches are presented in Figures III.20–III.23. These results allow a clear visual comparison of current purity, phase accuracy, and harmonic behaviour.

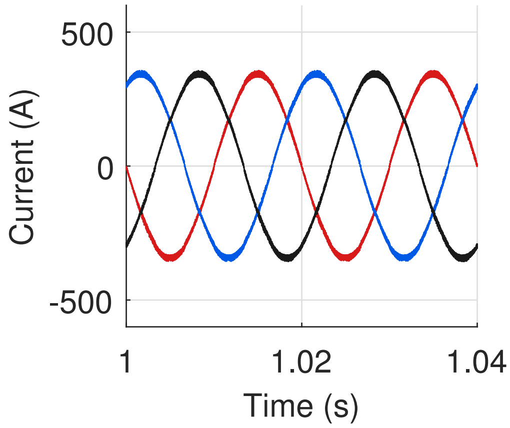

Injected Current Waveform

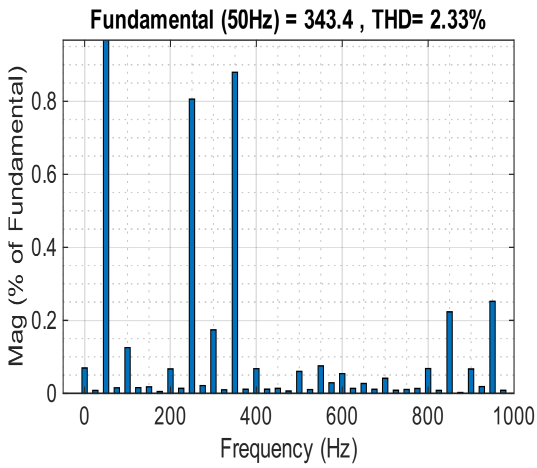

Current Total Harmonic Distortion (THD)

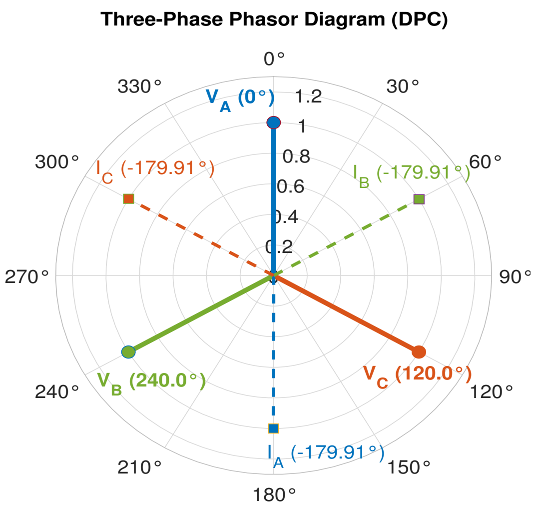

Voltage–Current Phase Diagram

Figure III.20: DPC – Control Performance

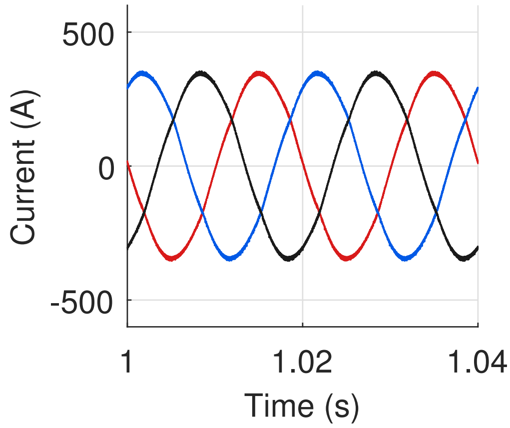

Injected Current Waveform

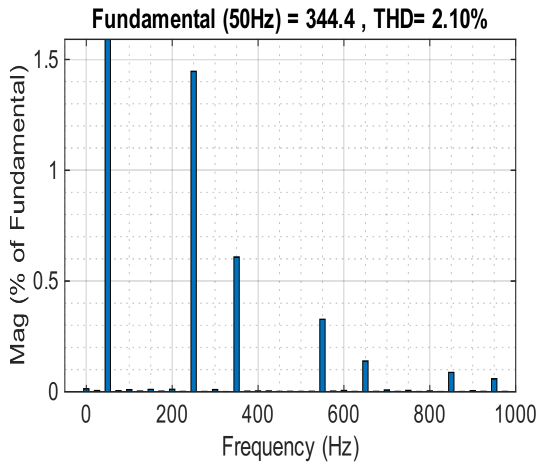

Current Total Harmonic Distortion (THD)

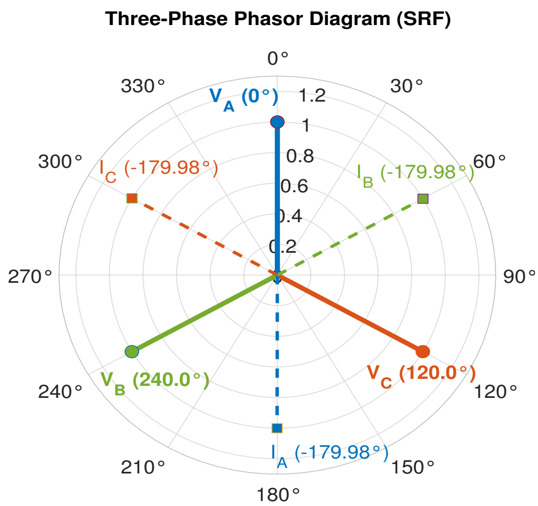

Voltage–Current Phase Diagram

Figure III.21: SRF – Control Performance

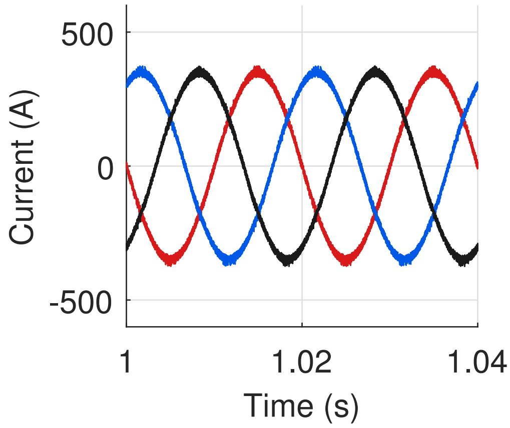

Injected Current Waveform

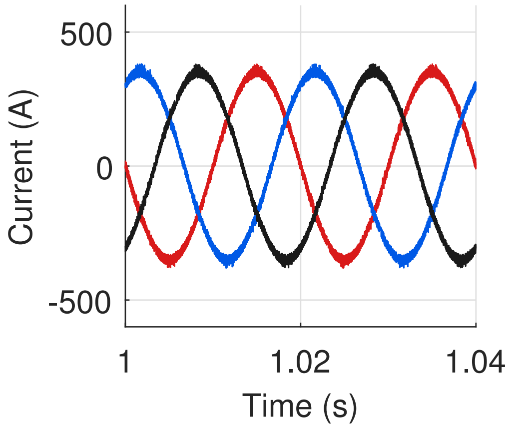

Injected Current Waveform

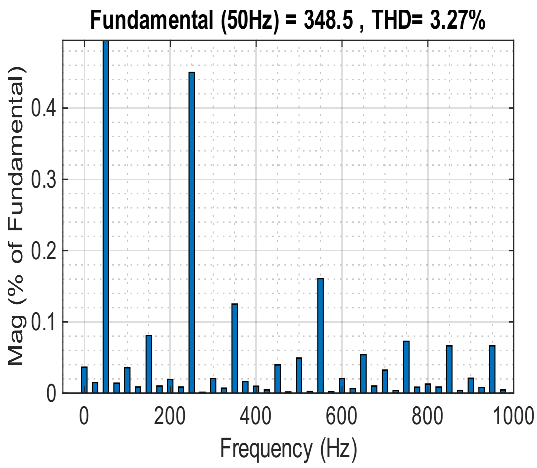

Current Total Harmonic Distortion (THD)

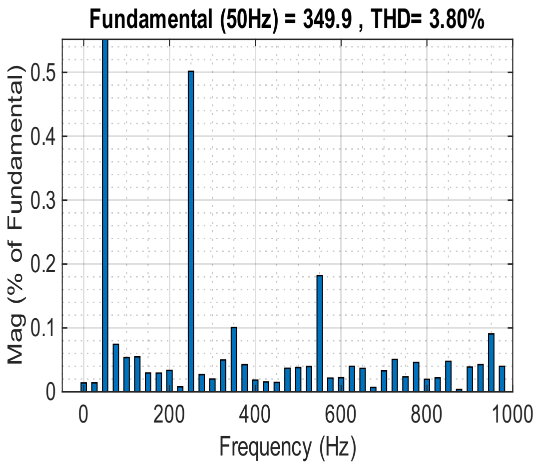

Current Total Harmonic Distortion (THD)

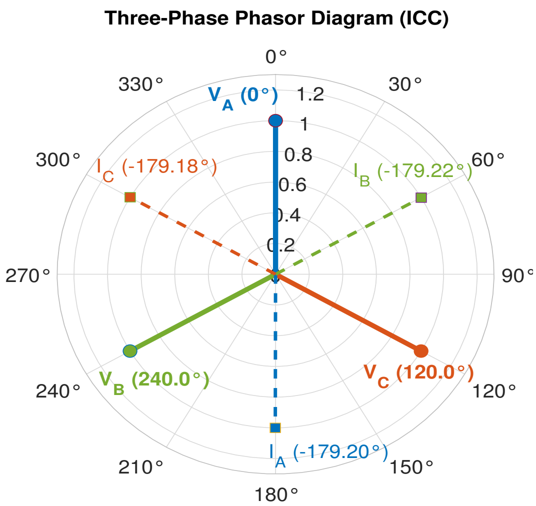

Voltage–Current Phase Diagram

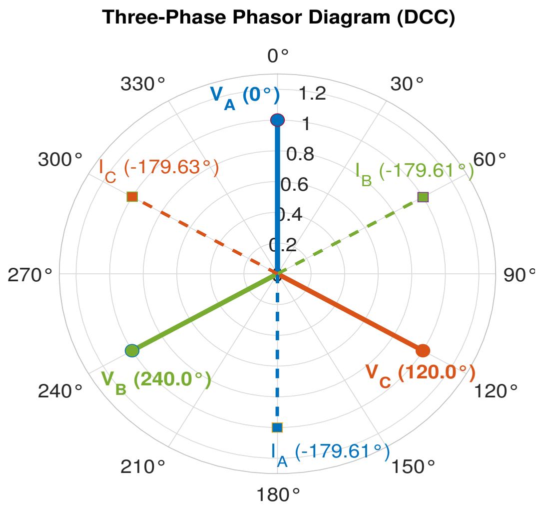

Voltage–Current Phase Diagram

Figure III.22: ICC – Control Performance

Figure III.23: DCC – Control Performance

The simulation results presented in Figures III.20–III.23 reveal clear differences in the harmonic performance and phase alignment achieved by the evaluated inverter control strategies. Overall, the Synchronous Reference Frame (SRF) method demonstrates the best current quality, achieving the lowest total harmonic distortion (THD) of approximately 2.10% under the tested operating conditions. This superior performance is mainly attributed to its decoupled control structure, which enables accurate regulation of the current components and ensures highly sinusoidal waveforms with precise phase tracking during steady-state operation.

The Direct Power Control (DPC) strategy follows closely, with a THD value of about 2.33%. This confirms its effectiveness in regulating instantaneous active and reactive power while maintaining low harmonic distortion and strong phase coherence with the grid voltage.

In contrast, the Indirect Current Control (ICC) approach exhibits a higher THD of approximately 3.27%. This increase can be primarily associated with the slower dynamic response of the inner current control loop and the presence of switching-induced ripples. Although stable voltage and current waveforms are preserved, the elevated harmonic content indicates reduced filtering effectiveness compared with SRF and DPC.

The Direct Current Control (DCC) method records the highest THD, reaching nearly 3.80%. This behaviour is mainly due to the direct switching mechanism, which introduces more pronounced current ripples. While the injected current remains within acceptable operational limits, the increased distortion reflects inherent limitations in maintaining waveform purity.

The analysis of the phase angle between the grid voltage and the injected current further corroborates these observations. All investigated strategies achieve near-ideal phase alignment close to -180°, confirming proper synchronisation with the grid. Nevertheless, the SRF method exhibits the most accurate phase tracking at approximately -179.98°, followed closely by DPC at -179.71°. Slightly larger deviations are observed for ICC (-179.20°) and DCC (-179.61°). Although these deviations do not significantly affect the overall power transfer, they highlight the superior dynamic coordination and control precision achieved by SRF and DPC.

Overall, the results indicate that while all examined control strategies operate within acceptable performance limits and comply with grid-connection requirements, the SRF approach provides the highest waveform quality, followed by DPC. In comparison, ICC and DCC exhibit relatively higher harmonic content and minor reductions in phase accuracy.

III.6 Conclusion

This chapter has presented a comprehensive performance assessment of grid-connected photovoltaic (PV) systems through detailed simulation studies covering system topology, maximum power point tracking (MPPT) algorithms, and inverter control strategies. The obtained results consistently demonstrate the superiority of the single-stage configuration, which offers reduced power losses, enhanced operational efficiency, and a simplified control structure, making it particularly well suited for large-scale practical applications.

The evaluation of MPPT algorithms under diverse operating scenarios indicates that metaheuristic-based techniques—especially the Grey Wolf Optimiser (GWO)—provide the best trade-off between fast convergence and high tracking accuracy. In contrast, the conventional Incremental Conductance (INC) algorithm, although computationally efficient, shows notable limitations under rapidly changing irradiance and partial shading conditions. The Particle Swarm Optimisation (PSO), Cuckoo Search (CS), and Whale Optimisation Algorithm (WOA) also exhibit stable and reliable performance, confirming their suitability for practical PV applications.

With regard to inverter control strategies, the Synchronous Reference Frame (SRF) approach achieves the lowest total harmonic distortion and the highest current quality, followed closely by Direct Power Control (DPC). Although Indirect Current Control (ICC) and Direct Current Control (DCC) present relatively higher harmonic levels, their performance remains within acceptable grid-connection limits. These results highlight the critical role of control strategy selection in ensuring power quality and compliance with grid standards.

Overall, the combined use of a single-stage PV topology, metaheuristic MPPT techniques, and advanced inverter control strategies establishes a robust and efficient framework for reliable grid-connected PV system operation. Building upon these simulation-based findings, the following chapter focuses on the practical implementation of the proposed system, where the designed configurations and algorithms are experimentally validated under realistic operating conditions. This transition provides an essential link between theoretical analysis and real-world performance, enabling a comprehensive evaluation of the system's effectiveness in practical environments.

Chapter IV

Design, Implementation, and Experimental Validation of a Grid-Connected PV System

IV.1 Introduction

Following the comprehensive simulation-based analysis presented in the previous chapter, this section advances towards the practical realisation of the grid-connected photovoltaic (PV) system. The transition from modelling and simulation to physical implementation is a critical stage in validating theoretical assumptions and verifying the actual performance of the proposed designs and control strategies under real-world operating conditions.

This chapter details the complete process of developing and testing the experimental PV platform, encompassing both hardware and control system implementation. It begins with the design of the inverter and its associated gate driver circuitry, forming the core of the power conversion interface between the photovoltaic generator and the grid. Particular attention is given to ensuring system robustness, safety, and fidelity to the simulation models previously developed.

Subsequently, the experimental setup is presented, highlighting the measurement instruments, data acquisition systems, and configuration used for system validation. A series of controlled experiments are conducted to assess the effectiveness of the maximum power point tracking (MPPT) algorithms and the performance of the inverter control strategies under various irradiance conditions, including both uniform and partial shading scenarios.

The obtained experimental results are then analysed and compared with simulation outcomes to evaluate consistency, accuracy, and dynamic performance. In particular, the investigation focuses on the quality of the grid-injected current and voltage signals, total harmonic distortion (THD), and current balance among the phases—key indicators of system compliance with grid standards and overall operational stability.

Finally, the discussion consolidates the experimental findings, highlighting the strengths and limitations of each control method, and provides insights into the practical challenges encountered during implementation. These results serve as a foundation for further optimisation of the system and confirm the feasibility of deploying the proposed PV control and conversion architecture in real grid-connected applications.

IV.2 Preparation and Development of the Experimental Platform

IV.2.1 Inverter Design and Hardware Implementation

As outlined in the preceding chapters, the inverter constitutes a fundamental component in grid-connected photovoltaic (PV) systems, as it undertakes the conversion of direct current (DC) generated by the PV array into alternating current (AC) synchronised with the grid voltage and frequency. Among the available topologies, the two-level, three-phase inverter stands out due to its structural simplicity, reliable performance, acceptable efficiency, and practical ease of implementation at the hardware level.

The scope of this thesis extends beyond theoretical analysis, encompassing the design and practical implementation of the inverter, together with experimental validation of its performance in alignment with PV system requirements. This work involves the design of the power stage, the development of the gate drive circuitry, the realisation of a dedicated printed circuit board (PCB), and the integration of protective circuits to enhance output quality and mitigate electrical stresses. This integrated approach offers a comprehensive platform suitable for future improvements and seamless integration with grid-connected PV systems. The implementation can be divided into two principal parts, as detailed below.

IV.2.1.1 Power Conversion Stage

The power stage represents the operational core of the inverter, where DC power is converted into three-phase AC power. It consists of three legs connected in parallel to the DC-link, each comprising two semiconductor switches (typically IGBTs or MOSFETs) connected in series, accompanied by anti-parallel freewheeling diodes.

Insulated Gate Bipolar Transistors (IGBTs) are extensively employed in three-phase inverters, owing to their advantageous features such as high input impedance through gate isolation, fast switching capability, robust thermal stability, ease of gate drive, and their ability to withstand high blocking voltages while offering controllable switching behaviour for short-circuit protection. For this design, FGH60n60 Field-Stop IGBTs were selected, rated for a continuous current of up to 60 A and a blocking voltage of 600 V. These devices exhibit both fast switching characteristics and strong thermal reliability, making them particularly suitable for the switching frequencies required in PV applications, thereby providing flexibility across a range of practical power levels.

The theoretical circuit diagram was initially developed using Proteus and subsequently translated into a PCB layout.

To enhance output quality, improve system efficiency, and increase inverter reliability, RCD snubber circuits were incorporated. These limit the voltage overshoots associated with rapid switching, thereby safeguarding the IGBTs against electrical stress. Furthermore, the DC-link capacitors were deliberately placed externally, offering greater flexibility in selecting their capacitance values to suit various experimental scenarios or future optimisations. Collectively, these design decisions guarantee stable and efficient performance under realistic operating conditions.

IV.2.1.2 Gate Driver Circuit Design

The bipolar gate drive circuit plays a critical role in ensuring the proper and efficient operation of the IGBTs, by supplying the appropriate voltage and current levels for fast and precise switching, while simultaneously minimising power losses.

In this design, as illustrated in Figure IV.1, isolated 24 V supplies were generated using six 220/24 V transformers, thereby ensuring complete electrical isolation for each gate drive unit. The supply voltage was further divided using a 511 Ω resistor and a 15 V Zener diode, to provide +15 V and –8 V drive levels. This arrangement achieves a balance between accurate regulation and the galvanic isolation required between the low-voltage control domain and the high-voltage gate drive domain.

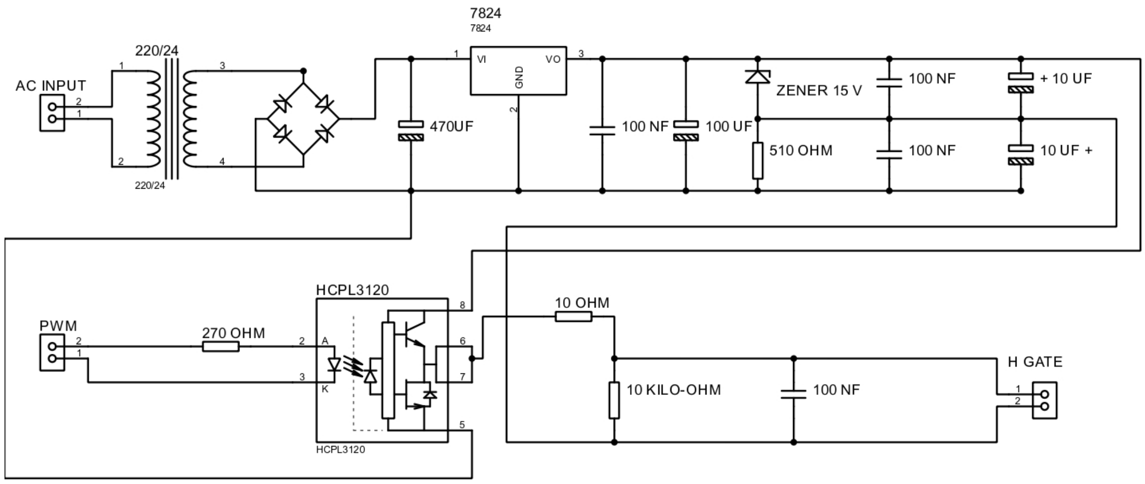

Figure IV.1: Schematic diagram of the gate drive circuit.

From the primary 24 V source, the optocoupler HCPL-3120 was employed as the core signal isolation and drive device. It not only ensures optical isolation between the control circuitry and the high-voltage power stage, but also delivers the necessary drive voltages (+15 V for turn-on and –8 V for turn-off) with robust immunity to high dv/dt conditions during switching. In addition, the HCPL-3120 integrates key protection features, including undervoltage lockout (UVLO), thereby safeguarding the IGBTs under abnormal operating conditions and ensuring stable and reliable operation.

The positive gate bias (+15 V) ensures rapid and efficient turn-on of the IGBT devices, while the negative gate bias (–8 V) prevents false turn-on events caused by rapid voltage transients. This dual-level approach provides additional flexibility in fine-tuning the switching dynamics, leading to improved control accuracy, faster transient response, and enhanced overall inverter performance.

The inverter design presented in this thesis demonstrates a cohesive integration of theoretical study, simulation, and practical implementation. The developed system not only fulfils the operational requirements of grid-connected PV inverters, but also offers a flexible experimental platform amenable to further development.

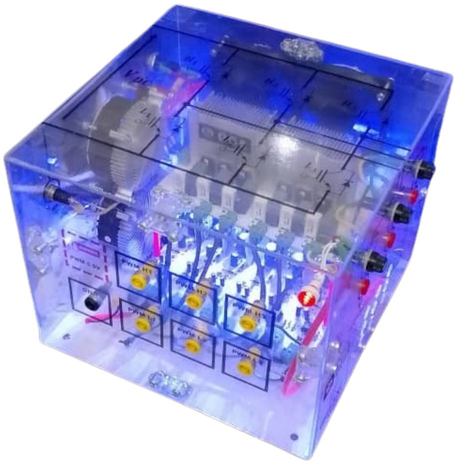

Figure IV.2: Final implemented inverter system.

As illustrated above, this inverter should not be regarded solely as a preliminary research prototype, but as a practical system that bridges academic investigation and industrial application, paving the way for future enhancements and integration into renewable energy solutions.

IV.2.2 Experimental Setup for System Validation

As part of the experimental verification of the performance of a single-stage grid-connected photovoltaic system, a dedicated test platform was developed in the **LGEB** laboratory. Figure IV.3 illustrates the general schematic of the system, which consists of two photovoltaic panels supplying a custom-built three-phase inverter. The inverter is connected to the electrical grid through an *L-type* filter and a three-phase autotransformer.

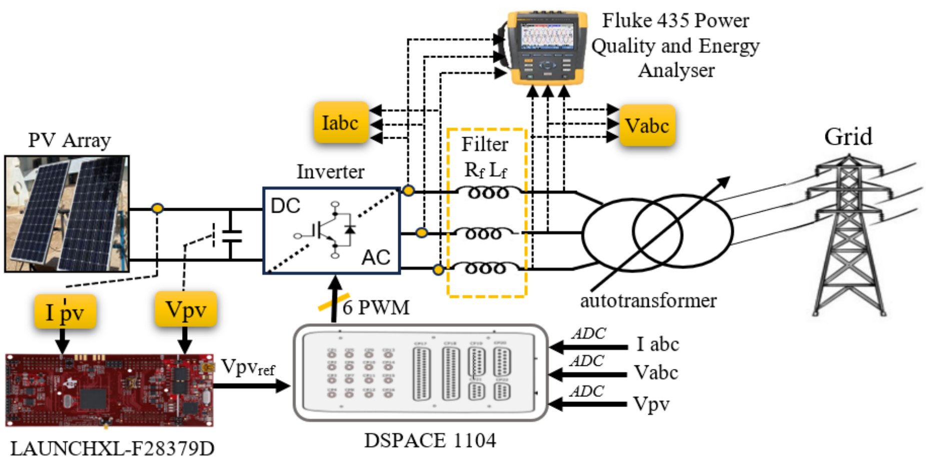

Figure IV.3: General schematic of the grid-connected photovoltaic experimental system.

The implementation of the proposed control framework was distributed across two complementary hardware platforms:

- the **DSP F28379D** digital controller from *Texas Instruments*.
- the **dSPACE 1104** board.

This division of tasks was introduced with the aim of enhancing computational efficiency, improving sampling performance, and ensuring the reliable operation of the grid-connected photovoltaic system.

The **DSP F28379D** is a member of the *C2000* family, specifically designed for real-time control in power electronics and renewable energy applications. It features a dual-core architecture operating at a frequency of up to 200 MHz, high-resolution PWM units, and multiple 16-bit ADC channels capable of acquiring data both rapidly and accurately. In addition, the integration of a floating-point unit (FPU) facilitates the execution of real-time algorithms by reducing the computational burden associated with complex mathematical operations. Owing to these advantages, the DSP was assigned the task of executing the maximum power point tracking (MPPT) algorithm and generating the corresponding reference voltage for the photovoltaic array.

The calculated reference voltage is subsequently transmitted to the **dSPACE 1104** platform, which is an advanced system for rapid control prototyping. This board integrates seamlessly with the *MATLAB/Simulink* environment, enabling automatic code generation and real-time parameter tuning via the *ControlDesk* interface. It also offers a wide range of analogue and digital input/output channels, allowing effective interaction with the inverter stage and measurement devices. Benefiting from these features, the dSPACE 1104 was employed to implement the inverter control strategy, ensuring synchronisation with the grid and maintaining operational stability under varying conditions.

This functional distribution – with the MPPT algorithm executed on the DSP F28379D and inverter control implemented via the dSPACE 1104 – achieves an efficient allocation of computational load, enhances the system's dynamic response, and ensures accurate operation of the photovoltaic system as a whole.

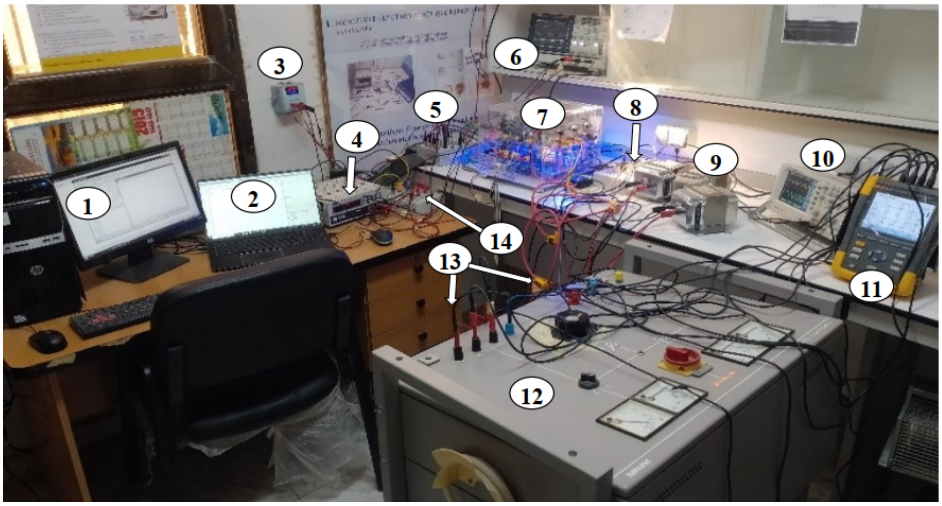

Figure IV.4: Photograph of the realised experimental platform in the LGEB laboratory.

Figure IV.4 presents a photograph of the realised experimental platform. The hardware configuration included a DC-link capacitor rated at 2200 μF, an *L-type* inductor of 10 mH, and a three-phase autotransformer rated at 21/380 V. The experiments were conducted on **11 March 2024** under clear weather conditions with gradual variations in solar irradiance. The main components of the experimental setup are listed below:

1. Control computer dedicated to the dSPACE 1104.
2. Laptop computer used to interface with the LAUNCHXL-F28379D.
3. Input from the photovoltaic panel array.
4. Development board LAUNCHXL-F28379D.
5. Real-time control unit dSPACE DS1104.
6. Oscilloscope for DC-side measurements.
7. Three-phase inverter.
8. Voltage and current sensors for the AC side.
9. L-type filter.
10. Oscilloscope for AC-side measurements.
11. Power quality analyser Fluke 435.
12. Three-phase autotransformer.
13. Voltage and current probes (Fluke).
14. Voltage and current sensors for the DC side.

IV.3 Experimental Results and Discussion

IV.3.1 MPPT System Performance

IV.3.1.1 Under Uniform Solar Irradiance

In this study, the photovoltaic system consists of two solar panels connected in series, as illustrated in Figure IV.5. The main electrical parameters of this module under standard test conditions (STC) are summarised in Table IV.1.

To characterise the panels, measurements were conducted using the **LAUNCHXL-F28379D** launchpad combined with DC voltage and current sensors. Under uniform irradiance, the power–voltage (P–V) and current–voltage (I–V) curves, shown in Figure IV.6, exhibit a single and distinct Maximum Power Point (MPP), confirming the stable and efficient behaviour of the PV system.

Figure IV.5: Experimental setup of the PV system.

Table IV.1: Electrical specifications of the PV module under STC.

Parameter	**Value**
Rated Maximum Power (P_{max})	190 W
Voltage at P_{max} (V_{mp})	36.6 V
Current at P_{max} (I_{mp})	5.20 A
Open-Circuit Voltage (V_{oc})	45.2 V
Short-Circuit Current (I_{sc})	5.62 A

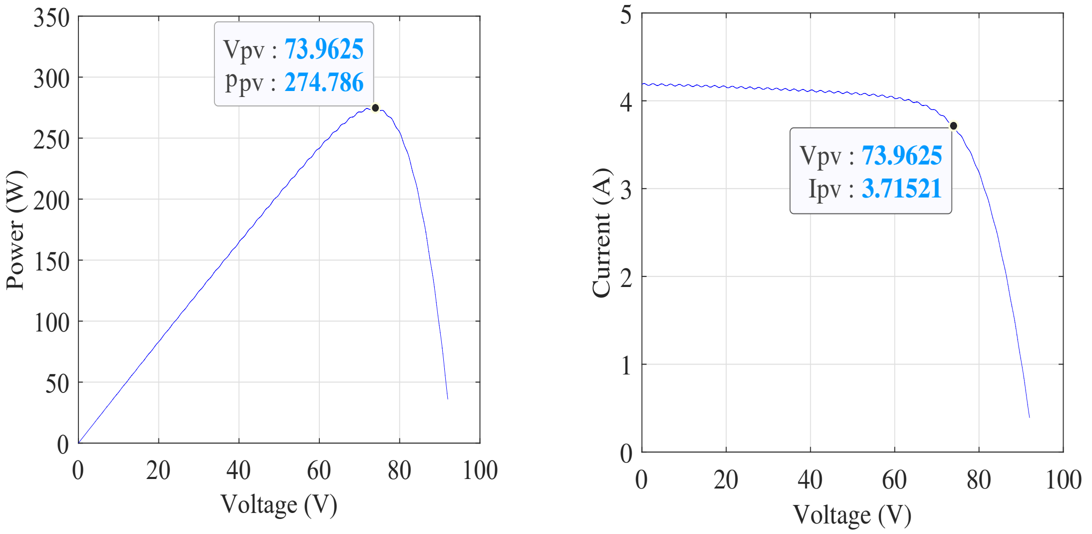

(a) P–V characteristic under uniform irradiance.

(b) I–V characteristic under uniform irradiance.

Figure IV.6: P–V and I–V characteristics of the PV system under uniform irradiance.

Following this characterisation, five MPPT algorithms—PSO, CS, WOA, GWO, and INC—were applied under the same uniform irradiance to evaluate their dynamic performance and tracking accuracy. Figures IV.7–IV.11 show the corresponding experimental outcomes.

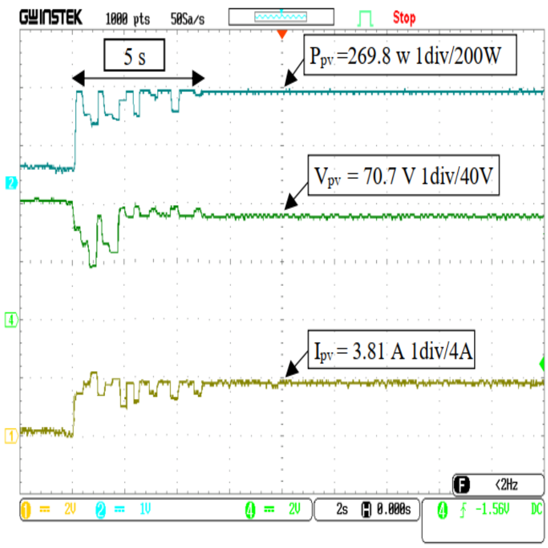

Figure IV.7: Experimental result using PSO.

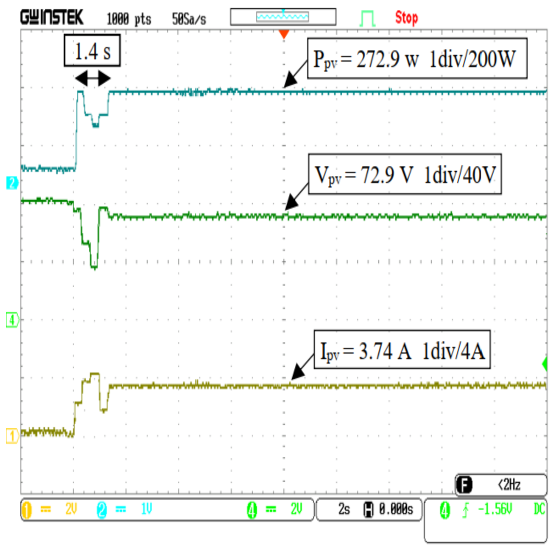

Figure IV.8: Experimental result using GWO.

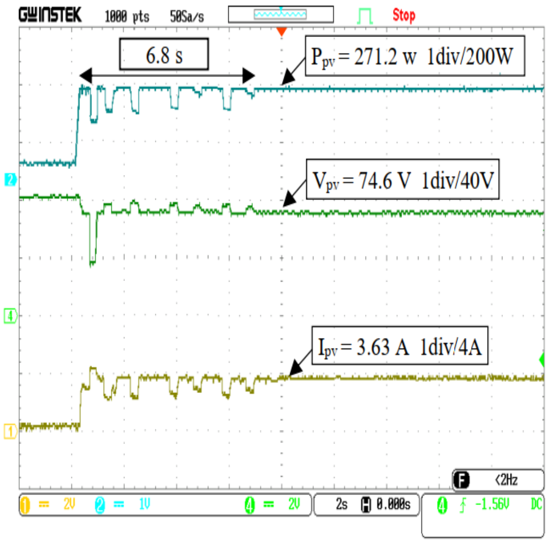

Figure IV.9: Experimental result using WOA.

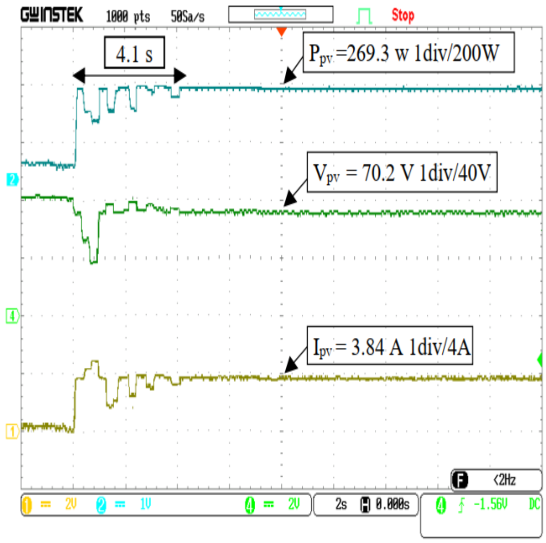

Figure IV.10: Experimental result using CS.

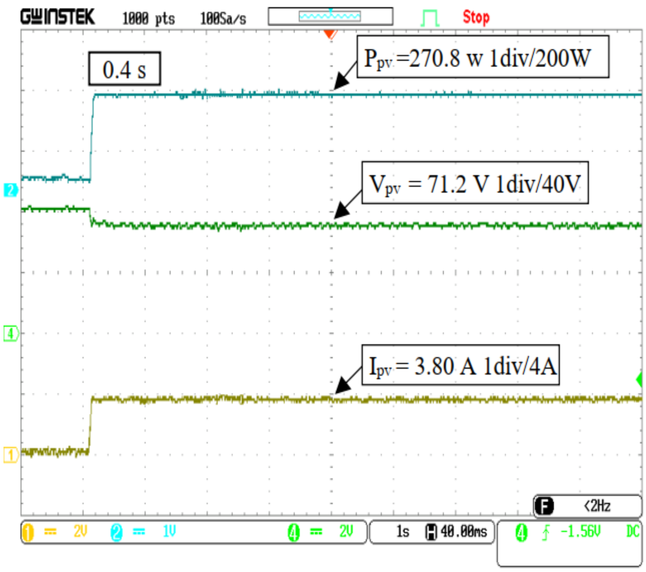

Figure IV.11: Experimental result using INC.

IV.3.1.2 Under Partial Shading Conditions

The same measurement setup was used to assess the panel behaviour under partial shading. As illustrated in Figure IV.12, this condition resulted in the appearance of one Global Maximum Power Point (GMPP) at 191.7 W and two Local Maximum Power Points (LMPPs) at 94.33 W and 67.54 W on the P–V curve. These results clearly demonstrate that shading introduces multiple local peaks, thereby reducing the overall efficiency of the photovoltaic system and increasing the complexity of tracking the true maximum power point.

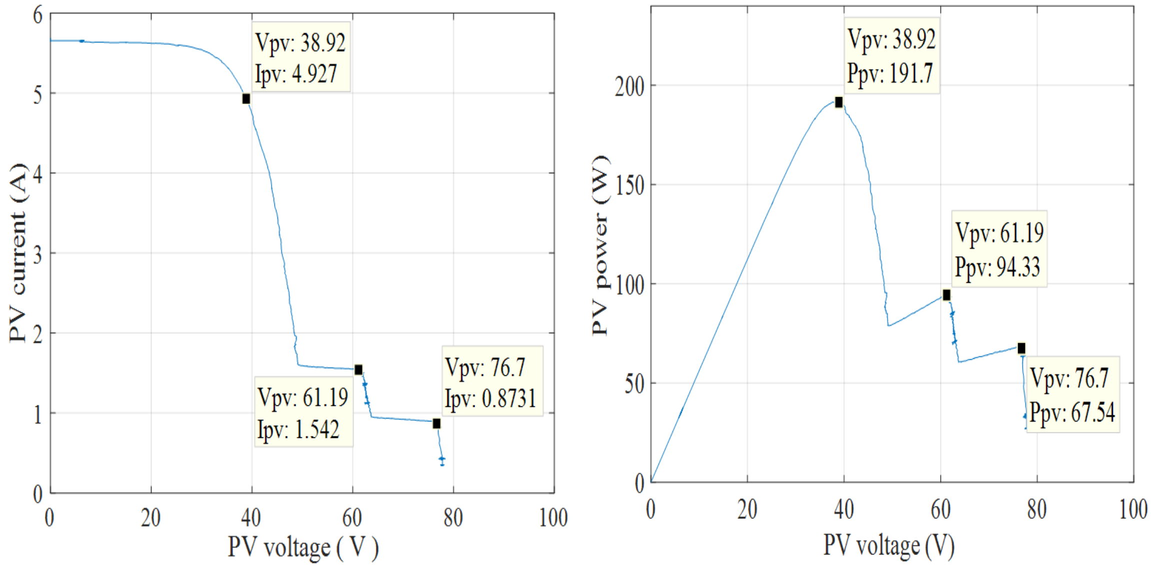

(a) I–V characteristic under partial shading. (b) P–V characteristic under partial shading.

Figure IV.12: P–V and I–V characteristics of the PV system under partial shading conditions.

These current–voltage (I–V) and power–voltage (P–V) characteristics provide a clear representation of the behaviour of the photovoltaic system under partial shading conditions. They also constitute a reference framework for evaluating the dynamic response illustrated in Figures IV.15–IV.17 and the tracking efficiency of the implemented maximum power point tracking (MPPT) algorithms in the subsequent experimental analysis.

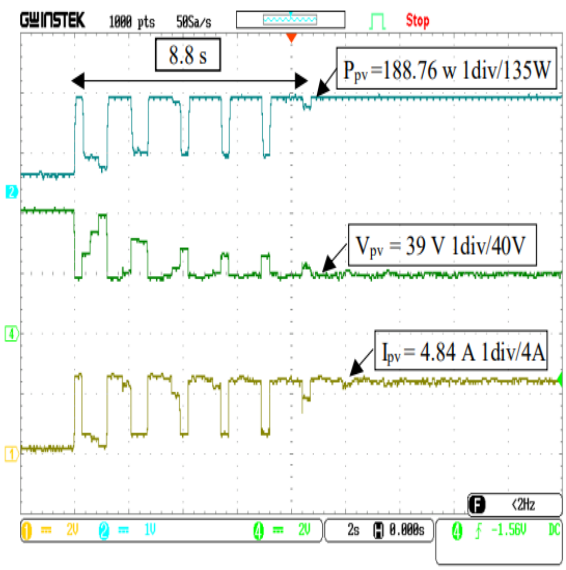

Figure IV.13: Experimental result PSO.

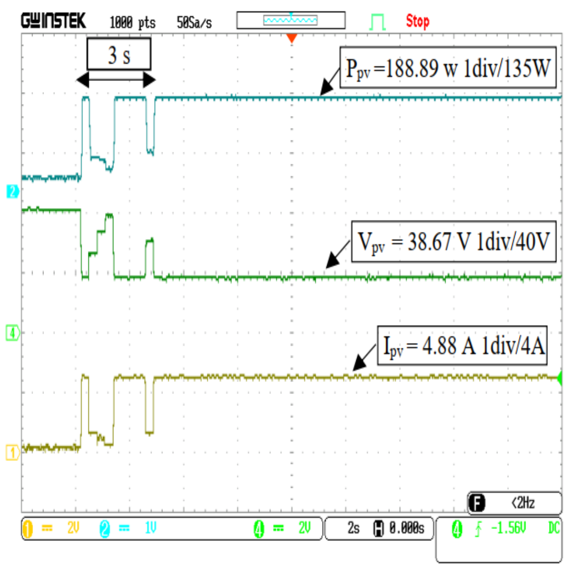

Figure IV.14: Experimental result CS.

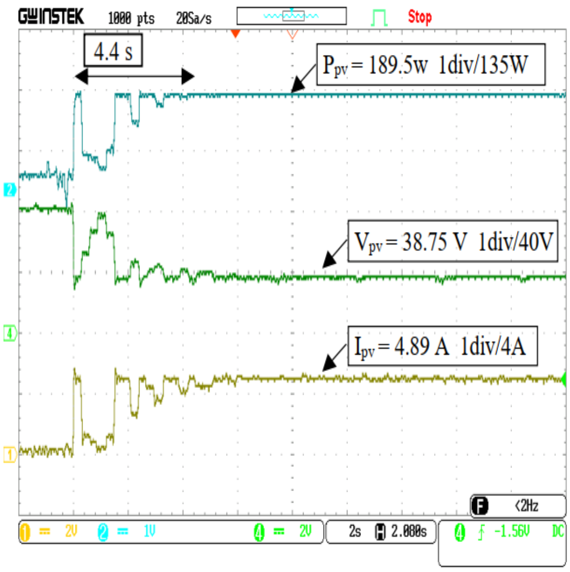

Figure IV.15: Experimental result WOA.

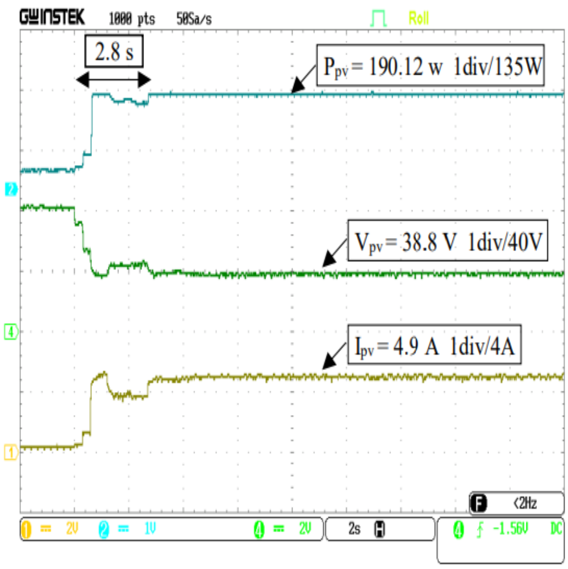

Figure IV.16: Experimental result GWO.

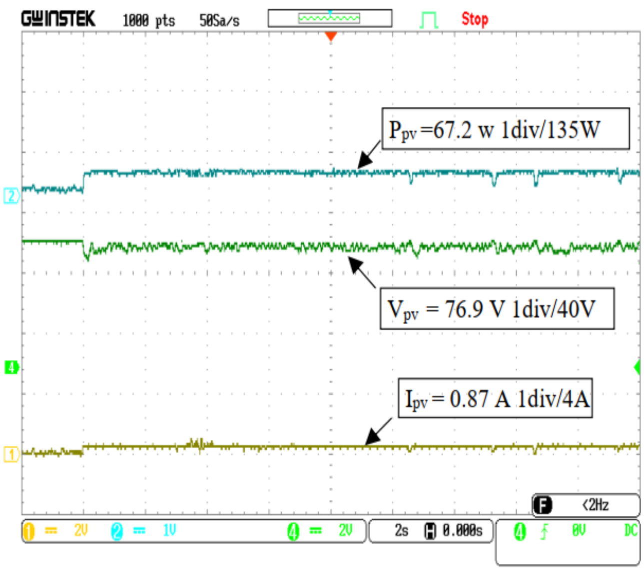

Figure IV.17: Experimental result using INC.

IV.3.1.3 Analysis and Discussion of Experimental Results

To provide a clearer comparative insight, and based on the results presented in Figures IV.15–IV.17. The Figure IV.18 presents a quantitative summary of the steady-state performance of the five MPPT algorithms under both uniform irradiance and partial shading conditions. The figure illustrates each algorithm's extracted power and corresponding convergence time, highlighting the relative differences in their accuracy and dynamic behaviour.

To provide a clearer comparative perspective,

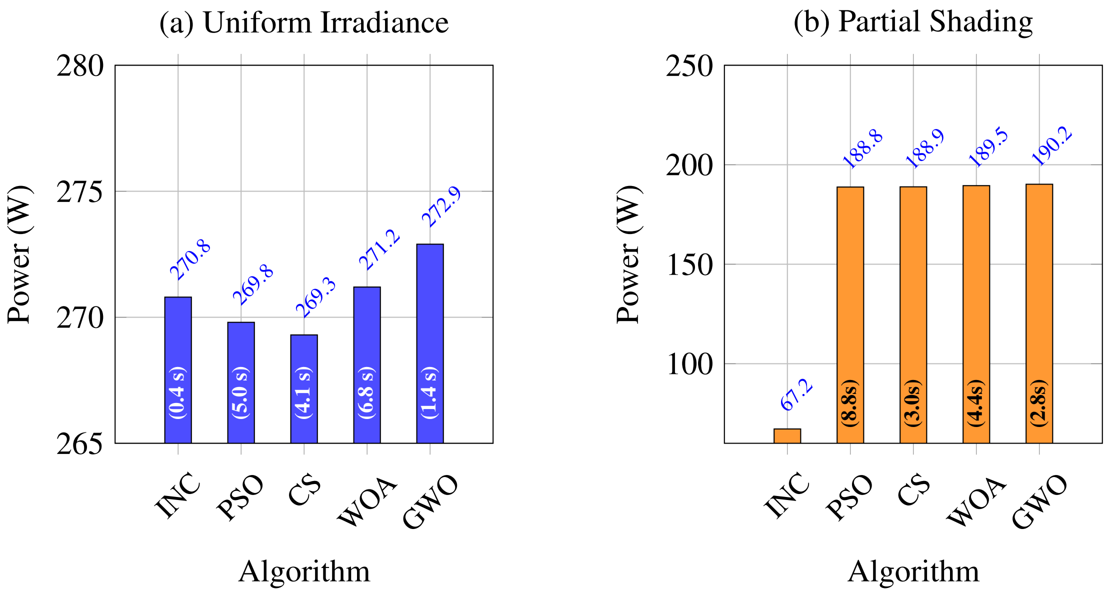

Figure IV.18: Comparison of MPPT algorithms under (a) uniform irradiance and (b) partial shading conditions.

Under experimental conditions, all algorithms successfully tracked the operating point of the photovoltaic system; however, their accuracy and dynamic responses varied notably. As presented in Figure IV.18(a), the **GWO** algorithm once again achieved the **highest extracted power of 272.9 W**, confirming its superior tracking capability observed in the simulation stage. The output voltage (72.9 V) remained very close to the MPP voltage illustrated in Figure IV.6, while the current value (3.74 A) indicated efficient utilisation of the PV array. Nevertheless, the convergence time increased to **1.4 s**, which is expected in real hardware implementations due to electronic delays and sensor response limitations.

The **Incremental Conductance (INC)** algorithm maintained the **fastest response** (0.4 s), consistent with its simulation behaviour, though at the expense of slightly lower accuracy, producing an extracted power of 270.8 W. This outcome reflects its reactive and rapid nature, yet also highlights its lower tracking stability under practical conditions characterised by electrical noise and parameter fluctuations.

Among the remaining metaheuristic techniques, **WOA**, **PSO**, and **CS** exhibited longer convergence times, ranging between 4 s and 6.8 s, indicating slower adaptation to the system's nonlinearities and measurement constraints. Nevertheless, their final power outputs (269–271 W) remained within acceptable limits, confirming stable yet less efficient tracking compared with GWO.

Overall, the **GWO algorithm** once again demonstrated the **best balance between power extraction, response speed, and dynamic stability**, confirming its robustness for real-time PV operation. The discrepancies between the experimental and simulation results can be attributed to inverter dynamics, sampling rate limitations, and analogue circuit delays. Furthermore, the strong performance of GWO reflects its capability to handle small fluctuations in voltage and current during the search for the MPP, making it a promising candidate for real-time PV control applications.

Under **partial shading conditions**, Figure IV.18(b) shows that the extracted power of all algorithms decreased compared with uniform irradiance, which is expected due to uneven solar distribution and the emergence of multiple local power peaks. Nevertheless, the performance differences among the tested algorithms were significant.

The **GWO algorithm** once again demonstrated the **highest tracking accuracy**, achieving an extracted power of **190.2 W** at 38.8 V and 4.90 A, with a convergence time of 2.8 s. This confirms its ability to locate the global maximum power point (GMPP) despite the presence of several local maxima, showcasing strong robustness and search efficiency under complex irradiance profiles.

The **WOA** and **CS** algorithms achieved similar performances, with power outputs of 189.5 W and 188.9 W, respectively. The CS method converged slightly faster (3.0 s) than WOA (4.4 s), indicating a marginally better dynamic response to non-uniform conditions. Meanwhile, the **PSO** algorithm extracted 188.8 W but exhibited the slowest response (8.8 s), reflecting its tendency to become trapped near local peaks before reaching the global optimum.

Conversely, the **Incremental Conductance (INC)** method completely failed to locate the global MPP, stabilising at a low-power point (67.2 W) with a high voltage of 76.9 V and a very low current of 0.87 A. This demonstrates its inherent limitation under partial shading, where the P–V curve becomes highly non-linear and multiple local maxima exist.

Overall, the metaheuristic-based algorithms, particularly GWO, proved substantially more effective than the classical INC method in managing partial shading. Their stochastic and population-based search mechanisms allow them to escape local maxima and identify the true global operating point. Hence, the GWO algorithm remains the most promising candidate for MPPT applications in PV systems exposed to dynamically changing and partially shaded environments.

IV.3.2 Grid-Injected Characteristics under Different Operating Conditions

Before presenting the experimental waveforms related to the grid side, it is worth emphasising that, under steady solar irradiance or moderate partial shading conditions, most Maximum Power Point Tracking (MPPT) algorithms tend to converge towards nearly the same operating point. Consequently, no considerable differences are observed in the injected voltage, current, or power waveforms. Therefore, presenting the results of every algorithm would add redundancy without providing additional analytical value. To maintain clarity and highlight the most relevant aspects, only **representative curves** are shown to illustrate the general performance behaviour of the system. The differences between the algorithms are discussed only when they become visibly significant or have a meaningful impact on grid-side operation or stability.

IV.3.2.1 Analysis of Injected Power under Different Operating Conditions

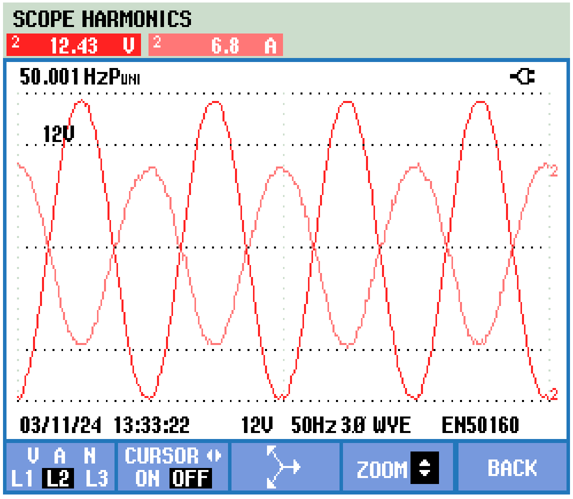

(a) Measured injected voltage and current under uniform irradiance.

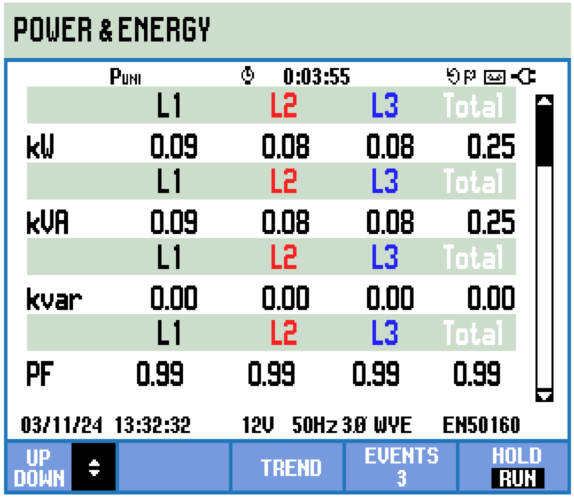

(b) Measured injected power under uniform irradiance.

Figure IV.19: Experimental voltage, current, and power waveforms of the grid-injected signals under uniform irradiance conditions.

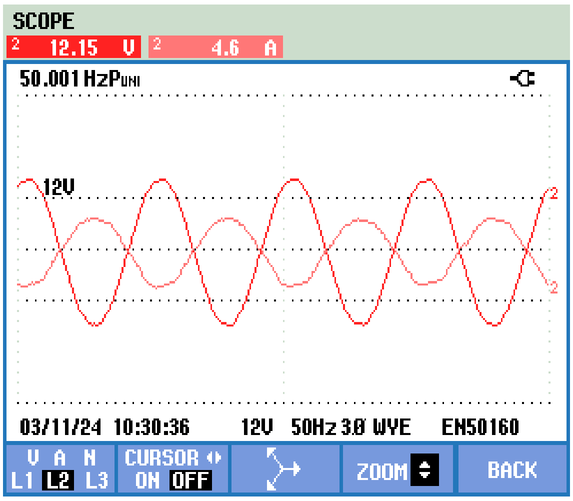

(a) Measured injected voltage and current under partial shading.

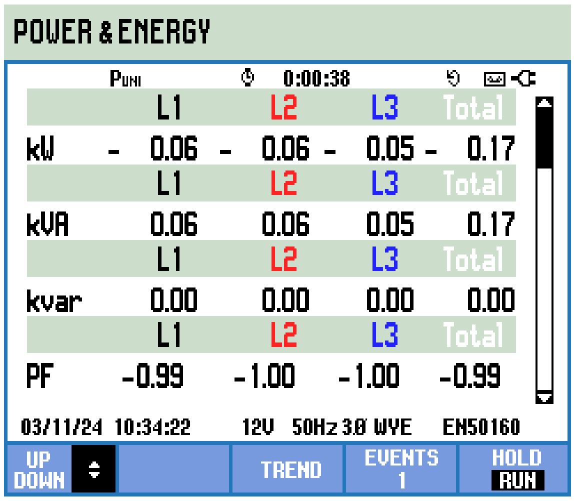

(b) Measured injected power under partial shading.

Figure IV.20: Experimental voltage, current, and power waveforms of the grid-injected signals under partial shading conditions.

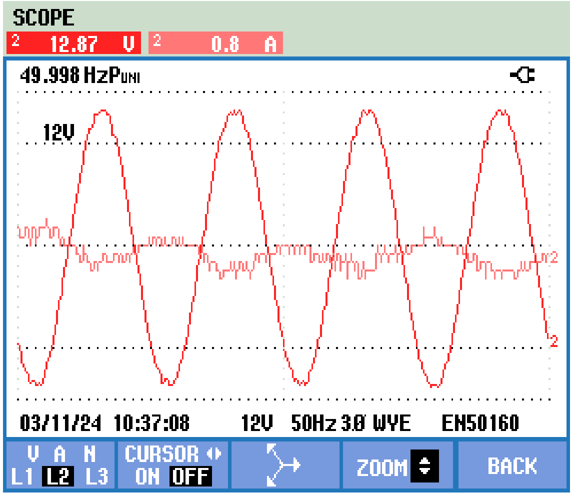

(a) Measured injected voltage and current under partial shading with the INC algorithm.

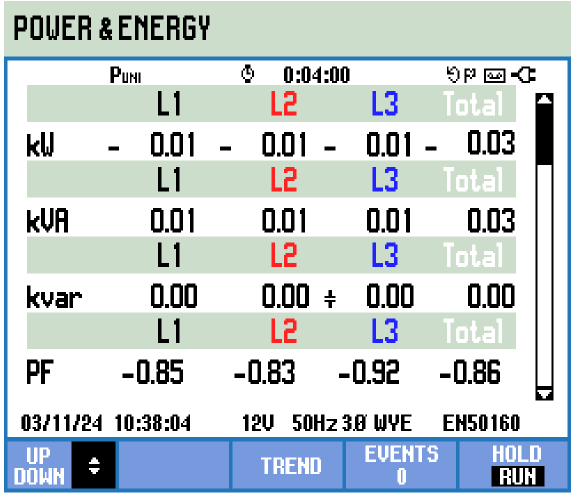

(b) Measured injected power under partial shading with the INC algorithm.

Figure IV.21: Experimental voltage, current, and power waveforms of the grid-injected signals under partial shading using the INC MPPT algorithm.

IV.3.2.2 Analysis of Current Unbalance in Grid-Injected Phases

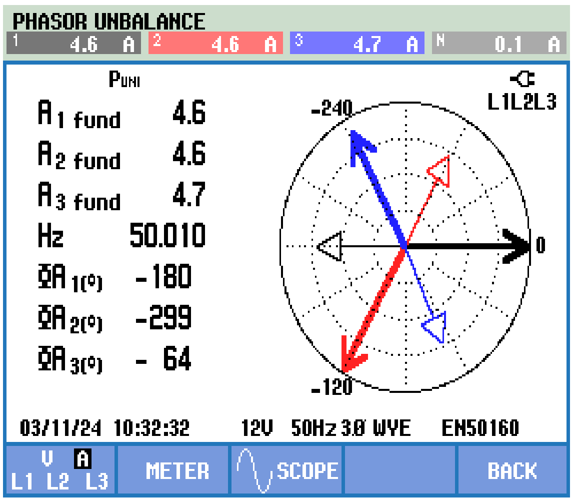

(a) Current unbalance observed using DCC and ICC control.

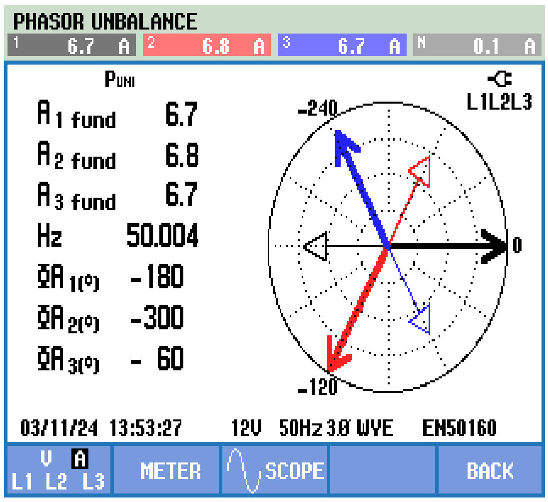

(b) Current unbalance observed using SRF and DPC control.

Figure IV.22: Observed current unbalance characteristics in the grid-connected PV inverter under experimental conditions.

IV.3.2.3 Total Harmonic Distortion (THD) Analysis

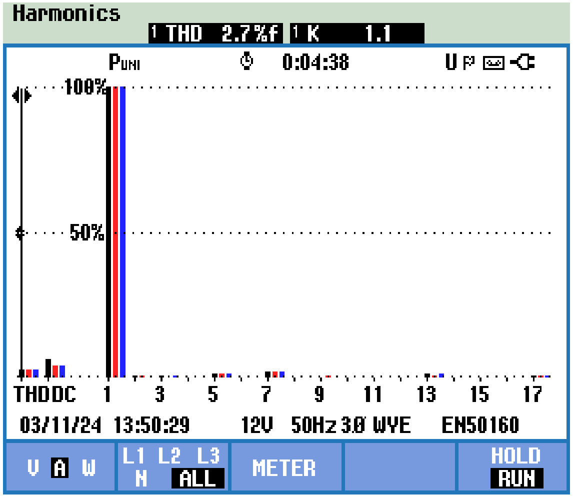

(a) Measured current THD using DPC control.

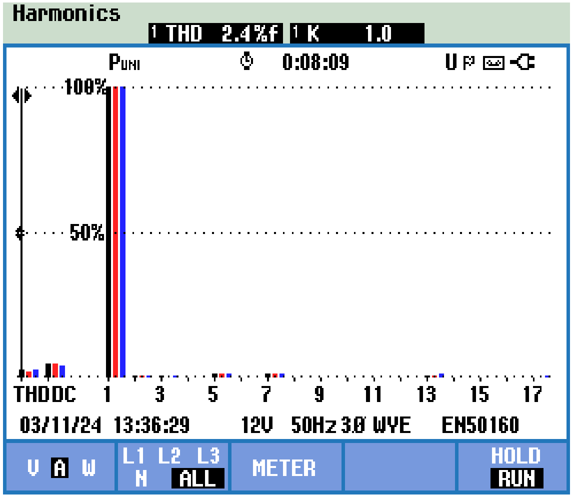

(b) Measured current THD using SRF control.

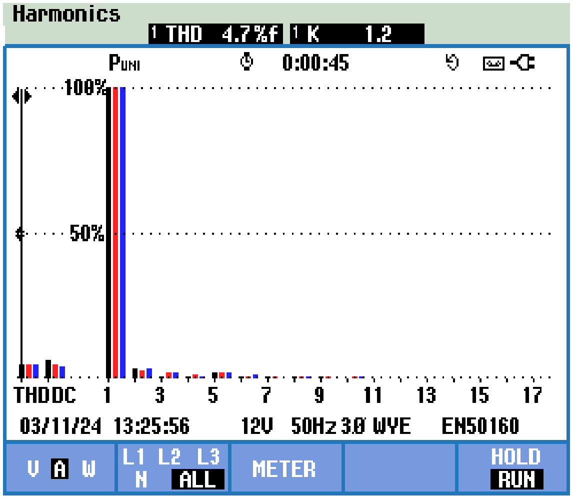

(c) Measured current THD using DCC control.

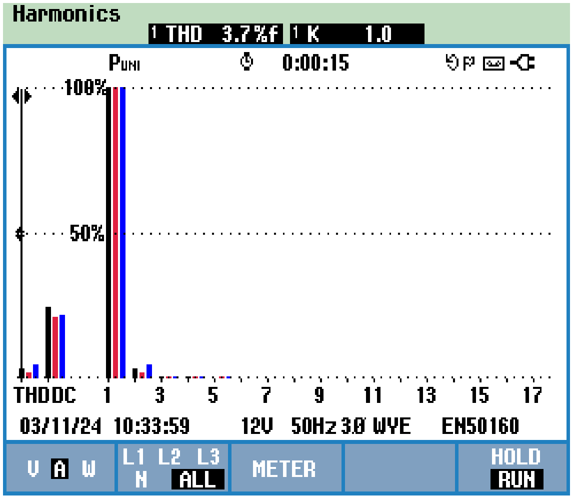

(d) Measured current THD using ICC control.

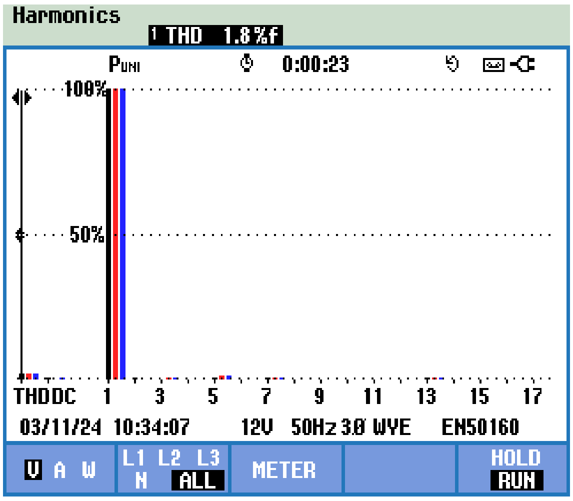

(e) THD of grid voltage.

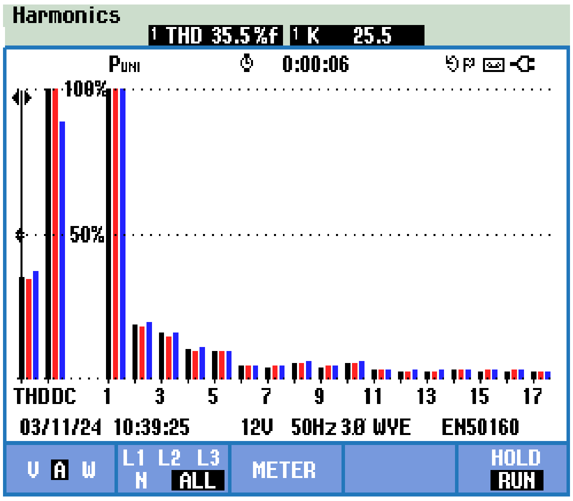

(f) THD under partial shading with the INC.

Figure IV.23: Measured total harmonic distortion (THD) of current and voltage under various inverter control strategies using the Fluke Power Analyzer.

IV.3.3 Analysis of Power Quality and Control Strategies in Grid Connection

The experimental results presented in Figures IV.19–IV.21 for the injected signals show that both the voltage and current waveforms exhibit good conformity, with a phase shift of approximately 180°, confirming that power transfer occurs towards the grid. Under uniform irradiance conditions, the measured voltage and current in the steady-state operation were about 12.43 V and 6.8 A, respectively, corresponding to an injected power of approximately 0.25 kW and a high power factor of nearly 0.99. In comparison, the extracted PV array power was around 272 W, indicating that the difference is mainly due to inverter and grid-interface losses.

When partial shading was applied, both voltage and current decreased to around 12.15 V and 4.6 A, yielding an injected power of 0.17 kW while maintaining the same power factor (PF $\approx$ 0.99). However, the *Incremental Conductance (INC)* algorithm exhibited a clear inability to escape the local maximum power point under these conditions. Consequently, the voltage and current dropped to 12.87 V and 0.8 A, respectively, resulting in a very low injected power of about 0.03 kW and a decreased power factor of 0.85. These findings highlight the limitations of conventional MPPT techniques such as INC in handling non-uniform irradiance and demonstrate the advantage of recent metaheuristic algorithms in achieving more robust and adaptive global tracking.

IV.3.3.1 Comparative analysis of injected power quality

The comparative analysis revealed that the performance of grid control strategies differs not only in terms of the total harmonic distortion (THD) but also in their dynamic response and resilience to voltage or current disturbances, as shown in Figure IV.23–IV.24. Among the examined methods, the Synchronous Reference Frame (SRF) and Direct Power Control (DPC) achieved the best results in waveform purity and operational stability, whereas Indirect Current Control (ICC) and Direct Current Control (DCC) presented relatively lower quality responses.

The superiority of SRF can be attributed to the use of Park transformations, which decouple the active and reactive current components in the synchronised dq frame, allowing precise regulation of the injected current and near-unity power factor. Since the control is performed on quasi-DC signals, the SRF method effectively minimises harmonic content, yielding a low THD ($\approx$ 2.4%) and smooth, stable operation even under moderate fluctuations of irradiance or grid voltage.

On the other hand, DPC relies on real-time monitoring of instantaneous power flow and directly selects the appropriate inverter switching state based on the deviation between reference and measured power. This direct structure offers faster transient response and excellent power quality with a THD of approximately 2.7%. Moreover, DPC maintains robustness against minor grid voltage disturbances without requiring additional filters, which makes it particularly suitable for applications demanding rapid dynamic correction.

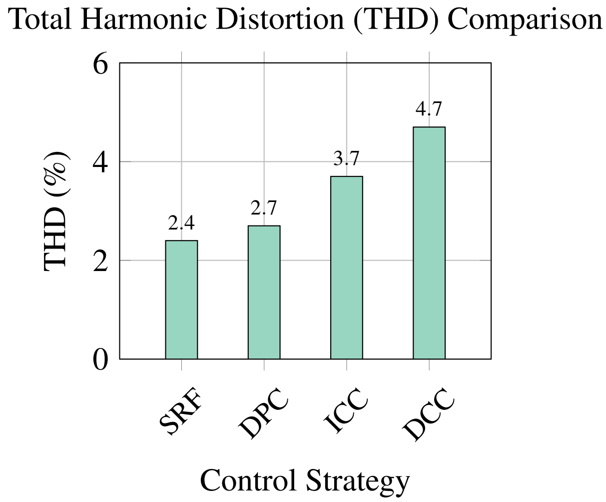

Figure IV.24: Comparison of Total Harmonic Distortion (THD) for different control strategies.

Conversely, both ICC and DCC exhibit slower dynamic performance because their operation depends on direct comparison between reference and measured currents through proportional–integral (PI) controllers. The switching-based nature of DCC produces small current ripples that increase THD to around 4.7%. These effects become more pronounced under partial shading, where maintaining current stability and phase balance becomes crucial.

IV.3.3.2 Phase and frequency stability analysis

Based on the results shown in Figure IV.22 ,The phase-angle evaluation demonstrates that the SRF and DPC controllers preserve highly stable synchronisation with the grid. The measured phase displacement across the three phases remains tightly clustered around the expected theoretical values, with angles of approximately $-60°$, $-180°$, and $-300°$. This consistency indicates accurate tracking of the grid voltage vector and strong robustness under dynamic operating conditions.

In comparison, the DCC and ICC controllers exhibit slightly larger angular deviations, recording phase values of about $-64°$, $-180°$, and $-299°$. Although these deviations reflect slower current-response dynamics, they remain sufficiently close to the reference values, ensuring acceptable synchronisation quality.

Regarding frequency performance, both SRF and DPC maintain an almost constant operating frequency of 50.004 Hz, confirming their superior precision in grid alignment. Conversely, DCC and ICC show small oscillatory variations around 50.010 Hz, attributable to delayed current regulation. Nonetheless, the fluctuations remain within acceptable stability margins.

IV.3.3.3 Overall performance evaluation

Overall, the results indicate that SRF provides the highest waveform purity due to its capability to control the active and reactive current components independently, while DPC offers the fastest transient behaviour through instantaneous power regulation. Both methods deliver excellent grid-injection quality, whereas DCC and ICC are more appropriate for low-cost or less dynamic systems where simplicity is prioritised over precision. These findings ultimately underline the importance of combining advanced MPPT algorithms such as GWO or WOA with high-accuracy grid control strategies (SRF or DPC) to achieve more efficient and stable photovoltaic power conversion systems.

IV.4 Conclusion

This chapter has presented one of the main contributions of this thesis, namely the experimental validation of a single-stage grid-connected photovoltaic (PV) system. The work encompassed the complete design, implementation, and experimental assessment of the proposed system, starting from the development of an upgraded three-phase inverter that provides a flexible experimental platform for the evaluation of different control strategies and Maximum Power Point Tracking (MPPT) algorithms. System performance was examined under a range of operating conditions, including uniform solar irradiance and partial shading scenarios, thereby ensuring a realistic and comprehensive validation framework.

The experimental results demonstrated that, under uniform irradiance conditions, the system operated with a high power factor close to 0.99 and achieved an injected grid power of approximately 0.25 kW, indicating efficient power conversion. Under partial shading conditions, the injected power decreased to about 0.17 kW, highlighting the impact of non-uniform irradiance on system performance. In this operating regime, the Incremental Conductance (INC) algorithm showed clear limitations in escaping local maxima, whereas metaheuristic-based MPPT techniques, particularly the Grey Wolf Optimisation (GWO) and Whale Optimisation Algorithm (WOA), exhibited superior adaptability and more effective tracking of the global maximum power point.

In terms of grid interaction, signal quality, and synchronisation, the Synchronous Reference Frame (SRF) and Direct Power Control (DPC) strategies provided the best overall performance, achieving low Total Harmonic Distortion (THD) levels of approximately 2.4% and 2.7%, respectively, alongside stable operation. By contrast, the Indirect Current Control (ICC) and Direct Current Control (DCC) strategies resulted in higher current distortion levels.

The superior performance of the SRF approach can be attributed to its use of Park transformations, which enable an effective decoupling of active and reactive current components, allowing precise current regulation and operation at a near-unity power factor.

Overall, the findings of this chapter confirm that the proposed system architecture ensures stable grid power injection and high-quality current waveforms in compliance with grid standards. Moreover, the experimental results underline the effectiveness of combining advanced MPPT algorithms—such as GWO or WOA—with accurate grid control strategies, such as SRF or DPC, in order to enhance power conversion efficiency and improve the dynamic stability of grid-connected photovoltaic systems.

General Conclusion

This thesis has presented a comprehensive study of grid-connected photovoltaic (PV) systems, encompassing mathematical modelling, optimisation, numerical simulation, and experimental validation. The work was organised in a progressive and coherent manner to develop an integrated understanding of PV system behaviour, from theoretical foundations to practical implementation, while accounting for technical challenges and real-world industrial constraints.

The theoretical analysis demonstrated that the optimisation of photovoltaic system performance relies on three interrelated pillars, which together form the basis of effective strategies for performance enhancement, system stability, and operational efficiency:

- **First pillar:** Maximum Power Point Tracking (MPPT), which represents the most critical component by ensuring fast dynamic response, high tracking accuracy, and robustness against variations in irradiance, temperature, and partial shading conditions.
- **Second pillar:** The quality of power injected into the electrical grid, which is primarily influenced by the inverter control strategy through its impact on current waveform quality, total harmonic distortion (THD), and grid synchronisation capability.
- **Third pillar:** System topology selection, which has received relatively limited attention in previous studies, concerns the choice between single-stage and two-stage architectures, given its decisive role in efficiency improvement, loss reduction, and control structure simplification.

Based on this framework, the simulation phase initially focused on analysing different PV system topologies to identify an optimal structure that balances efficiency and control simplicity. A comparative analysis between single-stage and two-stage configurations demonstrated that:

- Single-stage systems achieve higher efficiency, with an approximate loss reduction of 5% compared to two-stage systems, while benefiting from simpler control structures.
- Two-stage systems offer greater operational flexibility; however, this advantage is accompanied by increased losses and higher control complexity.

After selecting the optimal topology, various MPPT algorithms were evaluated, including classical methods such as Incremental Conductance (InC) and advanced metaheuristic techniques such as Grey Wolf Optimisation (GWO), Particle Swarm Optimisation (PSO), Cuckoo Search (CS), and the Whale Optimisation Algorithm (WOA). These algorithms were tested under uniform irradiance, rapid environmental variations, and partial shading conditions. The results demonstrated that:

- Classical methods (INC), provide fast and satisfactory performance under uniform irradiance but fail to track the global maximum power point under partial shading conditions, leading to noticeable energy losses.
- Metaheuristic algorithms exhibit superior global tracking capability and effective avoidance of local optima, with an inherent trade-off between convergence speed and tracking accuracy.
- Among the evaluated algorithms, GWO emerged as the most balanced solution in terms of speed, accuracy, and stability.

Several inverter control strategies were analysed to ensure high-quality power injection and compliance with grid-connection requirements, including the Synchronous Reference Frame (SRF), Direct Power Control (DPC), Indirect Current Control (ICC), and Direct Current Control (DCC). The results confirmed that:

- All investigated strategies achieve acceptable performance and comply with international grid-connection standards.
- The SRF and DPC strategies provide superior current waveform quality, reduced total harmonic distortion, and enhanced grid synchronisation capability.

Since simulation results alone are insufficient to fully validate system performance, particular emphasis was placed on experimental verification, which constitutes a key contribution of this thesis. The experimental results demonstrated that:

- The practical feasibility of real-time implementation of advanced control algorithms was successfully achieved through the design and implementation of an improved inverter prototype based on the DSP-F28379D digital signal processor.
- The effectiveness and reliability of MPPT algorithms and inverter control strategies were experimentally validated under both uniform irradiance and partial shading conditions.
- Experimental results showed strong agreement with simulation outcomes, with minor discrepancies attributed to unavoidable practical disturbances.

- Metaheuristic MPPT algorithms, particularly GWO, were experimentally confirmed to outperform classical methods in achieving global maximum power point tracking under partial shading conditions.
- Classical MPPT methods were verified to perform effectively under uniform irradiance but to converge toward local optima under partial shading conditions.
- All investigated inverter control strategies were experimentally validated to meet international standards, with SRF and DPC demonstrating clear performance advantages.

Overall, this thesis establishes a unified and efficient optimisation framework for grid-connected PV systems by integrating system topology selection, MPPT algorithms, inverter control strategies, and rigorous experimental validation within a high-efficiency single-stage architecture suitable for practical and industrial applications.

Based on the outcomes of this thesis, future research directions may focus on the following aspects:

- The development of advanced control strategies for the integration of large-scale photovoltaic systems into smart grid environments, with particular emphasis on dynamic grid interaction, voltage and frequency support, and enhanced operational reliability.
- The extension of microgrid applications through the design of control algorithms capable of ensuring seamless transitions between grid-connected and islanded operating modes, while maintaining effective power sharing, voltage stability, and supply continuity.
- The enhancement of the existing experimental platform by incorporating multi-level hierarchical control structures (primary, secondary, and tertiary levels), supported by reliable and low-latency communication architectures, enabling coordinated operation of distributed energy resources.
- The exploitation of smart inverter capabilities to provide grid ancillary services, including voltage support, reactive power compensation, harmonic mitigation, and participation in frequency regulation, thereby contributing to improved flexibility, reliability, and sustainability of modern power systems.

Bibliographic References

[1] International Renewable Energy Agency (IRENA), "Renewable capacity highlights 2024," 2024.

[2] A. Press, "Renewable energy jumps to new high, powered by china solar boom," 2025.

[3] Reuters, "Record renewables growth fuels cost competitiveness - irena report shows," 2024.

[4] International Renewable Energy Agency (IRENA), "Renewable energy roadmap: Algeria," 2023.

[5] R. Miles, K. Hynes, and I. Forbes, "Photovoltaic solar cells: An overview of state-of-the-art cell development and environmental issues," *Progress in Crystal Growth and Characterization of Materials*, vol. 51, no. 1-3, pp. 1–42, 2005.

[6] A. Sorokin, S. Bobashev, T. Feigl, K. Tiedtke, H. Wabnitz, and M. Richter, "Photoelectric effect at ultrahigh intensities," *Physical Review Letters*, vol. 99, no. 21, p. 213002, 2007.

[7] N.-G. Park, T. Miyasaka, and M. Grätzel, *Organic-inorganic halide perovskite photovoltaics*. Cham, Switzerland: Springer, 2020.

[8] M. BOUNABI, *Study of topologies and architectures of DC-AC photovoltaic converters connected to the grid*. PhD thesis, National Polytechnic School, Algeria, 2019.

[9] T. Bilal, *Contribution to Monitoring and Performance Analysis of Photovoltaic Systems*. PhD thesis, National Polytechnic School, Algeria, 2022.

[10] L. Abdelhamid, *Implementation of photovoltaic inverter controller on DSP*. PhD thesis, National Polytechnic School, Algeria, 2016.

[11] ScienceDirect, "Grid-connected photovoltaic systems," *ScienceDirect*, 2023.

[12] C. E. Reviews, "Best off-grid solar system." `https://www.cleanenergyreviews.info/blog/bestoff-grid-solar-system`, 2020. Accessed: Mar. 03, 2022.

[13] D. Naghaviha, H. Nikkhajoei, and H. Karimi, *Step-by-Step Design of Large-Scale Photovoltaic Power Plants*. Wiley, 1st ed., 2022.

[14] C. E. Reviews, "What is a hybrid inverter." `https://www.cleanenergyreviews.info/blog/whatis-a-hybrid-inverter`, 2021. Accessed: Mar. 02, 2022.

[15] V. M. Phap and L. T. T. Hang, "Comparison of central inverter and string inverter for solar power plant: Case study in vietnam," *Journal of Nuclear Engineering & Technology*, vol. 9, no. 3, pp. 11–23, 2019.

[16] S. B. Kjaer, J. K. Pedersen, and F. Blaabjerg, "A review of single-phase grid-connected inverters for photovoltaic modules," *IEEE Transactions on Industry Applications*, vol. 41, pp. 1292–1306, September/October 2005.

[17] R. Teodorescu, M. Liserre, and P. Rodríguez, *Grid Converters for Photovoltaic and Wind Power Systems*. Wiley, 2011.

[18] M. Venkatesan, R. Rajeswari, and K. Keerthivasan, "A survey of single phase grid connected photovoltaic system," in *2012 International Conference on Emerging Trends in Science, Engineering and Technology (INCOSET)*, pp. 404–408, IEEE, 2012.

[19] O. L. Santos, "Contribution to the dc-ac conversion in photovoltaic systems: Module oriented converters." `https://hal.archives-ouvertes.fr/`, April 2015.

[20] M. Calais, J. Myrzik, T. Spooner, and V. G. Agelidis, "Inverter for single phase grid connected systems – an overview," in *Proceedings of the IEEE Power Electronics Specialists Conference (PESC)*, vol. 2, pp. 1305–1310, 2002.

[21] Z. J. Čorba, V. A. Katić, B. P. Dumnic, and D. M. Milićević, "In-grid solar-to-electrical energy conversion system modeling and testing," *Thermal Science*, vol. 16, no. Suppl. 1, pp. S159–S171, 2012.

[22] G. P. Adam, O. Anaya-Lara, G. M. Burt, D. Telford, B. Williams, and J. McDonald, "Modular multilevel inverter: Pulse width modulation and capacitor balancing technique," *IET Power Electronics*, vol. 3, no. 5, pp. 702–717, 2010.

[23] T. Orlowska-Kowalska, F. Blaabjerg, and J. Rodríguez, *Advanced and Intelligent Control in Power Electronics and Drives*, vol. 531. Springer, 2014.

[24] M. Azizi, O. Husev, and D. Vinnikov, "Single-stage buck–boost inverters: A state-of-the-art survey," *Energies*, vol. 15, no. 5, p. 1622, 2022.

[25] K. R. Reddy, V. N. Reddy, M. V. Kumar, and S. K. Tummala, "Configurations and control strategy of a single stage grid connected pv system," in *E3S Web of Conferences*, vol. 184, p. 01074, EDP Sciences, 2020.

[26] R. Dogga and M. Pathak, "Recent trends in solar pv inverter topologies," *Solar Energy*, vol. 183, pp. 57–73, 2019.

[27] A. Ghilani, A. Terki, A. M. Ghodbane, Z. Alili, and O. Belaroussi, "Optimal conversion topologies for grid-connected pv systems: A comparative study of single-stage and two-stage configurations," *ITEGAM-JETIA*, vol. 12, no. 57, pp. 408–415, 2026.

[28] S. E. Evju, "Fundamentals of grid connected photovoltaic power electronic converter design," specialization project, Department of Electric Engineering, Norwegian University of Science and Technology, December 2006.

[29] R. Mayfield, "The highs and lows of photovoltaic system calculations," *Electrical Construction & Maintenance*, July 2012. Accessed on November 10, 2012.

[30] Midcontinent Independent System Operator (MISO), "Miso guideline for ieee std 1547-2018 implementation: Recommendations on requirements impacting transmission systems," November 2019.

[31] A. Refaat, A. Khalifa, M. Elsakka, Y. Elhenawy, A. Kalas, and M. Elfar, "A novel metaheuristic mppt technique based on enhanced autonomous group particle swarm optimization algorithm to track the gmpp under partial shading conditions—experimental validation," *Energy Conversion and Management*, vol. 287, p. 117124, 2023.

[32] A. Asnil, K. Krimadinata, E. Astrid, and I. Husnaini, "Enhanced incremental conductance maximum power point tracking algorithm for photovoltaic system in variable conditions," *Journal Européen des Systèmes Automatisés*, vol. 57, no. 1, pp. 33–43, 2024.

[33] Y. Houam, A. Terki, and N. Bouarroudj, "An efficient metaheuristic technique to control the maximum power point of a partially shaded photovoltaic system using crow search algorithm (csa)," *Journal of Electrical Engineering & Technology*, vol. 16, pp. 381–402, 2021.

[34] N. Priyadarshi, P. Sanjeevikumar, M. S. Bhaskar, F. Azam, I. B. Taha, and M. G. Hussien, "An adaptive ts-fuzzy model-based rbf neural network learning for grid integrated photovoltaic applications," *IET Renewable Power Generation*, vol. 16, no. 14, pp. 3149–3160, 2022.

[35] A. Ghilani, A. Terki, A. M. Ghodbane, and Z. Alili, "Experimental validation of pso and gwo-based mppt for a single-stage three-phase grid-connected pv system under partial shading," *Journal Européen des Systèmes Automatisés*, vol. 57, no. 2, pp. 123–135, 2024.

[36] M. Alhaj, M. Bendaoud, A. E. Fathi, Z. Boudjema, and H. Messaoud, "Hybrid ann–gwo mppt with mpc-based inverter control for efficient ev charging under partial shading conditions," *Transactions of the Institute of Measurement and Control*, vol. 46, no. 3, pp. 1234–1245, 2024.

[37] A.-B. A. Al-Hussein, F. R. Tahir, and V.-T. Pham, "Fpga implementation of synergetic controller-based mppt algorithm for a standalone pv system," *Computation*, vol. 13, no. 3, p. 64, 2025.

[38] E. AI, "Revolutionizing embedded systems through on-device processing," *International Journal of Scientific Research in Computer Science, Engineering and Information Technology*, vol. 10, pp. 123–130, Feb. 2025. Accessed: 2025-05-01.

[39] A. Bouhouta, *Improving the Power Quality of Grid Connected PV Systems Using Power Electronic Converters*. Ph.d. thesis, University of Medea, Algeria, Mar. 2023.

[40] Y. T. Tan, D. S. Kirschen, and N. Jenkins, "A model of pv generation suitable for stability analysis," *IEEE Transactions on Energy Conversion*, vol. 19, pp. 748–755, December 2004.

[41] M. Bacha and A. Terki, "Diagnosis algorithm and detection faults based on fuzzy logic for pv panel," *Materials Today: Proceedings*, vol. 51, pp. 2131–2138, 2022.

[42] L. V. Bin, C. Yanbo, and W. Chengshan, "Design of grid-connected photovoltaic system using soft cut-in control," in *International Conference on Geoscience, Power, Energy, & Industry Applications*, (Tianjin University, Tianjin, China), pp. 1–5, April 2009. Sustainable Power Generation and Supply.

[43] J. Wiles, "Pv math." `http://www.iaei.org/magazine/2009/01/pv-math/`, 2009. Accessed on November 10, 2012.

[44] D. Zabia, H. Afghoul, and O. Kraa, "Maximum power point tracking of a photovoltaic system under partial shading condition using whale optimization algorithm," in *International Conference on Artificial Intelligence in Renewable Energetic Systems (IC-AIRES)*, pp. 121–132, Springer, 2021.

[45] T. K. Selma, *Implementation on FPGA of an Algorithm for the Characterization of Solar Modules*. Ph.d. thesis, Department of Electronics, University of Blida1, Algeria, 2021.

[46] Y. Amara, R. Boukenoui, R. Bradai, and H. Salhi, "Design and control of two-stage standalone photovoltaic generation system," in *2018 International Conference on Communications (ICC)*, IEEE, 2018.

[47] A. Ballouti, F. Djahli, A. Bendjadou, N. Belhaouchet, and A. Benhamadouche, "Mppt system for photovoltaic module connected to battery adapted for unstable atmospheric conditions using vhdl-ams," *Arabian Journal for Science and Engineering*, vol. 39, pp. 2021–2031, 2014.

[48] A. K. Pati and N. C. Sahoo, "A new approach in maximum power point tracking for a photovoltaic array with power management system using fibonacci search algorithm under partial shading conditions," *Energy Systems*, vol. 7, pp. 145–172, 2016.

[49] C. W. Tan and M. Jamri, "Modeling and control of a photovoltaic energy system using the state-space averaging technique," *American Journal of Applied Sciences*, vol. 7, no. 5, pp. 682–691, 2010.

[50] A. Menadi, *Commande Par Les Techniques Intelligentes D'un Système Photovoltaïque Connecté Au Réseau*. Phd thesis, Université Mohamed Khider Biskra, 2016.

[51] S. Li, "A maximum power point tracking method with variable weather parameters based on input resistance for photovoltaic system," *Energy Conversion and Management*, vol. 106, pp. 290–299, 2015.

[52] K. A. Kim and P. T. Krein, "Photovoltaic converter module configurations for maximum power point operation," in *Proceedings of the University of Illinois Urbana-Champaign Research*, (Urbana, IL, USA), 2010.

[53] H. N. Zainudin and S. Mekhilef, "Comparison study of maximum power point tracker techniques for pv systems," in *Proceedings of the International Conference at Cairo University*, (Cairo, Egypt). Paper ID 278.

[54] Q. A. Al-Shetwi, M. Z. Sujod, M. A. Hannan, M. A. Abdullah, A. S. Al-Ogaili, and K. P. Jern, "Impact of inverter controller-based grid-connected pv system on the power quality," *Alexandria Engineering Journal*, vol. 59, no. 3, pp. 1379–1393, 2020.

[55] S. K. Sahoo, S. Sukchai, F. F. Yanine, and E. F. Fernandez, "Review and comparative study of single-stage inverters for a pv system," *Renewable and Sustainable Energy Reviews*, vol. 91, pp. 962–986, 2018.

[56] M. A. Ghodbane, T. M. Benchouia, M. Chebaani, M. Becherif, A. Gloea, A. Ghilani, and Z. Alili, "Sensorless wind speed estimation using pso for multi-objective finite-state pre-

dictive torque control in grid-connected wind turbines," *Journal Européen des Systèmes Automatisés (JESA)*, vol. 58, no. 3, pp. 421–434, 2025.

[57] N. Altin and S. Ozdemir, "Three-phase three-level grid interactive inverter with fuzzy logic based maximum power point tracking controller," *Energy Conversion and Management*, vol. 69, pp. 17–26, 2013.

[58] K. Tsang and W. Chan, "Model based rapid maximum power point tracking for photovoltaic systems," *Energy Conversion and Management*, vol. 70, pp. 83–89, 2013.

[59] M. A. Zeddini, S. Krim, and M. F. Mimouni, "Experimental validation of an advanced metaheuristic algorithm for maximum power point tracking of a shaded photovoltaic system: A comparative study between three approaches," *Energy Reports*, vol. 10, pp. 161–185, 2023.

[60] S. I. Saadi and I. K. Mohammed, "Power control approach for pv panel system based on pso and inc optimization algorithms," *Journal Européen des Systèmes Automatisés*, vol. 55, no. 6, pp. 825–834, 2022.

[61] V. C. Tella, B. Agili, and M. He, "Advanced mppt control algorithms: A comparative analysis of conventional and intelligent techniques with challenges," *European Journal of Electrical Engineering and Computer Science*, vol. 8, no. 4, pp. 6–20, 2024.

[62] A. Almutairi, A. G. Abo-Khalil, K. Sayed, and N. Albagami, "Mppt for a pv grid-connected system to improve efficiency under partial shading conditions," *Sustainability (Switzerland)*, vol. 12, no. 24, pp. 1–18, 2020.

[63] R. Nisha and G. S. K., "Metaheuristic algorithm based maximum power point tracking technique combined with one cycle control for solar photovoltaic water pumping systems," *Frontiers in Energy Research*, vol. 10, 2022.

[64] J. Ahmed and Z. Salam, "A soft computing mppt for pv system based on cuckoo search algorithm," in *4th International Conference on Power Engineering, Energy and Electrical Drives (POWERENG)*, (Istanbul, Turkey), pp. 558–562, IEEE, 2013.

[65] J. Ahmed and Z. Salam, "A maximum power point tracking (mppt) for pv system using cuckoo search with partial shading capability," *Applied Energy*, vol. 119, pp. 118–130, 2014.

[66] X.-S. Yang and S. Deb, "Multiobjective cuckoo search for design optimization," *Computers & Operations Research*, vol. 40, no. 6, pp. 1616–1624, 2013.

[67] N. Aouchiche, “Conception d’une commande mppt optimale à base d’intelligence artificielle d’un système photovoltaïque,” ph.d. thesis, Université de Technologie de Belfort–Montbéliard, France, 2020.

[68] J. C. Lin, S. Ren, P. Fournier-Viger, J. Su, and B. Vo, “Advances in intelligent information hiding and multimedia signal processing,” in *Advances in Intelligent Systems and Computing*, vol. 64, pp. 101–110, Springer, 2017.

[69] D. B. Prakash and C. Lakshminarayana, “Optimal siting of capacitors in radial distribution network using whale optimization algorithm,” *Alexandria Engineering Journal*, 2016.

[70] I. Jamal, M. F. Elmorshedy, S. M. Dabour, E. M. Rashad, W. Xu, and D. J. Almakhles, “A comprehensive review of grid-connected pv systems based on impedance source inverter,” *IEEE Access*, vol. 10, pp. 89101–89123, 2022.

[71] A. Q. Al-Shetwi, W. K. Issa, R. F. Aqeil, T. S. Ustun, H. M. Al-Masri, K. Alzaareer, M. G. Abdolrasol, and M. A. Abdullah, “Active power control to mitigate frequency deviations in large-scale grid-connected pv system using grid-forming single-stage inverters,” *Energies*, vol. 15, no. 6, p. 2035, 2022.

[72] G. Abad, *Predictive Direct Control Techniques of the Doubly Fed Induction Machine for Wind Energy Generation Applications*. Phd thesis, Mondragon University, Arrasate, Spain, 2008.

[73] Y. Bekakra, L. Zellouma, and O. Malik, “Improved predictive direct power control of shunt active power filter using gwo and alo–simulation and experimental study,” *Ain Shams Engineering Journal*, vol. 12, no. 4, pp. 3859–3877, 2021.

[74] S. Ouchen, H. Steinhart, M. Benbouzid, and F. Blaabjerg, “Robust dpc-svm control strategy for shunt active power filter based on h regulators,” *Electrical Power and Energy Systems*, vol. 117, p. 105699, 2020.

[75] T. C. Minh, *Coupling of Photovoltaic Inverters and Grid: Control Aspects and Disturbance Rejection*. Ph.d. thesis, University of Grenoble, Grenoble, France, 2012.

[76] A. Rennane and D. S. Koussa, “Evaluation of the performance of the phase-locked loop (pll) for the interconnection of a renewable energy source to the electric grid,” *Revue des Energies Renouvelables*, vol. 17, no. 2, pp. 227–243, 2014.

[77] A. Ghoshal and V. John, “A method to improve pll performance under abnormal grid conditions,” in *National Power Electronics Conference (NPEC)*, (Indian Institute of Science, Bangalore, India), 2007.

[78] P. Tripathy, B. Misra, and B. Nayak, "Phase-locked loop based synchronization schemes for three-phase unbalanced and distorted grid: A review," *International Journal of Applied Power Engineering*, vol. 13, no. 4, pp. 934–943, 2024.